# Space-borne spectrodirectional estimation of forest properties

Jochem Verrelst

Space-borne spectrodirectional estimation of forest properties

Jochem Verrelst

Thesis committee

Thesis supervisor
Prof. Dr. sc. nat M.E. Schaepman
Professor of Geo-Information Science with special attention for remote sensing
Wageningen University, The Netherlands
Professor of Remote Sensing
University of Zurich, Switzerland

Thesis co-supervisors
Dr. ir. J.G.P.W. Clevers
Associate Professor, Laboratory of Geo-Information Science and Remote Sensing
Wageningen University, The Netherlands

Dr. sc. nat. B. Koetz
Earth Observation Engineer - EO science, Application and Future Technology Department
European Space Agency - ESRIN, Italy

Other members
Prof. Dr. H.H.T. Prins   Wageningen University, The Netherlands
Prof. Dr. A.K. Skidmore   ITC, Enschede, The Netherlands
Prof. Dr. P. Defourny   Université Catholique de Louvain, Belgium
Prof. Dr. J.F. Moreno Mendez   University of Valencia, Spain

This research was conducted under the auspices of the C.T. de Wit Graduate School for
Production Ecology and Resource Conservation (PE&RC)

Space-borne spectrodirectional estimation of forest properties

Jochem Verrelst

Table of contents

Chapter 1

General introduction

Paragraph 1.3.2 based on paragraph 8.3 (written by J. Verrelst) in: Schaepman, M.E., Ustin, S.L., Plaza, A.J., Painter, T.H., Verrelst, J., & Liang, S. (2009). Earth system science related imaging spectroscopy-An assessment. *Remote Sensing of Environment, 113*, S123-S137

1.1 Earth Observation and forest monitoring

Forests presently cover approximately 30% of the terrestrial Earth surface and function as habitats for organisms, as soil conservers and as carbon pools, thereby constituting one of the most important aspects of the Earth's biosphere (www.fao.org/forestry). Nevertheless, with the upcoming global warming, forests are under threat. Although forests have responded to global warming in the past, the rate of change predicted in the 21st century and the resulting feedback effects on global climate is likely to be unprecedented (Saxe et al., 2001; Chapin et al., 2005; Hyvönen et al., 2007). To forecast climate change impacts and adaptations, it is a requisite to be equipped with spatially-explicit and up-to-date bio-indicators of the health status of the Earth's global forest cover (e.g. photosynthetic activity, carbon and nutrient sequestration, defoliation, biomass; e.g. see http://fhm.fs.fed.us/). Earth Observation (EO) offers unique opportunities to provide continuous and repetitive data of the Earth forest cover, from local to global scale. In many parts of the world space-based EO technologies constitute the sole cost-effective data source suitable to report upon forest conditions. Owing to the advantages of EO, many national and international agencies have already implemented operational EO data streams in forest inventory and monitoring programs (e.g. Canadian Forest Service, US-GEOSS Forest Monitoring, GMES Service Element Forest Monitoring).

This thesis focuses on the use of state-of-the-art optical EO data for forest properties mapping. Optical EO data are able to deliver biochemical and structural canopy properties. Optical sensors sample the Earth's reflected visible, near infrared (NIR) and short-wave infrared (SWIR) solar electromagnetic radiation to deliver images of the Earth's surface. However, an optical sensor only measures the spatially distributed radiation fluxes reflected from the Earth's surface in the direction of the sensor. Optical EO measurements are thus fundamentally not capable to provide directly the canopy properties that are of interest for forest monitoring. An intermediate step is necessary to transform the EO measurements into estimates of the vegetation structure or biochemistry. To perform such a transformation, some understanding of the involved physics is required.

The physical process that makes optical EO possible is the interaction between radiation and matter, called radiative transfer (RT) (Lillesand et al., 2004). Radiative transfer in vegetation comprises reflection, transmission, absorption and emission, intrinsically related to the vegetation elements. These vegetation elements cause variations in absorbance and transmittance across wavelengths via multiple scattering processes throughout the canopy and background (i.e. understory, soil). This implies that EO data can only provide information on vegetation properties that have a direct impact on and are sensitive to the measured radiation fluxes (Ross, 1981; Goel, 1988; Asner, 1998; Dawson et al., 1999; Chen et al., 2000). In turn, the explicit retrieval of vegetation properties based on EO data is limited to variables directly involved in the radiative transfer within the canopy, called the radiative state variables (Verstraete & Pinty, 1996). These state variables can either have a biochemical nature (e.g., chlorophyll content, pigments) or a structural nature (e.g. leaf area index (LAI), canopy cover).

The knowledge of the state variables and interacting RT processes is encapsulated into a variety of models.

Fundamentally, the interpretation of EO data always implies the use of a model (Widlowski, 2002). This model can be *empirical*, as in the case of various statistical methods that correlate raw data or vegetation indices with variables of interest, or can be *physical,* as in the case of RT models whereby information about the variables that influence the propagation of radiation fluxes is extracted based on physical rules (e.g. Myneni et al., 1995; Gobron et al., 2000).

Despite the large variety of models and derived products, our current understanding of the interaction between radiation and forest properties is still far from complete. There are (*i*) limitations on the side of the models; (*ii*) there is the intrinsic complexity of the forest canopy to be accounted for, and (*iii*) there is the ongoing technological boost towards more powerful EO instruments such as imaging spectroscopy and multi-angular instruments, which requires an upgrading of our knowledge of the involved mechanisms at a refined spatial, spectral and/or angular scale. These points are essentially interconnected and will be briefly outlined in the next sections within the context of forest monitoring. They will finally lead to the objectives of this thesis that aims to contribute to the broader scientific debate on how multi-angular imaging spectroscopy can serve monitoring canopy biochemical and structural properties.

1.2 EO models

1.2.1 *Empirical models: vegetation indices*

With respect to empirical approaches, vegetation indices (VIs) are among the oldest and most widely used tools in EO mapping applications. VIs are simple numerical indicators that reduce multispectral (two or more bands) data to a single variable for predicting and assessing vegetation characteristics. Along with the development of optical sensors a broad diversity of VIs have been developed, aiming for specific purposes (i.e., greenness, chlorophyll content, secondary pigments: e.g. carotene, xanthophylls), spatial scales (e.g. leaf, canopy, global) and spectral resolutions (i.e. broadband vs. narrowband). Nevertheless, what all vegetation indices have in common is that:

- Data are reduced to one single layer, which is assumed informative about the structural or biochemical condition of the vegetation. VIs are powerful when fast and local-to-regional assessments are needed;

- VIs create only empirical relationships and are thus limited in transferring to other images;

- Besides sensitivity to vegetation properties, VIs can additionally be affected by a number of perturbing factors, including: atmospheric effects, clouds, soil effects, anisotropy effects, sensor-specific spectral effects.

Although quite often effective, this leads to the awareness that VIs are intrinsically limited by the empiricism of their design. In any quantitative application that requires a given level of accuracy, all the perturbing factors could result in errors or uncertainties that reduce the predictive power of VIs below a desired threshold. Furthermore, and more importantly, for the majority of VIs their sensitivity towards perturbing factors at canopy level has not been systematically studied, particularly with respect to anisotropic effects or in relation to canopy heterogeneity. This seriously limits the use of these indices, especially when calculated from EO data for forest monitoring applications. Knowledge of the roles perturbing factors play is very important when implementing VIs in operational monitoring schemes (Glenn et al., 2008). Linking VIs with physical models can help to assess these uncertainties (Myneni et al., 2002).

1.2.2 *Physical models: radiative transfer (RT) models*

Since statistical or empirical approaches lack transferability and robustness, this has led to the advancement of physical models for estimating biochemical/structural state variables from canopy spectra. Physical radiative transfer models describe the transfer and interactions of solar radiation inside the canopy based on physical laws and thus provide an explicit link between the biochemical and structural characteristics of vegetation scattering elements (e.g. the leaf) and the canopy reflectance (Ross, 1981; Goel and Thompson, 2000).

Leaf level

RT processes at the leaf level take place at the molecular level, e.g., the absorption characteristics of the foliar biochemical components, such as electronic transitions in the chlorophyll pigments or the bending and stretching vibrations of the biochemical bonds (Lichtenthaler, 1987; Curran, 1989). Apart from biochemical components, the foliage optical properties are primarily a function of internal leaf structure, leaf surface roughness and water content (Ross, 1981; Fourty et al., 1996; Middleton et al., 1997; Bousquet et al., 2005). Leaf RT models attempt to explain how radiation interacts with the above-mentioned biophysics and biochemistry (Jacquemoud and Baret, 1990; Dawson et al., 1998; Ganapol et al., 1998). Popular leaf-level radiative transfer models are PROSPECT (Jacquemoud & Baret, 1990) and LIBERTY (Dawson et al., 1998).

Canopy level

While the optical properties of the leaves can be described by a leaf-level RT model, estimates of vegetation properties based on EO data from air- or space-borne platforms have to be ultimately assessed at the canopy level. Such canopy models are described by a number of state variables. State variables typically encompass LAI, canopy cover, the nonphotosynthetic canopy elements and the understory as the main factors driving the EO

signal (Spanner et al., 1990; Huemmrich & Goward, 1997; Asner, 1998). In principle, these state variables determine the relative contributions of the canopy scattering elements, which can be typified as photosynthetic vegetation (PV) and nonphotosynthetic vegetation (NPV).

There are four broad categories of canopy reflectance models, although some models contain elements of more than one category:

- The simplest canopy RT models are the 1D or *turbid media* (homogeneous canopies) models. Turbid medium models describe the canopy as a horizontally homogeneous layer of scattering and absorbing particles of a given density and orientation (e.g. Verhoef, 1984). These models (e.g. the SAIL family) are suited for describing dense leafy canopies such as closed forests, which can be described as being horizontally homogeneous, but are inappropriate for describing forests that are more heterogeneous.

- *Geometrical-optical models* (e.g. Li & Strahler, 1992) describe the canopy using a series of regular geometric shapes, placed on the soil surface in a prescribed way. The fractions of different components are calculated based on the 3D geometric optical principles. Canopy reflectance is determined by the interception of light and shadowing by the geometric objects and the reflectance from the ground surface. These types of models can be applied to describe sparse canopies such as shrublands or open forests.

- The finest modeling degree is *Monte Carlo ray tracing*, which stochastically calculates photon trajectories within turbid or geometric canopies. A photon is tracked from its source until it exits the canopy, with scattering based on probabilistic interactions. Ray tracing is used to assess the influence of multiple scattering on spatial aggregation and angular dynamics over heterogeneous forests (e.g. Govaerts, 1998; Lewis, 1999; Disney et al., 2000). Only these sophisticated models, possessing the flexibility to render any kind of 3D scene, are able to represent stands with higher levels of complexities.

- *Hybrid models* combine elements of both the turbid medium, the geometric optical or the ray tracing models. In this case, the geometric shapes representing the canopy, for example, are treated as a turbid medium, or simple geometric shapes are introduced in a ray tracing environment. Often the amount of *a priori* knowledge can be a limiting factor when constructing a detailed 3D description of a canopy. In this case, a less detailed approach with a smaller number of input parameters might be preferred, e.g., such as FLIGHT (Forest LIGHT interaction model) (North, 1996). The model is hybrid because of the combination of a geometrical-optical model and Monte Carlo simulations of photon transport.

1.2.3 *Applying radiative transfer models*

The advantage of physical RT models is that they can be coupled (e.g. leaf with canopy level), thereby providing a physically based linkage between optical EO data and biochemical or structural state variables (Verhoef & Bach, 2003; Jacquemoud et al., 2009). Once having

such coupling established it allows inferring foliar biochemistry at canopy scale. Moreover, with a coupling not only the relationships between foliar biochemistry (e.g. chlorophyll content) and reflectance data (and derived vegetation indices) can be analyzed, but also the effects of additional factors perturbing these relationships, such as sun-target-sensor geometry and canopy structure (Zarco-Tejada et al., 2001). RT models can be applied in many ways for forestry applications; some can be run in the *forward* mode, some both in the forward and *inverse* modes.

Running RT models in its direct or *forward* mode enables creating a database covering a wide range of situations and configurations. Such forward RT model simulations allow for sensitivity studies of canopy parameters relative to diverse observation specifications, which can lead to an improved understanding of the EO signal as well as to an optimized instrument design of future EO systems (Myneni et al., 1995; Gobron, 1997; Jacquemoud et al., 2000; Pinty et al., 2001).

Inversion of the RT model enables retrieving vegetation characteristics from EO data. The unique and explicit solution for a model inversion depends on the number of free model parameters relative to the number of available independent observations. A prerequisite for a successful inversion is therefore the choice of a validated and appropriate RT model, which correctly represents the radiative transfer within the observed target (Pinty and Verstraete, 1992; Myneni et al., 1995). When a unique solution is not achieved (unified theorem of Hadamard well-posedness) then more *a priori* information is required to overcome the ill-posed problem, a condition that is not always achieved (Combal et al., 2003).

To overcome the problem of *a priori* information, semi-empirical models may function as a compromise. Semi-empirical models are simple models that contain aspects of both physical and empirical models by retaining some physical interpretation with empirical linkages to describe the pattern of reflectance anisotropy rather than maintain fidelity with biophysical parameters (Pinty et al., 1989; Su et al., 2009).

1.3 Forests and radiative transfer models

1.3.1 *Forest dynamics: the case of an Alpine old-growth forest*

Having the models for EO data interpretation available, a next step is to select the appropriate model for linking with a forested target. The design of the model should be such that it is able to mimic the radiative fluxes throughout the forest canopy at an acceptable degree of detail for reliable retrievals. Therefore, some knowledge of forest development is required. A forest is not static and becomes more heterogeneous in structure and composition over time (Franklin et al., 2002). Consequently, the spectral response of a forest is heavily dependent on its development stage. The most noteworthy dynamics causing spectral changes over time will be further discussed in the context of an Alpine coniferous forest; however, the growth dynamics are broadly applicable to boreal and temperate forests.

Forests are long-living ecosystems, i.e. they can grow up to 1000 years old (also termed old-growth or primary forest). During the development of a forest ecosystem, its structure undergoes dramatic changes in vertical and horizontal dimension during aging (Brown and Parker, 1994; Franklin and Van Pelt, 2004). Both individual structures and their spatial arrangements are relevant to the understanding of key processes in the development of a long-living forest. For instance, young (typically between 10 and 30 years) and old-growth forests (exceeding 150 years) offer extreme contrasts in foliage distribution. In young forests, foliage is concentrated high in the canopy with little or none lower in the canopy. In old-growth forests, foliage and living branches are distributed continuously from the ground to the top of the canopy (Franklin et al., 2002). Apart from heterogeneity, the increment of woody elements such as dead standing trees and coarse woody debris (CWD) are other features that characterize old-growth forests (Keddy & Drumnond, 1996); a high density of CWD may account for as much as 90% of forest floor mass (Woldendorp & Keenan, 2005).

From an EO perspective, the spectral trajectory over many decades of old-growth forests is hence governed by (*i*) an increase of NPV (e.g. dead standing trees, CWD) at the expense of PV, and (*ii*) a more heterogeneous 3D distribution of PV and NPV elements. This implies that for old-growth forests EO-based retrieval of foliar biochemistry is affected by the complex combination of structural heterogeneity and optical scattering properties of accumulating woody elements.

1.3.2 *Radiative transfer models and forests*[1]

Old-growth forests play an important role in species diversity through niche diversification and may act as important carbon sinks, due to the long period of forest stability (Knohl et al., 2003; Luyssaert et al., 2008). Despite the relevance of old-growth forests, a comprehensive review in scientific literature (in *Remote Sensing of Environment*) revealed that the majority of physically-based approaches have been applied on young to mature forests, rather than the more structurally complex canopies of old-growth forests. Figure 1.1 displays studies of applications of RT models in the last decade. RT models can be categorized as (*i*) 1D or turbid-medium models; or (*ii*) when the canopy space consists of crown architectural elements, as 3D models. In Figure 1.1, the symbols indicate whether biophysical (open symbols) or biochemical (closed symbols) variables are quantified. At a glance, the intuitive perception that relatively simple 1D models are still preferred in the scientific community (e.g. Huang et al., 2008) is not confirmed by this figure. Some studies have evidently relied on the turbid-medium type of models such as the SAIL family, yet the majority of the encountered studies effectively applied canopy models in 3D space. For most of the presented

---

[1] paragraph based on paragraph 8.3 (written by J. Verrelst) in: Schaepman, M.E., Ustin, S.L., Plaza, A.J., Painter, T.H., Verrelst, J., & Liang, S. (2009). Earth system science related imaging spectroscopy-An assessment. *Remote Sensing of Environment, 113*, S123-S137

forestry applications RT models are linked with optical EO data through numerical inversion methods with the purpose of inferring one or more state variables. For other forestry applications RT models are run in forward mode to generate synthetic data, e.g. for mapping purposes based on spectral unmixing or classification techniques.


Figure 1.1: Stand age study site compared for year of publication per radiative transfer model used. The open symbols represent biophysical retrievals (e.g. fraction cover, LAI), while the closed symbols represent biochemical retrievals (e.g. chlorophyll). Symbols are plotted on the averaged age. The grey lines represent the full range of stand age of the used study site. (Referenced legend *a*: Bruniquel-Pinel & Gastellu-Etchegorry, 1998; *b*: Gemmell, 1998; *c*: Gemmell and Varjo, 1999; *d*: Gastellu-Etchegorry et al., 1999; *e*: Gemmell, 1999; *f*: Brown et al., 2000; *g:*Demarez & Gastellu-Etchegorry, 2000; *h*: Kuusk & Nilson, 2000; *i*: Hu et al., 2000; *j*: Gao et al., 2000; *k*: Huemmrich, 2001; *l*: Gastellu-Etchegorry & Bruniquel-Pinel, 2001 *m*: Lacaze & Roujean, 2001; *n*: Gemmell et al., 2001*; o*: Kimes et al., 2002; *p*: Gemmell et al., 2002; *q*: Song et al., 2002; *r*: Wang et al., 2003; *s*: Shabanov et al., 2003; *t*: Gastellu-Etchegorry et al., 2003; *u*: Rautiainen et al., 2004; *v*: Zarco-Tejeda et al., 2004; *w*: Peddle et al., 2004; *x*: Fernandes et al., 2004; *y*: Meroni et al., 2004; *z, aa*: Kötz et al., 2004; *ab, ac*: Fang et al., 2003; *ad*: Zhang et al., 2005; *ae*: Rautiainen & Stenberg, 2005; *af*: Rautiainen, 2005; *ag*: Disney et al., 2006; *ah*: Schlerf & Atzberger, 2006; *ai:* Eriksson et al., 2006; *aj*: Soudani et al., 2006; *ak, al*: Cheng et al., 2006; *am*: Zhang et al., 2006; *an* Song et al., 2007; *ao*: Koetz et al., 2007; *ap*: Colombo et al., 2008; *aq*: Lang et al., 2007; *ar*: Malenovský et al., 2008; *as, at*: Kuusk et al., 2008; *au*: Huang et al., 2008; *av*: Suarez et al., 2008; *aw*: Verrelst et al., 2008b; *ax*: Quaife et al., 2008; *ay*: Moorthy et al., 2008).

A model-driven motivation for selecting younger, structurally more homogeneous stands may be the smaller degrees of uncertainty; hence these stands are better suited for model parameterization and validation. Simple, turbid medium models are well suited for dense

vegetation canopies, such as young, homogeneous stands. Also, due to the ill-posed nature of the inversion problem (Combal et al., 2003; Atzberger, 2004), a simplified approximation of the canopy representation may be required simply because larger numbers of variables will increase the uncertainty of the inversion. The abundant presence of understory and CWD typical in boreal coniferous forests poses nevertheless a problem for the correct image interpretation using simplified physically based models (Chen & Cihlar, 1996; Eklundh et al., 2001; Stenberg et al., 2004; Peltoniemi et al., 2005; Rautiainen et al., 2007).

Only very few contributions have discussed spectral characteristics of old-growth forests (Song et al., 2002; Song et al., 2007). In these studies, canopy structural variables and leaf optical properties were entered in a hybrid geometric-optical radiative transfer model (GORT) to mimic structural canopy changes characteristic of successional change. Figure 1.1 also suggests a significant imbalance towards canopy biophysical properties compared to canopy (or even leaf) chemistry. The retrieval of leaf chemistry is usually resolved by coupling a relatively simple leaf-level RT model with a canopy-level RT model. The woody component is typically fixed in these retrieval studies, an assumption that does not necessarily match reality (Roberts et al., 2004). A challenge remaining to be resolved is to make the models more adjustable to canopy compositional variability, e.g. in terms of variable proportions of foliage and woody elements, which is common in old-growth forests (Franklin et al., 2002). An assessment on the contributions of canopy woodiness to canopy reflectance for a wide range of canopies would be a first step to do.

Simple turbid medium RT models are likely unable to account for such structural and compositional changes. Geometrical-optical models, ray tracing models or hybrid models that have 3D functionalities are expected to be better equipped to simulate the radiative transfer fluxes within a heterogeneous, woody canopy. Owing to the capability of simulating radiative fluxes almost on a photon-by-photon basis, meanwhile preserving simplicity in generating 3D scenes, FLIGHT seems to be particularly suitable to link canopy variables with reflectance data. Having outlined canopy models and their relationships with forest, a next step is linking them with recent technologies in EO: imaging spectroscopy and multi-angular EO.

1.4 Imaging spectroscopy

While in the 90ies EO was limited to a few broad bands and a limited number of state variables could be estimated from broad spectral regions, with the advent of imaging spectroscopy during the last decennium EO has entered a new paradigm. Imaging spectrometers use many contiguous and narrow bands (up to more than one hundred). Such a high number of bands makes it possible to capture most absorption features in a vegetation reflectance spectrum (Green et al., 1998; Ustin et al., 2004). This opened new avenues for EO science: the availability of many narrow bands enabled to define new state variables, active in specific, usually small spectral regions.

Given this refined concept of state variables, various examples of the retrieval of foliar chemistry and canopy composition exist, using the spectral information dimension encapsulated in the narrow spectral bands of imaging spectroscopy instruments. Examples include: pigments (e.g. chlorophyll *a* & *b*, carotenoids), relationships with nutrients (e.g. nitrogen, phosphorus), foliage water content, dry matter, understory and canopy composition. See Schaepman et al. (2009) for an overview. A common and straightforward approach of using imaging spectroscopy data for inferring canopy properties is to apply narrowband vegetation indices (Majeke et al., 2008). However, questions related to up-scaling uncertainties (e.g., anisotropy effects, influence of structure) have to be resolved beforehand.

1.4.1 *Space-borne imaging spectrometer: CHRIS*

Until now, there are not many true imaging spectrometers in space, satisfying a strict definition of the criterion of contiguity over an extended spectral range, either the visible/near-infrared or from the visible into the shortwave infrared. The development of imaging spectrometer initiatives for space satellites remains difficult and very expensive in terms of payload design, maintenance and calibration. In any case, these difficulties have not deterred the space agencies to fund innovative missions carrying on board imaging spectrometry payloads (Schaepman et al., 2009). This is the case with CHRIS (Compact High Resolution Imaging Spectrometer) developed by a European consortium funded by European Space Agency (ESA). CHRIS is the sensor of interest in this thesis.

The imaging spectrometer CHRIS on board the PRoject for On Board Autonomy 1 (PROBA-1) satellite was launched on October 21, 2001 as a technology demonstrator. PROBA-1 is a small platform, weighing approximately 100 kg and measuring approximately 60×60×80 cm. CHRIS can acquire up to 62 spectral bands in the range of 400–1050 nm with a spectral resolution of 5–12 nm. The CHRIS/PROBA system has several unique features: the sensor can be commissioned from the ground station, allowing different acquisition modes in terms of both spectral channels and spatial resolution (Barnsley et al., 2004), with a nominal ground resolution between ~17 and 34 m. The nominal swath is 13 km. Five principal modes have been selected according to the requirements for five major application fields: aerosol, land cover, vegetation, coastal zones and water bodies.

Despite its flexible configuration, however, the uniqueness of CHRIS lies not only in its fine spectral sampling. The CHRIS sensor has been the first high spatial resolution sensor with advanced pointing capability, dedicated to the acquisition of nearly simultaneous images with multiple viewing angles. Thanks to its four reaction wheels the platform is highly maneuverable: along-track pointing allows a given site to be imaged five times during a single overpass. The system acquires the images at times when its zenith angle is approximately equal to a set of so-called fly-by zenith angles: ±0°, ±36° and ±55° (Barnsley et al., 2004). The added value of multi-angular EO is explained below.

1.5 Multi-angular Earth Observation

Traditional EO applications have mostly focused on extracting structural and biochemical information from the spectral domain; only recently space-borne multi-angular sensors became available to exploit the angular domain. Multi-angular EO sensors are designed to acquire imagery at varying angles explicitly to collect multiple looks over as short a timeframe as possible, taking into account the constraints imposed by the orbits of their platforms (Chopping, 2008). Multi-angular EO seeks to exploit the reflectance anisotropy of the Earth's surface that is described by the bidirectional reflectance distribution function (BRDF) that describes the angular distribution of spectral radiation scattered by a surface (Nicodemus et al., 1977). The BRDF describes the reflectance anisotropy of a target as a function of illumination geometry and viewing geometry; it depends on wavelength and is determined by the intrinsic surface properties. Sampling the angular distribution of surface-leaving radiation from multiple viewing angles therefore has an added value compared to mono-angular remotely sensed data which mostly give a view on the top of the canopy (nadir view).

Similar to the interpretation of EO data in the spectral domain, interpretation of EO data in the angular domain relies on the use of models (Wanner et al., 1997). These models should enable the pixel-by-pixel inversion of measured reflectance anisotropy over wide areas into useful products (Lucht et al., 2000). Although being most realistic, physical models are computationally too demanding to allow rapid inversion over wide areas, and the necessity of *a priori* knowledge for parameterization makes that they are inflexible to account for a range of surface cover types (Roberts, 2001). Semi-empirical models do not require *a priori* knowledge; usually three or four independent parameters are sufficient for describing the reflectance anisotropy of a target. As such, they are particularly useful for angular extrapolation and interpolation schemes in view of the limited angular sampling delivered by multi-angular EO platforms. Among the semi-empirical models, the Rahman–Pinty–Verstraete (RPV) model (Rahman et al., 1993) describes the reflectance anisotropy based on four parameters. Inversion of the model against angular reflectance data allows quantifying the surface reflectance anisotropy in one single parameter, the so-called Minnaert-*k* parameter.

1.5.1 *Spectrodirectional data for forest structure mapping*

Multi-angular EO data provide access to surface properties by exploiting their anisotropic reflectance characteristics. It is this reflectance anisotropy that enables information about the structural properties of the surface to be inferred (Asner et al., 1998; Deering et al., 1999; Sandmeier & Deering, 1999; Diner et al., 1999, 2005). Although not always straightforward, in the last few years multi-angular EO data have been used to develop a variety of approaches that map structural properties of forests, such as:

- Tree density estimates (Sabol et al., 2002; Wessels et al., 2004; Chopping et al., 2006, 2008, 2009)
- LAI (Pocewicz et al., 2007)
- Tree height (Kimes et al., 2006; Heiskanen, 2006, Chopping et al., 2008, 2009)
- Foliage clumping index (Chen et al., 2005; Leblanc et al., 2005)
- Canopy heterogeneity (Widlowski et al., 2001; Pinty et al., 2002).

While these studies demonstrated that there is some structurally-related information embedded in the angular domain, almost all of them were using the Multi-angle Imaging Spectroradiometer (MISR) on board the Terra platform (Diner et al., 1998). The advantage of the MISR instrument lies in its 9 viewing angles; however, the relatively high angular sampling is at the expense of a low spectral resolution (5 broad bands) and a coarse spatial resolution (275 m in red, 1100 m in the other broad bands). Although the use of MISR data led to an improved understanding of angular anisotropy of vegetation canopy reflectance and to the development of methods that derive structural information from it, basically all these methods were developed in the red spectral broadband because of it has the best spatial resolution. MISR is unable to record reflectance anisotropy over the full VNIR (visible and NIR), which is a gap to be filled because of the close coupling between optical and structural parameters (Roujean et al., 2004).

The rich information content of CHRIS data at a relatively high spatial resolution may refine our understanding on how vegetation properties impact the partitioning of the canopy-leaving radiation in the VNIR. More precisely, CHRIS may open opportunities to decouple the angular domain from the spectral domain, thereby linking the spectral domain with biochemistry and the angular domain with canopy structure at the tree canopy level. It is therefore of interest to investigate how space-borne spectrodirectional (combined multi-angular and spectroscopy) data can contribute to forest monitoring, specifically in the case of natural, heterogeneous old-growth forests.

1.6 Objectives

The main objective of this thesis is to evaluate how space-borne spectrodirectional data can contribute to the mapping and monitoring of biochemical and structural properties of a heterogeneous old-growth forest.

While anisotropy of vegetation canopy reflectance is known to be related to canopy structure, our knowledge about the embedded information richness of angular reflectance anisotropy as measured over the whole VNIR is limited. The imaging spectrometer CHRIS provides an excellent instrument to fill this knowledge gap.

One way to quantify the canopy reflectance anisotropy of an old-growth forest is by means of assessing the angular response of vegetation indices. Imaging spectroscopy data allow calculating a large range of vegetation indices at the canopy level that may be useful for forest

monitoring. The effects of canopy reflectance anisotropy on the performance of vegetation indices are nevertheless largely unknown. Therefore, the first hypothesis is: *Multi-angular imaging spectroscopy enables assessing the robustness of vegetation indices with respect to reflectance anisotropy.*

Due to the forest heterogeneity, it is expected that not only reflectance anisotropy but also structural and compositional canopy variables affect the efficacy of vegetation indices in assessing foliar biochemistry (e.g. chlorophyll content). The role perturbing variables play in the performance of indices can be theoretically analyzed and quantified by means of forward RT modeling. Therefore the second hypothesis is: *Radiative transfer models can provide a theoretical framework for assessing the efficacy of vegetation indices over heterogeneous forested areas.*

Having theoretically identified some cause-effect relationships between reflectance anisotropy and canopy variables in the VNIR, a next step is to analyze how space-borne measured canopy anisotropy can be applied to derive mappable forest structural properties. Inversion of the RPV model with CHRIS data can be useful for this purpose. The RPV model enables to decompose and quantify reflectance anisotropy at one single wavelength in one single parameter, the Minnaert-*k* parameter. A systematic evaluation of the information content of the Minnaert-*k* parameter across the spectral domain may lead to improved canopy structure mapping. Therefore the third hypothesis is: *The Minnaert-k parameter allows to systematically estimate the dynamics of reflectance anisotropy across the VNIR wavelengths.*

This research should ultimately lead to an improved exploitation of the angular and spectral domain with the purpose of developing a mapping routine that quantifies structural heterogeneity with a level of detail that cannot be reached by mono-angular optical data. Therefore the final hypothesis is: *Simultaneous exploitation of the angular and spectral domain should lead to improved forest heterogeneity mapping.*

Based on the above hypotheses the following research questions will be investigated in this thesis:

A. To what extent does the anisotropic reflectance of vegetated surfaces as measured by CHRIS influence the performance of vegetation indices, and what are the underlying mechanisms (investigated in chapter 2)?

B. Can foliar chlorophyll content be reliably estimated in woody, heterogeneous forest types using vegetation indices (investigated in chapter 3)?

C. How does reflectance anisotropy of a heterogeneous forest behave across the spectral VNIR domain as measured by CHRIS (investigated in chapter 4)?

D. Can spectrodirectional CHRIS data be applied for forest heterogeneity mapping (investigated in chapter 5)?

1.7 Outline of this thesis

The core of this thesis (Chapters 2–5) is based on a series of four peer-reviewed papers. Each chapter is introduced here by stating its research goals and by outlining its relationship with other relevant work.

Chapter 2 explores the influence of reflectance anisotropy on a suite of broadband and narrowband vegetation indices as measured by CHRIS and tries to explain some mechanisms underlying the observed angular variation.

Chapter 3 goes further in evaluating the efficacy of vegetation indices at the canopy scale. By coupling a leaf reflectance model (PROSPECT) with a canopy reflectance model (FLIGHT) the contribution of canopy variables in perturbing the performance of chlorophyll-sensitive vegetation indices is theoretically analyzed.

Chapter 4 uses CHRIS images of coniferous forests under winter conditions. The RPV model is used to quantify the anisotropic behavior into a single parameter: the Minnaert-k parameter. This study exploits the unique structurally-related information content that is embedded in the angular domain.

Chapter 5 aims at developing a mapping application based on the Minnaert-k parameter. The underlying idea is that the information content derived from the angular domain can be combined with the information content derived from the spectral domain to yield improved forest cover heterogeneity mapping.

Finally, **chapter 6** concludes this thesis with conclusions, discussion of the main findings and suggestions for future work.

Chapter 2

Angular sensitivity analysis of vegetation indices derived from CHRIS/PROBA data

Jochem Verrelst, Michael E. Schaepman, Benjamin Koetz, Matthias Kneubühler

Angular sensitivity analysis of vegetation indices derived from CHRIS/PROBA data

Abstract

View angle effects present in spectral vegetation indices can either be regarded as an added source of uncertainty for variable retrieval or as a source of additional information, enhancing the variable retrieval; however, the magnitude of these angular effects remains for most indices unknown or unquantified. We use the ESA-mission CHRIS/PROBA (Compact High Resolution Imaging Spectrometer onboard the Project for On-board Autonomy) providing space-borne imaging spectrometer and multi-angular data to assess the reflectance anisotropy of broadband as well as recently developed narrowband indices. Multi-angular variability of Hemispherical Directional Reflectance Factor (HDRF) is a prime factor determining the indices´ angular response. Two contrasting structural vegetation types, pine forest and meadow, were selected to study the effect of reflectance anisotropy on the angular response. Calculated indices were standardized and statistically evaluated for their varying HDRF. Additionally we employed a coupled radiative transfer model (PROSPECT/FLIGHT) to quantify and substantiate the findings beyond an incidental case study. Nearly all tested indices manifested a prominent anisotropic behavior. Apart from the conventional broadband greenness indices e.g. Simple Ratio Index (SRI), Normalized Difference Vegetation Index (NDVI), light use efficiency and leaf pigment indices e.g. Structure Insensitive Pigment Index (SIPI), Photochemical Reflectance Index (PRI) and Anthocyanin Reflectance Index (ARI) did express significant different angular responses depending on the vegetation type. Following the quantification of the impact, we conclude that the angular-dependent fraction of non-photosynthetic material is of critical importance shaping the angular signature of these VIs. This work highlights the influence of viewing geometry and surface reflectance anisotropy, particularly when using light use efficiency and leaf pigment indices.

Keywords: vegetation indices, multi-angular remote sensing, narrowband indices, light use efficiency, coniferous canopy, reflectance anisotropy, photochemical reflectance index

2.1. Introduction

Spectral vegetation indices (VIs) are designed to assess vegetation photosynthetic activities, leaf area, biomass and physiological functioning (Myneni et al., 1995) on the land surface while reducing the effects of extraneous factors such as background substrate, atmosphere and illumination effects (Vincent, 1997) and so enabling multi-temporal and cross-sensor comparisons (e.g. Goetz, 1997; Lenney et al., 1996). However, it has been demonstrated already that VIs do not only minimize but, in fact, can also exaggerate impacts of solar zenith and view angle (Jackson et al., 1990, Kimes et al., 1985; Pinter et al., 1987). VIs do suffer from directionality not only because of the reflectance anisotropy of surfaces due to vegetation type, canopy structure, non-photosynthetic material, background contributions and shadowing (Kimes et al., 1985; Leblanc et al., 1997; Qi et al., 1995), but also because of the inherent viewing geometry of (large swath) sensors. The Normalized Difference Vegetation Index (NDVI), the most frequently used index in remote sensing applications, usually has higher values at larger viewing angles than at nadir position (Huete et al., 1992; Jackson et al., 1990; Pinter et al., 1987). Typically, over vegetation canopies near infrared (NIR) photons are more affected by multiple scattering than red photons that cause an increase of the spectral contrast between the NIR and red band (Kimes, 1983). In addition, surface reflectance anisotropy affects the relationship of red and NIR reflectance values, resulting in slightly varying directional responses per vegetation type (Leblanc et al., 1997; Qi et al., 1995). Also for other indices, such as the Soil Adjusted Vegetation Index (SAVI) and the Global Environmental Monitoring Index (GEMI), similar patterns for various vegetation types were observed with higher values at off-nadir angles than at nadir position (Gemmell & McDonald, 2000; Huete et al., 1992). These and other studies (e.g. Deering et al., 1999) demonstrated that broadband indices are equally dependent on variations in sun–target–sensor geometry, as in single band measurements, and thus caution is required when using spectral vegetation indices.

One way to cope with the influence of directional effects is through the development of correction approaches either by following an empirical or a physical logic. Huete et al. (1992) minimized variations in SAVI-view angle response with a simple empirically derived cosine function, although this approach does not allow extrapolation to other indices. A number of methods have been recently proposed using physical Bidirectional Reflectance Distribution Function (BRDF) models to reduce uncertainties caused by sun/view angle and surface variations (Bacour et al., 2006; Csiszar et al., 2001; Huete et al., 2002; Los et al., 2005). For example, the angular concerns and the regional heterogeneity of the surface area of the MODIS VI products are standardized by BRDF models (Schaaf et al., 2002) to produce nadir equivalent reflectance values from which the indices are computed (Huete et al., 2002; Van Leeuwen et al., 1999).

An alternative to minimizing the impact of directional effects to the status of a source of error, is the exploitation of the anisotropic characteristics of the surface for improving indices´

performances. Followers of the multi-angular approach advocated that a multi-angular viewing improved the performance of indices (e.g. NDVI) for discriminating cover and leaf area index (LAI), when compared to nadir viewing because it explicitly accounts for structural heterogeneity and canopy shading (Diner et al., 1999; Gemmell & McDonald, 2000).

In any case, whether directional effects are treated either as superfluous information or as a source of additional information is only important if the magnitude and significance of the angular variability is assessed, quantified, and finally included in interpretation of the data. Apart from the conventional broadband indices, a notion of the directional response is for most indices absent. Particularly for the recently developed narrowband indices have directional effects not yet been adequately addressed.

Recently developed narrowband indices are often no longer exclusively based on broad spectral bands located in the well-known red and NIR spectral regions but are found anywhere within the 400 to 2500 nm wavelength range having typically a spectral resolution of 2 to 15 nm. Many of these indices originate from studies on specific absorption features of pigments and structure in single leaves e.g. Photochemical Reflectance Index (PRI) and were, with the advent of space-borne imaging spectrometry (Ustin et al., 2004), upscaled to canopy level (e.g. Asner et al., 2004; Nichol et al., 2000; Nichol et al., 2002; Peñuelas & Inoue, 2000; Rahman et al., 2001). These indices possess the capability to assess – formerly undetectable – biochemical and biophysical properties such as variation in photosynthetic Light Use Efficiency (LUE) (e.g. Gamon et al., 1997; Peñuelas et al., 1995; Stylinski et al., 2002; Trotter et al., 2002), which is a primary driver of Net Primary Production (NPP) and thus ecosystem functioning (Monteith, 1972). To date only a small subset of narrowband indices has been systematically tested at canopy level (e.g. He et al., 2006; Schlerf et al., 2005; Xavier et al., 2006; Zarco-Tejada et al., 2005), and even less were tested on their directional response. This lack of directional testing limits the potential use of the vegetation indices for consistent and accurate longterm monitoring of vegetation on larger to global scales.

The objective of this work is to assess and consistently compare on a statistical basis the magnitude of surface reflectance anisotropy of commonly used spectral reflectance indices. Further some of the key factors governing the reflectance anisotropy have been identified and investigated using a coupled radiative transfer (RT) model. The selected indices are categorized into broadband and narrowband greenness, light use efficiency and leaf pigments. Because reflectance properties of land surface are anisotropic in nature, indices are assumed to be sensitive to changing viewing angles depending on the spectral bands used and the degree of surface anisotropy present in the observed scene. The pushbroom CHRIS (Compact High Resolution Imaging Spectrometer) sensor mounted on the PROBA (Project for On-Board Autonomy) platform offers a unique availability of continuous spectral bands and multi-angular views from space. This wealth of data enabled the assessment of the angular

variability for a wide range of broadband and narrowband indices, exemplified over two Alpine vegetation types exhibiting different degrees of reflectance anisotropy.

2.2. Data

2.2.1. Study site

The test site for this study is located in the eastern Ofenpass valley, which is part of the Swiss National Park (SNP) in South East Switzerland (10°13′48″E/ 46°39′45″N). The Ofenpass represents a dry inner-alpine valley with rather limited precipitation (900–1100 mm/a) at an average altitude of about 1900 m asl. The south-facing slope of the Ofenpass valley floor is considered as the core test site and has long been a subject to ecological studies (e.g. Kötz et al., 2004) and described extensively (Schaepman et al., 2005). Two dominant subalpine ecosystems characterized by contrasting anisotropy features (Koetz et al., 2005), being an old-growth coniferous forest and a meadow, were chosen as vegetation types to assess angular sensitivity.

The evergreen coniferous forest is dominated firstly by mountain pine (*Pinus Montana* ssp.*arborea*) and secondly by stone pine (*Pinus cembra*), being of interest for natural succession. The forest ecosystem can be classified as woodland associations of *Erico-Pinetum mugo*. The understory is characterized by low and dense vegetation composed mainly of *Vaccinium, Ericaceae*, and *Seslaraia* species. The second vegetation type, a subalpine meadow, can be characterized as poor grassland over calcareous soils. The mixed grassland ecosystem belongs to the floristic association *Seslerio-Caricetum sempervirentis.*

2.2.2. Satellite data

The CHRIS sensor on PROBA provides co-registered, spectral contiguous bands at 17 m ground sampling distance, in the spectral wavelength range from 415 nm to 1050 nm. PROBA is an experimental ESA space platform that enables the sensor to capture images from five viewing angles. CHRIS Mode 3 (Land) data were acquired over the SNP on 2004-06-27, 10:41 AM, under partly cloudy conditions (1/8th cloud cover) and low aerosol conditions (Aerosol Optical Depth (AOD) < 0.086 at 412 nm, < 0.022 at 862 nm). Data specifications are shown in Table 2.1 and the viewing geometry is shown in Figure 2.1. Solar position can be regarded as constant for all five CHRIS Fly-by Zenith Angles (FZA), since the time difference between first and last recording during the satellite overpass was less than two minutes. In the current along-track pointing configuration, the FZA is equivalent to the nominal view angle, which might deviate from the actual observation angle. Actual view angle for the nadir scene was +21.21° in the forward-looking direction (28° off the solar principal plane). FZA +36° was acquired exactly in the solar principal plane. FZA +55° differed only 14° from the solar principal plane and is further referred as forward-scatter. The

backscatter angles of FZA −36° and FZA −55° differed 53° and 45°, respectively, from the solar principal plane and lie in backscatter direction.

Table 2.1: CHRIS specifications for Land Mode 3

| Sampling	Image area	View angles	Spectral bands	Spectral range
~17 m @ 556 km altitude	13 x 13 km (744 x 748 pixels)	5 nominal angles @ 0°, ±36°, ±55°	18 bands with 6-33nm width	447−1035 nm
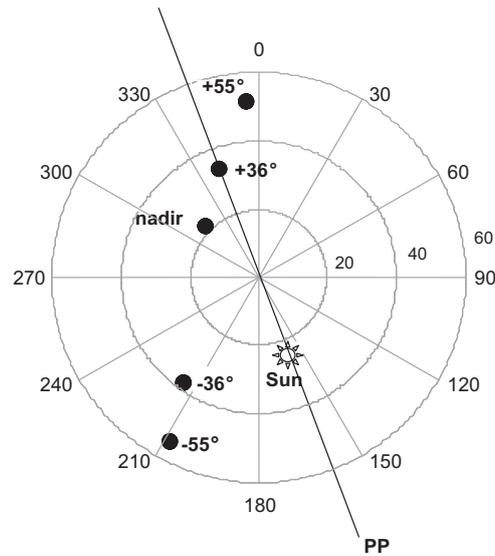
Figure 2.1: Polar plot of CHRIS image acquisition and illumination geometry as of June 27, 2004. PP: Principal Plane.

The CHRIS image set was geometrically and radiometrically corrected following an approach dedicated for rugged terrains (Kneubühler et al., 2005). The geometric correction relies on a parametric approach taking into account the viewing geometry, and geometric distortion due to the sensor, platform and topography. Atmospheric correction of the CHRIS radiance data was performed using the physically based radiative transfer model ATCOR-3 (Richter, 1998), which is based on MODTRAN-4. ATCOR-3 enables the processing of data from tilted sensors by accounting for varying path lengths through the atmosphere, varying transmittance and for terrain effects by incorporating digital terrain model (DTM) data and their derivatives (slope and aspect, sky view factor and solar illumination) (Richter & Schläpfer, 2002). One particularity of this approach is that ATCOR-3 corrects for path scattered radiance and adjacency effects, however not for hemispherical irradiance. The ATCOR-3 generated 'surface reflectance' is therefore representing Hemispherical Directional Reflectance Factor (HDRF), following the reflectance terminology of Schaepman-Strub et al. (2006).

The evaluated accuracy of the acquisition geometry of CHRIS/PROBA in the core of the Ofenpass test site after preprocessing resulted in a geolocation uncertainty for nadir and off-nadir scenes of 0.5–1 pixels (Kneubühler et al., 2005). All preprocessing efforts of CHRIS data finally resulted in geometrically corrected HDRF data with a spatial resolution of 17 m. The core test site was located in the scene centre line of each scene, implying that cross-track effects could be considered as negligible.

A cloud present above this site, particularly when observed from the +55° FZA, was masked out for all scenes, considerably limiting the inclusion of a number of potential forest pixels at lower slopes.

2.3. Methods

Among the most commonly used indices, we selected those that fit the wavelengths, or closely approach, the centre wavelength positions of the spectral resolution of CHRIS Land Mode 3 (Figure 2.2). The VIs were calculated using the remote sensing software package ENVI (ITTVIS, Boulder, CO, USA). Calculated indices were subsequently standardized and studied for their angular effects by means of an Analysis of Variance Repeated Measurements (ANOVA RM) and an independent sample students' *t*-test.
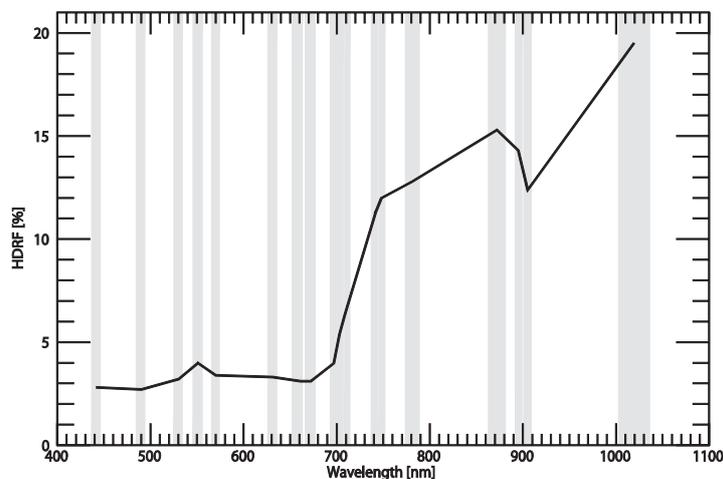

Figure 2.2: A typical canopy reflectance (438–1035 nm) of Swiss pine forest from the CHRIS sensor with its respective bandwidths (Mode 3).

The indices listed in Table 2.2 were selected to be calculated from multi-angular CHRIS HDRF data. We use four general categories of VIs according to their plant physiological functioning: (*a*) broadband greenness VIs (1–3), being measures of the overall amount of photosynthetic material in vegetation; (*b*) narrowband greenness VIs (4–6), being measures of the overall amount and quality of pigment content in vegetation; (*c*) Light Use Efficiency (LUE) VIs (6–9), being measures of the efficiency with which vegetation is able to use

incident light for photosynthesis, and (*d*) leaf pigment VI (10), being a measure of stress-related pigments present in vegetation. In case an index could not be calculated for a certain scene pixel (e.g. because of cloud cover, or non-vegetation cover), such a pixel was not included in the study. After pixel cleaning indices values for 353 meadow pixels for the 5 scenes were collected, whilst for forest 3488 pixels were collected.

Vegetation indices were calculated from HDRF data for each scene. Even though the Atmospherically Resistant Vegetation Index (ARVI) intends to minimize atmospheric effects, we still preferred to apply ARVI on HDRF data. This allowed preserving consistency in the quantitative inter-index evaluation of the angular signatures, and following Santer et al. (2007) in dark dense vegetation (DDV) trends of ARVI are not significantly different from spectral radiance or HDRF data. However, the primary use of ARVI is for top-of-the-atmosphere radiance data (Kaufman & Tanré, 1992), while in this case we use the DDV approximation to justify the use of ARVI derived from HDRF. In all other situations than the one above, ARVI must be derived from TOA radiances.

Despite the dedicated atmospheric correction, the impression arose that the extreme topography still exerted influence on reflectance anisotropy and, in turn, on indices' values. The influence that topographic attributes may have on VIs is discussed in Deng et al. (2007), where many subtle but important variations in topography–vegetation relationships were observed. Since the Alps face an erratic topography which is often paired with changing land cover characteristics, the inclusion of topography might significantly perturb surface reflectance anisotropy. To limit our approach in uncertainty, we decoupled topographic effects from our analysis. Multiple regression analysis assessed stepwise the contribution of topographic attributes, which are slope and solar illumination, to the variability of indices' values. These attributes accounted for up to 13% of the variations of the indices' values for each angular scene. To ensure that topographic effects are sufficiently decoupled in further analysis a topographic subset was thresholded. At the valley floor the topography is relatively flat and smooth consisting of monotonous coniferous forests and patches of uniform subalpine meadow. Restricting the study site to homogenous topographic conditions of the south-facing slope less than 8° and full sunlight conditions (solar illumination > 90%), enabled a reduction of topographic influences on the indices' values to about 3% for meadow and about 2% for forest. Such small correlation coefficients led to the assumption that considered topographical attributes were sufficiently decoupled. Within the remaining forest data pool an equal number of forest pixels and meadow pixels were randomly sampled (#308), ensuring a sound basis for statistical comparison.

Finally, all indices were normalized against their averaged nadir value, so nadir-position values were set at 1. Normalization provided an opportunity to compare statistically the angular shape of the indices within the same magnitude. A coupled RT model (PROSPECT/FLIGHT (Jacquemoud & Baret, 1990; North, 1996) was then applied to assess scale independent and in a physical manner the underlying driving factors governing the angular signatures.

Table 2.2: Overview of selected vegetation indices

	Index	Formula	Description	Reference
a: Broadband Greenness				
1	NDVI: normalized difference vegetation index	$(R_{NIR} - R_{RED}) / (R_{NIR} + R_{RED})$	Measure of green vegetation cover. (CHRIS$_{mid}$: NIR = 781 nm, RED = 672 nm)	Tucker, 1979
2	SRI: simple ratio index	R_{NIR} / R_{RED}	Measure of green vegetation cover. (CHRIS$_{mid}$: NIR = 781 nm, RED = 672 nm)	Tucker, 1979
3	ARVI: atmospherically resistant vegetation index	$(R_{NIR} - (2R_{RED} - R_{BLUE})) / (R_{NIR} + (2R_{RED} - R_{BLUE}))$	Similar as NDVI while being less sensitive to aerosol effects (CHRIS$_{mid}$: NIR = 781 nm, RED= 672 nm, BLUE = 490 nm)	Kaufman & Tanre, 1992
b: Narrowband Greenness				
4	NDVI$_{705}$: red edge normalized difference vegetation index	$(R_{750} - R_{705}) / (R_{750} + R_{705})$	Leaf chlorophyll contents (CHRIS$_{mid}$: R_{703}, R_{748} nm)	Gitelson & Merzlyak, 1994
5	mSRI$_{705}$: modified red edge simple ratio index	$(R_{750} - R_{445}) / (R_{705} + R_{445})$	Narrowband SRI, compensates for high leaf surface (specular) reflectance (CHRIS$_{mid}$: R_{442}, R_{703}, R_{748} nm)	Sims & Gamon, 2002
6	mNDVI$_{705}$: modified red edge normalized difference vegetation index	$(R_{750} - R_{705}) / (R_{750} + R_{705} - R_{445})$	Narrowband NDVI, compensates for high leaf surface (specular) reflectance (CHRIS$_{mid}$: R_{442}, R_{703}, R_{748} nm)	Sims & Gamon, 2002
c: Light Use Efficiency				
7	PRI: photochemical reflectance index	$(R_{531} - R_{570}) / (R_{531} + R_{570})$	Index of photosynthetic radiation use efficiency. Sensitive to carotenoid/ chlorophyll ratio (CHRIS$_{mid}$: R_{530}, R_{570} nm)	Gamon et al., 1992
8	SIPI: structure insensitive pigment index	$(R_{800} - R_{455}) / (R_{800} + R_{705})$	Carotenoid/chlorophyll *a* while decreasing sensitivity to variation in canopy structure (CHRIS$_{mid}$: R_{442}, R_{703}, R_{781} nm)	Penuelas et al., 1995
9	RGRI: red green ratio index	Mean of all bands in the red range divided by the mean of all bands in the green range	Anthocyanins/chlorophyll (CHRIS$_{mid}$: R_{530}, R_{551}, R_{570}, R_{631}, R_{661}, R_{672}, R_{697} nm)	Gamon et al., 1999
d: Leaf Pigments				
10	ARI: anthocyanin reflectance index	$(R_{550})^{-1} - (R_{700})^{-1}$	Leaf anthocyanins content (CHRIS$_{mid}$: R_{551}, R_{703} nm)	Gitelson et al., 2001

R, reflectance. CHRIS$_{mid}$ denotes the centre of the used CHRIS bands in Mode 3 (http://www.chris-proba.org.uk/mission/bandsets2.html). The wavelengths in the Formula column stand for the original proposed VI wavelengths, while the wavelengths in the Description column stand for the CHRIS wavelengths that approached closest to the original proposed wavelengths.

2.3.1. Statistical analyses

Mean and Standard Error of Mean (SEM) were used to represent angular variability per vegetation type and ANOVA RMs were additionally calculated to compare per index off-nadir values to nadir values. ANOVA RMs were typically used to identify differences for two datasets measured over succeeding steps (e.g. time steps).

Accordingly, comparing the indices' off-nadir values to the nadir values, the underlying null hypothesis is that there is no effect of angularity. Resultant F values, which are a measurement of distance between individual distributions, will function as an angular sensitivity indicator. If the null hypothesis is correct then F is expected to be about 1, whereas a 'large' F value indicates a larger between-viewing-angle variance than a within-viewing-angle variance, and can thus be interpreted as being an angular effect. Given the assumption that a forest pronounces a higher anisotropy and is spatially more heterogeneous than a meadow, then it is of interest to verify how this reflects in magnitude of the F value. Absolute t values of the independent sample t-test provide a likewise measure of the (dis-) similarity of the angular shapes of both structural types.

2.3.2. FLIGHT simulations

The Forest LIGHT Interaction Model (FLIGHT) developed by North (1996) is a Monte Carlo numerical ray-tracer simulating photon propagation through a 3D heterogeneous leaf canopy. The model allows the representation of complex vegetation structures and a correct treatment of multiple scattering within the scene composed of various scatter elements. For 3D simulations, tree crowns are represented by geometric primitives with defined shapes and positions of individual trees with associated shadow effects. Within each crown envelope foliage is approximated by volume-averaged parameters with optical properties of both leaf and woody scattering elements. Canopy reflectance of a range of forest stands parameterized by field-measured canopy variables and CHRIS acquisition geometries have been simulated. The FLIGHT parameterization was based on averaged field measurements of four core test sites within the forest. Crowns were represented by cones; the canopy structure and optical specifications are further described in Kötz et al. (2004). The foliage optical properties were modeled by PROSPECT (Jacquemoud & Baret, 1990) coupled with FLIGHT while the spectral properties of the woody parts and understory were characterized by spectrometric field measurements (Kötz et al., 2004). Finally, the BRF output of FLIGHT is compared with the approximated HDRF of the CHRIS data. Since the HDRF approximation produced by ATCOR includes a hemispherical and adjacency component, the approximation – at least in its trend – is valid.

2.4. Results

The assessment of the angular sensitivity of the two considered structural canopy types required similar topographical conditions and normalization of the angular shapes to a reference level. Intra- and inter-angular statistical comparisons enabled subsequently good validation of the directional performance of the considered indices.

2.4.1. Assessment of angular sensitivity

The key feature in the statistical comparison exercise is the assessment of the angular response of the indices; however the true biophysical impact of this is not assessed in this study. The angular dynamics of the vegetation indices in response to meadow and forest are shown in Figure 2.3 and Figure 2.4 respectively. These figures show the nadir-normalized averaged values for the sampled pixels including ±1 Standard Error of Mean (SEM). As a reference the nadir value is plotted, which is 1, or −1 in case of PRI. Note that directional effects are most extreme in the solar principal plane (Myneni et al., 1997) implying that it should be taken into account that the maximum angular variability is most likely not reached in this study.
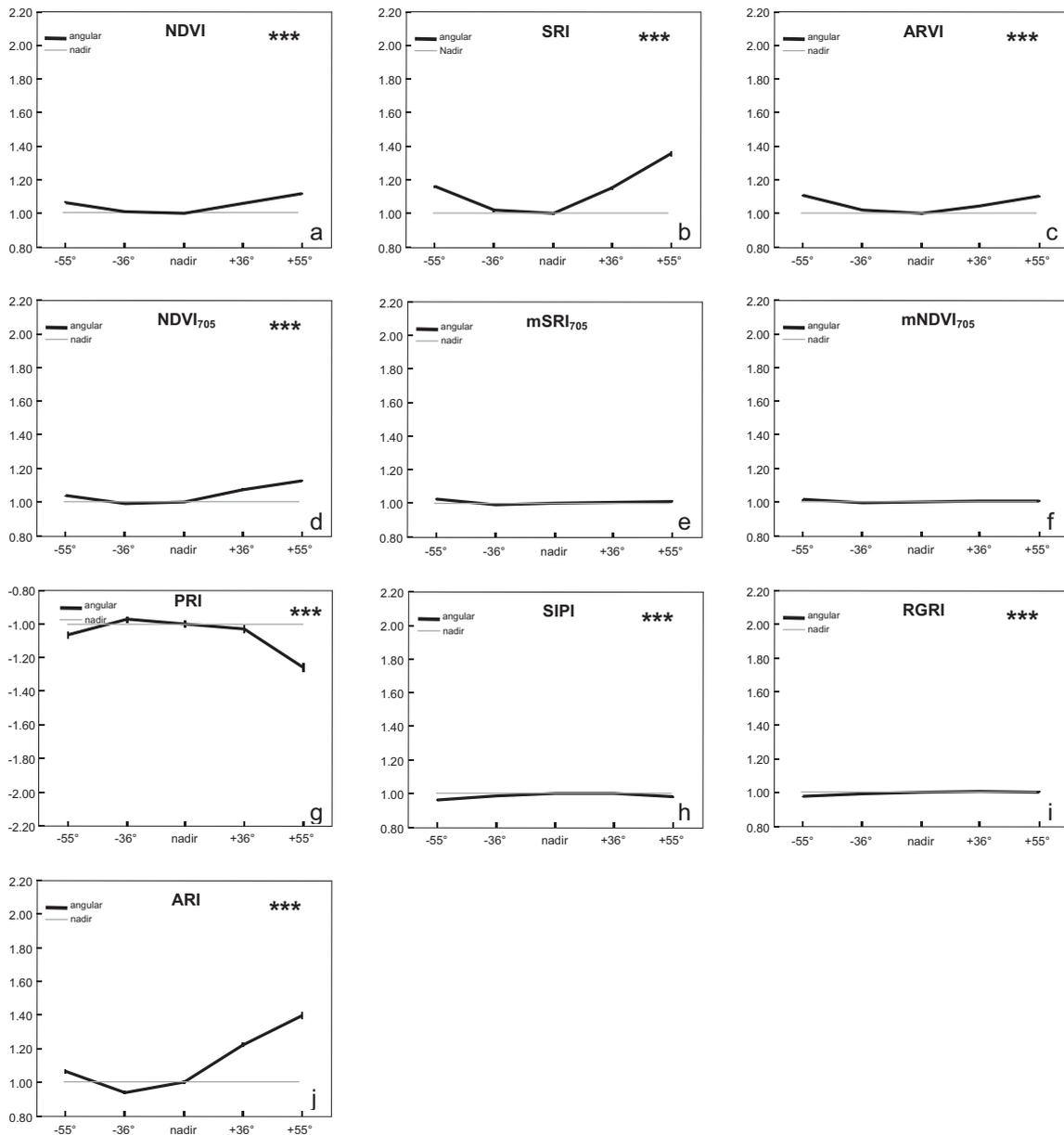
Figure 2.3: Averaged angular VIs values (normalized against its averaged nadir value) from meadow reflectance values. *x*-axis denotes viewing angles (negative angles are in back-scattering direction, positive angles are in forward-scattering direction). *y*-axis denotes normalized VIs. The error bars shown are ±1 SEM. Angular values were compared with nadir values by means of ANOVA RMs: significance levels: *$p < 0.05$, **$p < 0.01$, ***$p < 0.001$.
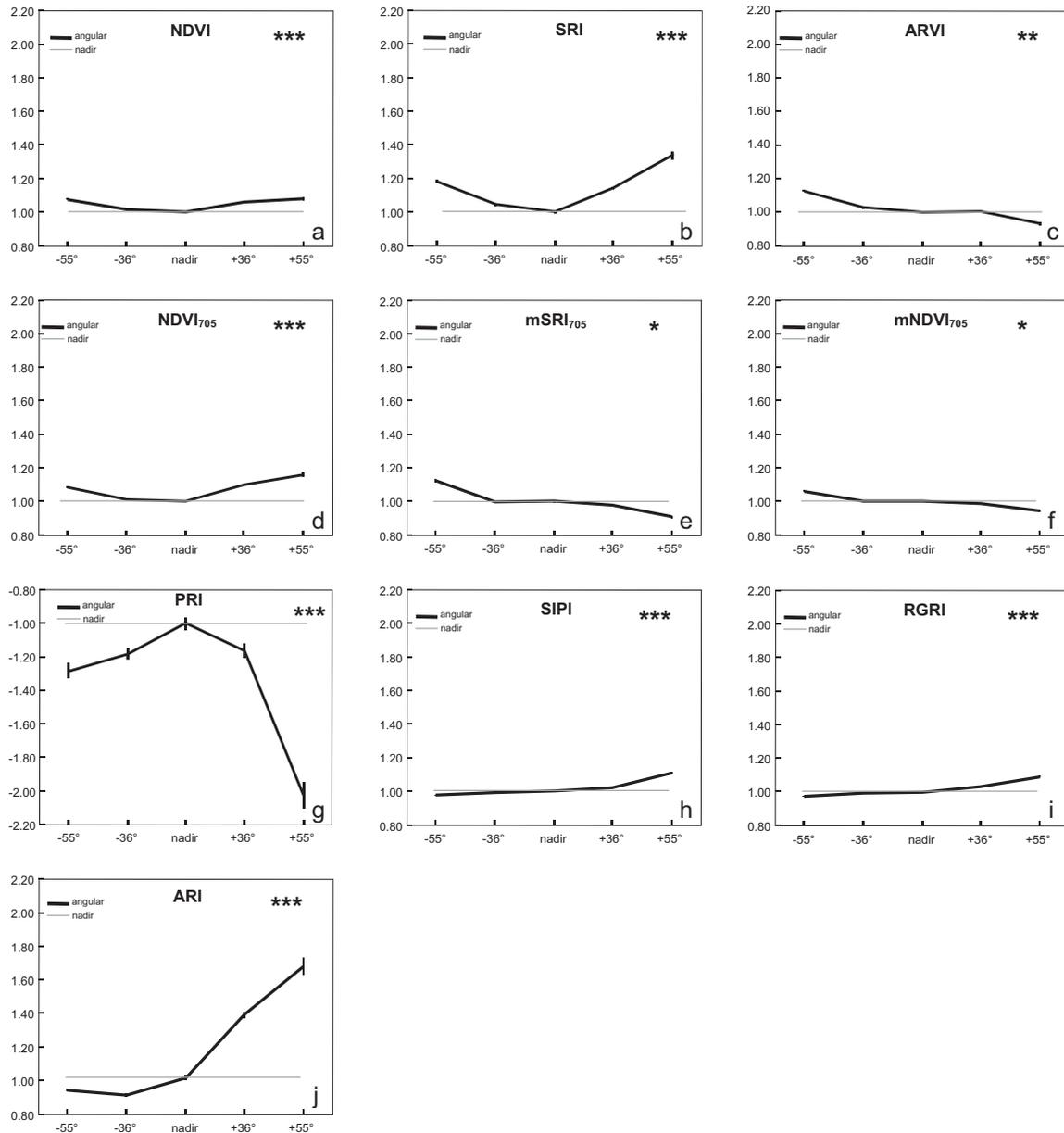
Figure 2.4: Averaged angular VIs values (normalized against its averaged nadir value) from forest reflectance values. *x*-axis denotes viewing angles (negative angles are in back-scattering direction, positive angles are in forward-scattering direction). *y*-axis denotes normalized VIs. The error bars shown are ±1 SEM. Angular values were compared with nadir values by means of ANOVA RMs: significance levels: *$p < 0.05$, **$p < 0.01$, ***$p < 0.001$.

Because of normalization and rescaling the values of some indices, typically operating at smaller ranges (e.g. nadir-average PRI around −0.02, nadir-average ARI around 0.007), are dramatically expanded. For others operating at around 1 or higher (SRI, ARVI, mSRI$_{705}$, SIPI, RGRI) normalization implied diminishing of actual values. For the sake of consistent interpretation, the graphs should be interpreted in combination with their statistical analysis.

ANOVA RMs' results are shown graphically in Figure 2.3 and Figure 2.4; *F* values of calculated ANOVAs are presented in Table 2.3. Apart from $mSRI_{705}$ and $mNDVI_{705}$, the indices exhibited significant differences for the two vegetation types.

Table 2.3: Percentages of change compared to nadir values for extreme viewing angles and ANOVA RM *F* values (off-nadir values compared to nadir values) for meadow and forest.

Index	−55° vs. nadir Meadow (%)	+55° vs. nadir Meadow (%)	−55° vs. nadir Forest (%)	+55° vs. nadir Forest (%)	ANOVA *F*-values meadow ($F_{1,614}$=)	ANOVA *F*-values Forest ($F_{1,614}$=)
NDVI	7	12	8	8	137.4***	116.3***
SRI	16	36	18	34	167.3***	200.2***
ARVI	11	10	13	−7	99.9***	10.4**
$NDVI_{705}$	4	13	9	16	122.8***	184.1***
$mSRI_{705}$	3	1	12	−9	4.5*	0.097 ($p = 0.761$)
$mNDVI_{705}$	2	1	6	−6	5.2*	0.05 ($p = 0.814$)
PRI	−6	−26	−32	−108	12.3***	74.359***
SIPI	−3	−1	−2	11	10.6***	129.126***
RGRI	−2	0	−3	9	29.6***	59.4***
ARI	6	40	−5	68	106.3***	120.1***

*$p < 0.05$, ** $p < 0.01$, ***$p < 0.001$.

2.4.2. Statistical results

ANOVA RM *F* values (4 off-nadir subsets, each compared to the nadir subset; subset = 308 pixels), shown in Table 2.3, were used to evaluate the magnitude of the angular variability compared to nadir values. Based on this small-scale statistical exercise with 2 vegetation types, the traditional broadband indices NDVI and SRI, $NDVI_{705}$ and ARI yielded the highest values for both structural types, especially forest, (in general: $F > 106$; $p < 0.001$) and can therefore be considered as most sensitive to changing viewing angles. Regardless of the apparently greatest angular response shown by the PRI graphs (Figure 2.3 and Figure 2.4), the *F* values for forest expressed relatively small numbers (*F* forest 74.4, *F* meadow 12.3, see Table 2.3). In contrast, no significant differences compared to nadir values were found when using mSR_{705} ($p = 0.761$) and $mNDVI_{705}$ ($p = 0.814$) over forest.

A greater degree of anisotropy (forest) did not always automatically translate into higher *F* values. In the case of NDVI, mSR_{705}, $mNDVI_{705}$ and prominently in the case of ARVI a higher *F* value for meadow than for forest was found. Here, near-nadir position showed a flat response; only when observed under larger viewing angles was the true anisotropy perceived.

Based on the ANOVA's of the two contrasting vegetation structures, VIs that show, in either case, significant ($p < 0.05$) angular variability (Table 2.3) will be referred to as 'anisotropic', whereas those VIs not revealing a prominent angular behavior are further referred as 'Lambertian', as is the case for mSR_{705} and $mNDVI_{705}$. The VIs were further ranked in Table 2.4 according to the summed *F* values of meadow and forest, ranging from displaying

primarily anisotropic sensitivity to exhibiting Lambertian behavior. Regarding the two ecosystems, the SRI, the simplest index, was most sensitive to changing viewing angles, followed by the NDVI$_{705}$ and NDVI. Because of the resulting low F value above meadow, PRI exhibited the smallest anisotropic behaviour, yet it was still largely significant.

Table 2.4: Ranked overview table based on statistical analysis ANOVA RM from most anisotropic to Lambertian (= no significant differences). Meadow and forest values were compared with an independent sample student's t-test ($n = 1540$).

Index	Summed meadow-forest ANOVA F-values	Angular Sensitivity	Meadow-forest comparison student' t and p-values
SRI	337.5	anisotropic	$t = 0.444$ ($p = 0.657$)
NDVI$_{705}$	306.9	anisotropic	$t = 6.519$***
NDVI	253.7	anisotropic	$t = -1.154$ ($p = 0.249$)
ARI	226.4	anisotropic	$t = 4.105$***
SIPI	139.7	anisotropic	$t = 17.280$***
ARVI	110.3	anisotropic	$t = -9.232$***
RGRI	89.0	anisotropic	$t = 16.120$***
PRI	86.7	anisotropic	$t = -10.488$***
mNDVI$_{705}$	5.2	Lambertian	$t = -3.344$**
mSRI$_{705}$	4.6	Lambertian	$t = -1.919$ ($p = 0.055$)

*$p < 0.05$, **$p < 0.01$, ***$p < 0.001$.

An independent sample student's t-test compared the influence of the two vegetation types on the indices' angular behavior. Apart from NDVI, SRI and mSRI$_{705}$, the angular response was for all remaining indices vegetation-type dependent (Table 2.4). The mNDVI$_{705}$ did express significant different angular shapes depending on the structural types; however, as shown earlier, mNDVI$_{705}$ did not express significant angular variability compared to nadir values. The student's t-test indicated that for the remaining narrowband indices and ARVI angular responses were not solely affected by viewing angles, but also by vegetation type. SIPI, RGRI and PRI yielded the highest student's t values, indicating that – from the set of tested indices – they were most affected by the contrasting vegetation types.

2.5. Discussion of VIs angular responses

The angular behavior of the single vegetation indices and influential factors are discussed in the next section in more detail. The greenness indices (SRI, NDVI, NDVI$_{705}$, mSRI$_{705}$, mNDVI$_{705}$ and ARVI) and the light use efficiency and leaf pigment indices (SIPI, RGRI, PRI and ARI) are discussed individually.

2.5.1. Greenness indices

Traditional broadband indices based on red and NIR are known to inherently exhibit anisotropic behavior, eventually additionally linked to vegetation type or soil conditions (Qi et al., 1995; Leblanc et al., 1997). Indeed, SRI (NIR/red) gave rise to the most pronounced angular variability with the highest values apparent in the extreme forward-scatter direction and the lowest values at nadir position (Figure 2.3b and Figure 2.4b). Measured NDVI shapes (Figure 2.3a and Figure 2.4a) were consistent with earlier studies (Galvão et al., 2004; Huete et al., 1992; Leblanc et al., 1997) and radiative transfer modeling (Sellers, 1985). The angular shape remained unchanged in the case of the narrowband red edge NDVI ($NDVI_{705}$) (Figure 2.3d and Figure 2.4d). In contrast, $mSRI_{705}$ and $mNDVI_{705}$, which were designed to eliminate the effect of leaf surface reflectance (Sims & Gamon, 2002), responded in Lambertian fashion to changing viewing angles (Figure 2.3e,f and Figure 2.4e,f). This Lambertian phenomenon can be explained by including the 445 nm reference band, the only modification compared to the $NDVI_{705}$. The angular distribution of this blue band was rather flat, with a slight decreasing trend in the extreme forward-scatter direction. A similar flattening in the blue was observed by Jin et al. (2002) and Abdou et al. (2006) when using Multi-angle Imaging SpectroRadiometer (MISR) surface BRF products. It was recognized that this phenomenon originates in part from the low values in the blue and uncertainties due to atmospheric correction.

ARVI, designed to minimize atmospheric effects in the sensor output by replacing the aerosol sensitive red wavelength used in the NDVI with a combination of the red and blue wavelength (Kaufman & Tanré, 1992), proved to be symmetrical around nadir for the meadow site (at both sides +10%) (Figure 2.3c and Figure 2.4c). Such a symmetrical trend was also observed in an earlier study over grass cover (Huete et al., 1992), and therefore a simple cosine adjustment was suggested to correct for viewing effects. ARVI angular response above forest, however, did not reveal a symmetrical trend. The inclusion of the blue band in the algorithm to correct for atmospheric effects flattened values around the nadir position though performed less successfully at large viewing angles.

2.5.2. Light use efficiency/leaf pigment indices

2.5.2.1. Photochemical Reflectance Index (PRI)

The measured PRI exhibited a very significant angular anisotropy for both meadow and forest canopies, but it was specifically perceived above forest canopy (Figure 2.4g). Average absolute forest PRI values, –0.014 (nadir) and –0.0234 (+55°) (values not shown), were coherent with canopy observation over evergreen shrub species (Stylinski et al., 2002) and with spruce stands (Lewis et al., 2005). The extent to which canopy structure, view and illumination angles are likely to influence the measured PRI values was further investigated based on the FLIGHT model similar to a modeling study by Barton and North (2001).

FLIGHT simulations were carried out considering field measurements taken in the core test site of the Swiss National Park (SNP). Over this site LAI values varied between 1.5 and 4.5, when derived from nadir observations (Kötz et al., 2004). In addition, the woody fraction (ca. 30%) is relatively high because of the advanced age of the pine forest and as forest management practice stopped 70 years ago. Consequently, given the relatively woody stands characterized by gaps between branches and trees, it may be reasonable to expect that observed proportions of photosynthetic vegetation (PV) and non-photosynthetic vegetation (NPV) depend on viewing angle. For instance, it is likely that at greater viewing angles lower proportion of PV and a greater proportion of NPV contribute to the observed canopy reflectance. This hypothesis was tested by FLIGHT simulations for which we increased the within-crown NPV proportions as a function of viewing angle (Figure 2.5). The resulting angular signature of the PRI based on the simulated BRF produced a concave shape similar as observed by CHRIS (Figure 2.4g). However, the PRI showed a convex shape when FLIGHT was parameterized with constant PV/NPV proportions for all view angles. Similar observations were published in the study of Barton and North (2001).
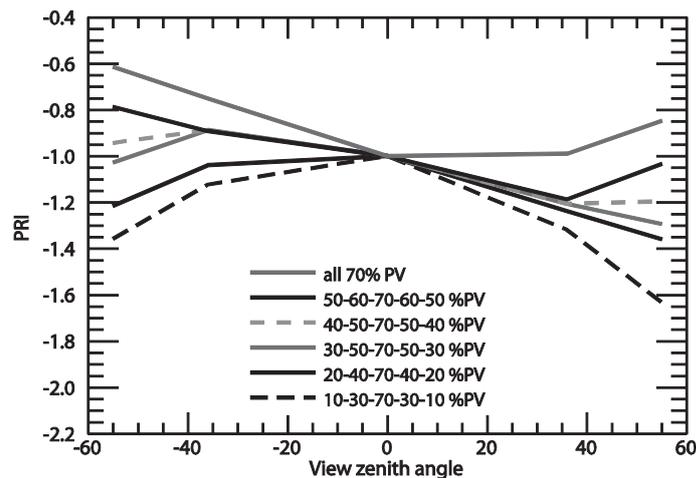
Figure 2.5: FLIGHT-simulated angular PRI values (normalized against their nadir value) for a coniferous forest. Viewing geometry is according to CHRIS FZAs (0°, ± 36°, ± 55°). Within-crown PV and NPV proportions varied with viewing angle (%NPV = 100 − %PV).

Shadow is another key factor in affecting the anisotropy of forest canopies (Gerard & North, 1997) and therefore the angular response of VIs. The shadowed canopy (forward-scattering values) demonstrated an unequivocally larger PRI drop (−108%) than the sunlit canopy (back-scattering values: −32%), which implies that shadow effects are prevalent in the PRI response. However, since a drop is apparent at both sides around nadir, one can conclude that shadow is not the prime driving factor.

The presented RT model simulations demonstrate that an index exclusively sensitive to leaf photosynthesis activity will be substantially distorted, both spatially and directionally, by the

contribution of NPV present in a canopy pixel (e.g. branches, trunks). Indeed, in the spatial domain, variations in NPV and background reflectance affect the performance of greenness VIs (e.g. NDVI, SRI) (Asrar et al., 1992; Baret & Guyot, 1991; Goward & Huemmrich, 1992). In the directional domain, it is the viewing angle that determines the proportion of photosynthetic, non-photosynthetic and background compounds that are exposed to solar radiation in that direction. Then, similar to spatial variations, varying NPV fractions along changing angles may equally impose effects on the angular VI signal. For canopies with LAI < 5.0, NPV has been shown to impose a significant effect on the canopy reflectance in woody plant canopies (Asner, 1998). This is especially the case in conifer canopies where the primary reflectance compounds (foliage, branches) are systematically organized at the shoot, branch, whirls, and crown level (Malenovský et al., 2008).

2.5.2.2. Structural Invariant Pigment Index (SIPI) and Red Green Ratio Index (RGRI)

Despite its apparent resemblance and flat shape, off-nadir values of SIPI (Figure 2.3h and Figure 2.4h) and RGRI (Figure 2.3i and Figure 2.4i) differed from nadir values (ANOVA RM, $p < 0.001$) and the total angular shape differed for both structural types (student's *t*-test, $p < 0.001$). The differences between both indices revealed only when considering the *F* values in Table 2.3. Whereas forest RGRI *F* was twice as large as *F* in meadow conditions, in case of SIPI, however, the forest *F* was more than ten times larger than the meadow *F*. The reason this behavior occurs can be partly explained because SIPI is designed to reduce the impact of leaf surface and mesophyll structure while estimating carotenoids to chlorophyll *a*. In a coniferous forest, carotenoids were not expected to play an important role but the greater variability of NPV and PV might account for a larger angular variability. The higher SIPI angular sensitivity over forest relative to RGRI can be partly understood because of the averaging of all red (600 nm to 699 nm) and all green (500 nm to 599 nm) channels in the RGRI. Indeed, for a range of varying view angle-specific PV−NPV settings, FLIGHT recorded an averaged relative flattening of −160% (SD: 81) in the far back-scattering direction and −74% (SD: 25) in the far forward-scattering direction when broadening the spectral range from a centre red band (CHRIS red_{mid}: 661 nm) and a centre green band (CHRIS $green_{mid}$: 551 nm) towards all red and green bands.

2.5.2.3. Anthocyanin Reflectance Index (ARI)

An Anthocyanin Reflectance Index in the form of $ARI = (R_{550})^{-1} - (R_{700})^{-1}$ estimates anthocyanin accumulation in intact senescing and stressed leaves (Gitelson et al., 2001). Whereas reflectance at 700 nm depends solely upon chlorophyll content, reflectance at 550 nm depends on both chlorophyll and anthocyanin content. Pronounced angular responses over meadow and coniferous stands emphasize the large variability that can occur. In backscatter direction values tended to fluctuate around or below nadir, in forward-scatter direction a prominent increase was apparent (Figure 2.3j and Figure 2.4j). Shadow effects and the influence of a likely greater fraction of observed non-photosynthetic material at larger off-nadir sensor view angles are again most likely contributing to the angular response. Due to the inversion of the two wavelengths, a larger decrease of reflectance at 550 nm rather than 700 nm implied a larger contrast and subsequently a rising ARI.

In general, one must be cautious when applying indices at the canopy level, which were originally based and adapted to leaf level observations. At leaf level a decrease in the green reflectance was related to an increase in anthocyanin content, whereas the reflectance in the blue, red and NIR ranges remained basically the same (Gitelson et al., 2001). At canopy level a decrease in green reflectance might have multiple causes; one of which is an increase in anthocyanin content. Woody compounds, litter, shadow, and soil conditions are other driving factors leading to a decrease in the green in a pixel. In turn the feedback on reflectance of these dynamics varies under changing viewing angles.

2.6. Summary and conclusions

Viewing geometry is a major determinant controlling the spectral behavior of vegetation canopies and thus affecting the quality of extracted biochemical parameters. The angular responses of four classes of vegetation indices were compared. Evidence from a sparse angular sampling of four off-nadir CHRIS recordings indicates the following:

Nearly all indices manifested a prominent reflectance anisotropy in the two alpine ecosystems. Indices where off-nadir values significantly differed from nadir values were labeled as being 'Anisotropic'. The traditional SRI, NDVI, NDVI$_{705}$, and ARI gave sign of greatest angular sensitivity. The greenness indices which use reflectance at 445 nm as a reference wavelength (mSRI$_{705}$, mNDVI$_{705}$) responded rather insensitive and have been labeled as being 'Lambertian'. Further, an independent sample *t*-test showed that, apart from NDVI, SRI and mSR$_{705}$, most indices did express varying angular shapes depending on the vegetation type. For those indices the specific surface reflectance anisotropy additionally affects the angular responses.

Reflectance anisotropy of broadband indices observed (NDVI, SRI, and ARVI) concurs with earlier observations (Galvão et al., 2004; Huete et al., 1992; Leblanc et al., 1997). Also Light Use Efficiency indices PRI, SIPI, RGRI and ARI gave rise to significant reflectance

anisotropy with an emphasis over forest and in forward-scatter direction. FLIGHT simulations showed that structural variability, in terms of the organization of PV and NPV elements, is a key player in shaping the angular signature of PRI. We therefore suggest that when applying a VI designed to assess leaf processes at canopy level, the accuracy of the biochemical parameter mapping can be greatly improved if the fractions of NPV and background (Canisius & Chen, 2007) are being taken into account.

Traditional broadband indices continue to be applied at large-scale analyses of ecosystem monitoring, for example the boreal forests (e.g. Beck et al., 2006; Goetz et al., 2006). Presently a growing fleet of narrow spectral resolution sensors are operational (e.g. MERIS, MODIS, Hyperion, ALI, etc) with capacities to upscale light use efficiency and leaf pigments indices at canopy level over large areas. Furthermore, indices products are increasingly subject to joint multi-temporal (e.g. Telesca & Lasaponara, 2006; Xiao et al., 2006) and cross-sensor studies (e.g. Chen et al., 2005; Ferreira et al., 2003).

This work highlights the importance of viewing geometry, and, by relying on the Helmholtz Reciprocity Principle (Magda et al., 2001), also solar geometry inevitably propagating in multi-temporal and multi-sensor studies. Because reflectance properties of the land surface are anisotropic in nature, sun–target–sensor geometry may create artificial noise imposed upon basically all VIs. Furthermore, space-borne and airborne sensors with large FOVs (e.g. Hymap: 61.3°, MERIS: 68.5°) are equally subject to within-scene viewing effects. In turn utmost caution is mandatory when inter-comparing results from an *anisotropy-sensitive* index acquired under varying sun–target–sensor configurations for a given land cover type. In the present era of multi-temporal and cross-sensor applications, standardization of vegetation indices is therefore desired to establish confidence in the reliability of its use. Standardization to correct for sensor-specific characteristics is nowadays achieved by applying cross-sensor translation equations (e.g. Miura et al., 2006; Teillet et al., 1997; Trishchenko et al., 2002; Steven et al., 2003), but a prerequisite to reduce cross-sensor uncertainty is that atmospheric corrections and processing strategies are adequately addressed (van Leeuwen et al., 2006). Standardization to correct for reflectance anisotropy is nowadays achieved by BRDF models from which VIs normalized to a standard geometry could be computed (e.g. Bacour et al., 2006; Csiszar et al., 2001; Huete et al., 2002; Los et al., 2005). Nevertheless, until now, these advanced approaches have remained restricted to the traditional broadband indices (e.g. NDVI). Now that a wealth of fine-tuned narrowband indices has been developed, evaluation of their compatibility and consistency may be a first step to allow for large-scale and multi-temporal studies.

On the other hand, research on the potential information content inherent to the directional dimension of many VIs regarding surface anisotropy has been largely left aside (however, see Barnsley et al., 1997; Pocewicz et al., 2007). Evidence from the employed work demonstrated that the angular shape of most of the studied indices, particularly narrowband indices, differs depending on the vegetation structural type. It is therefore suggested that exploiting the angular dimension, parallel to the indices' actual measures, opens opportunities

to provide a quick, additional, source of information regarding structural matters. Future work should further investigate how the angular variability of specific indices (e.g. PRI, SIPI) independently relates to structural features (e.g. LAI, fraction cover).

Finally, with the advent of having multi-angular imaging spectrometers in space, the decoupling of atmospheric and surface-induced reflectance anisotropy will gain in importance. On the one hand to achieve consistent retrievals of biochemical and structural variables at unprecedented accuracies over large swaths, time frames and regions; on the other hand to decrease retrieval uncertainties related to anisotropy effects. In any case, both approaches will be required simultaneously to allow for a consistent process monitoring of land and water surface properties (Schaepman, 2007). Vegetation indices as discussed in this contribution will then be a major contributor to the measurement of ecosystem changes and disturbance in an operational fashion.

Chapter 3

Effects of woody elements on simulated canopy reflectance: Implications for forest chlorophyll content retrieval

Jochem Verrelst, Michael E. Schaepman, Zbyněk Malenovský, Jan G.P.W. Clevers

Effects of woody elements on simulated canopy reflectance: Implications for forest chlorophyll content retrieval

Abstract

An important bio-indicator of actual plant health status, the foliar content of chlorophyll *a* and *b* (*Cab*), can be estimated using imaging spectroscopy. For forest canopies, however, the relationship between the spectral response and leaf chemistry is confounded by factors such as background (e.g. understory), canopy structure, and the presence of non-photosynthetic vegetation (NPV, e.g. woody elements) – particularly the appreciable amounts of standing and fallen dead wood found in older forests. We present a sensitivity analysis for the estimation of chlorophyll content in woody coniferous canopies using radiative transfer modeling, and use the modeled top-of-canopy reflectance data to analyze the contribution of woody elements, leaf area index (LAI), and crown cover (CC) to the retrieval of foliar *Cab* content. The radiative transfer model used comprises two linked submodels: one at leaf-level (PROSPECT) and one at canopy-level (FLIGHT). This generated bidirectional reflectance data according to the band settings of the Compact High Resolution Imaging Spectrometer (CHRIS) from which chlorophyll indices were calculated. Most of the chlorophyll indices outperformed single wavelengths in predicting *Cab* content at canopy level, with best results obtained by the Maccioni index ($[R_{780} - R_{710}] / [R_{780} - R_{680}]$). We demonstrate the performance of this index with respect to structural information on three distinct coniferous forest types (young, early mature and old-growth stands). The modeling results suggest that the spectral variation due to variation in canopy chlorophyll content is best captured for stands with medium dense canopies. However, the strength of the up-scaled *Cab* signal weakens with increasing crown NPV scattering elements, especially when crown cover exceeds 30%. LAI exerts the least perturbations. We conclude that the spectral influence of woody elements is an important variable that should be considered in radiative transfer approaches when retrieving foliar pigment estimates in heterogeneous stands, particularly if the stands are partly defoliated or long-lived.

Keywords: chlorophyll content, non-photosynthetic vegetation, old-growth forest, radiative transfer, PROSPECT, FLIGHT, chlorophyll indices

3.1. Introduction

The foliar content of the main photosynthetic pigments chlorophyll *a* and *b* (*Cab*) is widely regarded as a bio-indicator of the plant's actual health status, such as its stress condition (Lichtenthaler et al., 1996; Zarco-Tejeda et al., 2002; Gitelson et al., 2003; Sampson et al., 2003), and of vegetation gross primary productivity (Gitelson et al., 2006). Various leaf and canopy experiments have indicated that imaging spectroscopy is a powerful method for assessing variation in the chlorophyll content of leaves (e.g. Zarco-Tejada et al., 2000; Ustin et al., 2004; Kokaly et al., 2009). However, when the observational scale moves from leaf to canopy level, the relationship between reflected solar radiation and leaf chemistry tends to weaken (e.g. Trotter et al., 2002; Nichol et al., 2002; Ustin et al., 2009). The scattering and absorption properties caused by the foliar chemistry are then confounded by background reflectance and other dominating scatterers such as the foliage configuration and distribution of woody elements (e.g. Asner, 1998; Blackburn & Steele, 1999). Pigment indices that have originally been designed at leaf level (Ustin et al., 2009) are particularly likely to suffer from these additional heterogeneity factors (Barton and North, 2001; Suárez et al., 2008; Verrelst et al., 2008b).

At canopy level, a common approach for dealing with subpixel heterogeneity is to decompose a pixel into fractions of green photosynthetic vegetation (PV), non-photosynthetic vegetation and litter (NPV), and bare soil (Roberts et al., 1993). PV is characterized by strong absorbance peaks in the blue and red regions of the spectrum, predominantly due to the presence of *Cab*, while NPV is characterized by a gradual reflectance increase in the visible region of the spectrum. Although decomposition techniques (e.g. spectral unmixing) facilitate the study of ecosystem dynamics (e.g. Asner et al., 2003; Harris et al., 2003), they do not fully elucidate the complexity of the interaction of scattering elements with solar radiant energy.

An alternative approach is to estimate the foliar chemistry from optical remote sensing data by using inverted radiative transfer (RT) models. Canopy RT models describe the transfer and interaction of solar radiation inside the canopy on the basis of physical laws and thus provide a cause–effect relationship between scattering elements, their biochemical constituents, structure, and top-of-canopy (TOC) reflectance. Various studies have investigated the interaction of solar radiation with canopy biochemical variables through the use of coupled radiative transfer models (Demarez & Gastellu-Etchegorry, 2000; Zarco-Tejada et al., 2001; Zhang et al., 2008; Jacquemoud et al., 2009). These and other studies recognized that improved parameter retrieval from remote sensing data requires appropriate strategies for modeling the surface bidirectional reflectance distribution function (BRDF) that take account of canopy structure (crown shape, forest stand density, canopy heterogeneity), and background (e.g. Dawson et al., 1999; Sandmeier & Deering, 1999; Rautiainen et al., 2004; Schaepman, 2007). Though much work has been done on radiative transfer modeling, the relative importance of woody elements (NPV) in deriving canopy chlorophyll content has not been adequately evaluated. Only recently has the influence of the 3D structure of trunks and

branches on the reflectance in a young coniferous canopy been explicitly modeled and tested (Malenovský et al., 2008). But that study was done on a young production forest (< 30 years old), and in such forests the woody elements are only part of the living standing trees and are concentrated in the lower part of the canopy. In contrast, old-growth forests contain many woody components in the form of lying and standing deadwood (coarse woody debris: CWD) which is distributed within the canopy layer and on the forest floor, and can account for 18–40% of the total woody biomass (Siitonen, 2001). Not surprisingly, therefore, in these older forests, woody elements play a significant role in determining canopy reflectance (Asner, 1998), as they represent an important photon absorbing and scattering component. At the subpixel scale, forest aging processes will lead to more NPV scattering at the expense of PV scattering. As well as changing its canopy composition, an aging forest also becomes structurally more heterogeneous vertically and horizontally (Franklin et al., 2002), so therefore structural attributes will be important drivers of the canopy spectral response (Nilson & Peterson, 1994; Song & Woodcock, 2002).

Quantitative, physical-based RT modeling of 3D canopy architecture reveals the cause–effect relationship between the biochemical composition of the canopy and satellite observations. Old-growth forests present a challenge for the RT modeler, because those ecosystems have the most heterogeneous mix of green foliage and woody elements. A recent comprehensive overview of RT approaches used to model various stand ages over time (Schaepman et al., 2009) indicates that only a few RT-based studies have investigated old-growth forests, e.g. by studying the spectral trajectory of forest succession (Song & Woodcock, 2002; Song et al., 2007). Song and colleagues input canopy structural variables and leaf optical properties into a geometric-optical RT model and simulated the canopy spectral changes related to forest succession. Nevertheless, the model had difficulty accommodating the structural changes related to the materials comprising the canopy, such as the accumulation of woody elements during succession. Given that foliage elements and woody elements vary vertically and horizontally over time, we decided to investigate the influence of these structural changes on canopy reflectance in detail.

Monte Carlo (MC) ray-tracing models are very flexible and are capable of obtaining accurate canopy representations, yet they have the drawback of requiring a long processing time for simulation (Myneni et al., 1989; Widlowski et al., 2007). An appealing advantage of such models is that the interaction between radiation and the vegetation canopy is tracked almost on a photon-by-photon basis, making this kind of RT very realistic (c.f., Disney et al., 2000). For this reason, we opted to use the MC ray-tracing model FLIGHT (Forest LIGHT interaction model) (North, 1996) to simulate the influence of the structural dynamics occurring during forest development on TOC reflectance.

This paper reports on the influence of canopy compositional and structural effects when inferring chlorophyll content from modeled reflectance data. We created a reflectance data set for varying forest properties by coupling FLIGHT with a leaf-level RT model (PROSPECT) (Jacquemoud & Baret, 1990). Our hypothesis was that knowledge of the trends in simulated

spectral reflectance and derived vegetation indices for estimating chlorophyll content over a wide range of simulated stands with near-realistic canopy structural configurations will improve our understanding of leaf-to-canopy scaling. The objectives of the study were therefore twofold: 1) to evaluate the general performance of single wavelengths and chlorophyll-sensitive indices in predicting foliar chlorophyll content given woody and heterogeneous forest canopies, and 2) to evaluate in more detail the stand-specific influence of NPV and structural variables on the estimation of chlorophyll content by using the best performing index.

3.2. Methodology

3.2.1. Canopy radiative transfer model

As noted above, to study the perturbing effects of woody elements (NPV) on the estimation of *Cab* content we coupled a leaf RT model (PROSPECT) with a 3D canopy model (FLIGHT), hereafter called PROFLIGHT. PROSPECT idealizes the leaf as a stack of elementary plates composed of absorbing and diffusing constituents. The version of the model we used (Jacquemoud et al., 2000) is parameterized by chlorophyll content, dry matter content, leaf water content, and effective number of leaf layers. PROSPECT has been widely used in broadleaves for numerical inversion to estimate chlorophyll content. However, it has also been re-calibrated and used to simulate the optical properties of coniferous needles (e.g. Zarco-Tejada et al., 2004; Malenovský et al., 2006).

FLIGHT computes the TOC bidirectional reflectance factor (BRF) (Schaepman-Strub et al., 2006) by explicitly representing complex canopy structures, including crown overlapping and multiple scattering of solar radiant fluxes within the scene (North, 1996; Gerard & North, 1997). It traces the individual photons from their solar radiation source, through all relevant collisions, until the ray either is absorbed or exits the canopy. As photons enter a crown, they are scattered in accordance with probability density functions. Tree crowns are idealized by volumetric primitives of defined shapes with associated shadowing effects. Crown positions are estimated from a statistical distribution. In the individual crown envelopes, the foliage is approximated by statistical foliage properties using the optical properties of both leaf (PV) and woody elements (NPV). The NPV scattering elements are treated as opaque foliage elements, thus they scatter or absorb incident radiation only. PV scattering elements additionally transmit incident radiation. The lower bound of the canopy is a soil medium with an anisotropic scattering behavior (Hapke, 1981). The horizontal exchange of rays with neighboring areas is accounted for by cyclic boundary conditions, i.e. rays exiting laterally from the bounding box are rebound from the opposite plane at the same trajectory angle, to extend scattering to an infinitely extended forest. Subsequently, each generated scene canopy BRF is the result of a unique stand configuration, solar illumination direction (θ_s, ϕ_s), surface reflection direction (θ_r, ϕ_r), and spectral wavelength.

3.2.2. Model parameterization

The models used were parameterized with field data from an old-growth coniferous forest in the Swiss National Park, Switzerland (10°13′48″E/ 46°39′45″N) (Schaepman et al., 2004). This is one of the few areas in Western Europe not to have been influenced by humans during most of the 20th century: its forest has not been managed since the park was established in 1914. Since then, the forest has undergone a long process of change in stand structure and stand development. The forest, characterized by its old (165–200 years) pine stands (*P. montana* and *P. cembra*), is classified as a woodland association of *Erico-Pinetum mugo* (Zoller, 1995). Because of the high altitude (1900 m asl) and cold Alpine climate, decomposition proceeds slowly and therefore substantial quantities of large CWD can remain in the forest for many years. The forest floor is covered by CWD, *Ericaceae* and *Sesleria* shrub species. The overstory canopy is characterized by open and discontinuous stands, resulting in a relatively low crown cover (CC, between 50–80%), a low leaf area index (LAI, between 1.5–4.5) (Kötz et al., 2004), and a large proportion of woody elements (e.g. trunks, branches, CWD): one study found that 3% of the aboveground standing biomass in the park is comprised of foliage (7 Mg ha^{-1}) and 97% (250 Mg ha^{-1}) of wood (Risch et al., 2003). Over 20% of the trees in the park are standing dead trees killed by root-rot fungi; they are usually concentrated in infected patches (Dobbertin & Brang, 2001).

In addition to the old-growth mixed pine stand in the Swiss National Park, to illustrate the ranges and trends for chlorophyll content estimation, two other forest types differing in age and canopy structure characteristics were included in this study: a young Norway spruce (*Picea abies /L./ Karst.*) plantation in the Czech Republic, described in Malenovský et al. (2008), and a beetle-infested early mature Lodgepole pine (*Pinus contorta* Dougl. ex. Loud var. *latifolia* Engl.) stand in British Columbia, Canada (e.g. described in White et al., 2005). For a description of these stands and their indicative structural values, see Table 3.1.

Table 3.1: Three coniferous forests at distinct development phases: description and derived structural model parameters NPV = 100 − PV.

Name	Location	Description	Age	LAI	CC [%]	NPV [%]
Young Norway spruce stand	Moravian–Silesian Beskydy Mountains (Czech Republic) 49°50'N/ 18°54'E	Monoculture plantation forest. Foliage is concentrated in the dense, uniform overstory.	30	7−9	80−90	< 5
Old-growth Pine stand	Swiss National Park (Switzerland) 46°39'N/ 10°13'E	Mixture of *P. montana* and *P. cembras* stands (see section study site).	165−200	1.5−4.5	50−80	10−40
Early mature Lodgepole pine stand	Central interior of British Columbia (Canada) approx. 124°18'N/ 53°39' E	Dominant Sub-Boreal Spruce (SBS) biogeoclimatic zone. Occasional mountain pine beetle (*Dendroctonus ponderosae*) attacks. Rates of spread and attack intensity increased dramatically recently (White et al., 2005).	61−80	3−5†	60−80	5−50‡

†: Coarse-resolution LAI maps (Chen et al., 2002)

‡: Assessed

3.2.3. PROFLIGHT simulations

The detectability of variation in leaf chlorophyll content from spectral reflectance measurements depends on the species type (Belanger et al., 1995), the needle age (in the case of evergreen conifers: Jach & Ceulemans, 2000), the environmental stress load (Carter & Knapp, 2001), and the irradiation conditions within the canopy (Zhang et al., 2008). Changes in leaf chlorophyll content result in variation in leaf reflectance and transmittance spectra, which contribute to the canopy reflectance. In our approach, we simulated leaf-level *Cab*-related spectral variation and then input the resulting spectral variation into the canopy model in order to simulate canopy-level reflectance variations. The aim was to assess the contribution of canopy variables that potentially affect the invoked reflectance variations.

The variation in optical properties (reflectance, transmittance and absorption) of needle leaves (PV) related to chlorophyll content was simulated with PROSPECT. The chlorophyll content chosen ranged from 15 to 95 µg/cm^2 in increments of 10 µg/cm^2; such ranges are typical both in young and in mature needle leaf forest stands (Malenovský et al., 2006). The remaining PROSPECT variables – leaf mesophyll structure (N parameter), dry matter (C_d) and water content (C_w) – were derived from field measurements taken during the Fire Spread and Mitigation (SPREAD) campaign at the same site in the Swiss National Park as described in Kötz et al. (2004). They were subsequently aggregated to obtain values generic for the Swiss National Park study site (Table 3.2). During the above-mentioned campaign, the

spectral reflectance characteristics of understory, forest floor, and woody parts were measured with an ASD field spectroradiometer. The field spectra of understory vegetation, bark of branches, and bark of trunks were averaged (35 vegetated understory spectra, 15 bark spectra) to cover the spectral properties of the NPV and background components (Figure 3.1) needed for the radiative transfer parameterization. The floor of an old-growth forest typically comprises a complex layer of shrubs, herbaceous species, CWD, litter, and other ecosystem elements. In our study, "background" refers to the combined understory and forest floor, and its optical properties can essentially be conceptualized as a complex of PV and NPV elements. Patches of bare soil occur very rarely within the forest.

Table 3.2: Within-crown structural variation used in the simulations and field observations of stand variables relevant for FLIGHT parameterization ([a] NPV = 100 − PV, [b] 0.5 until LAI = 5, then increments of 1.0).

| Variable	Unit	Field observations	Range of simulated variation		
			Min.	Max.	Step
Needle parameters (PROSPECT)					
Water content	g/cm^2	0.044			
Dry matter	g/cm^2	0.036			
Mesophyll structure (N)	unitless	3.80			
Chlorophyll content	$\mu g/cm^2$		15	95	10
Within-crown structure					
Crown NPV[a]	%	30	0	80	10
LAI	−	2.5	1	10	0.5[b]
Crown cover (CC)	%	60	20	80	10
Leaf angle distribution		Spherical			
Stand structure					
Tree height	m	11.93 ± 2.9			
Crown radius	m	0.88			
Trunk height	m	7.0			
Trunk diameter	m	0.179 (on ground)			
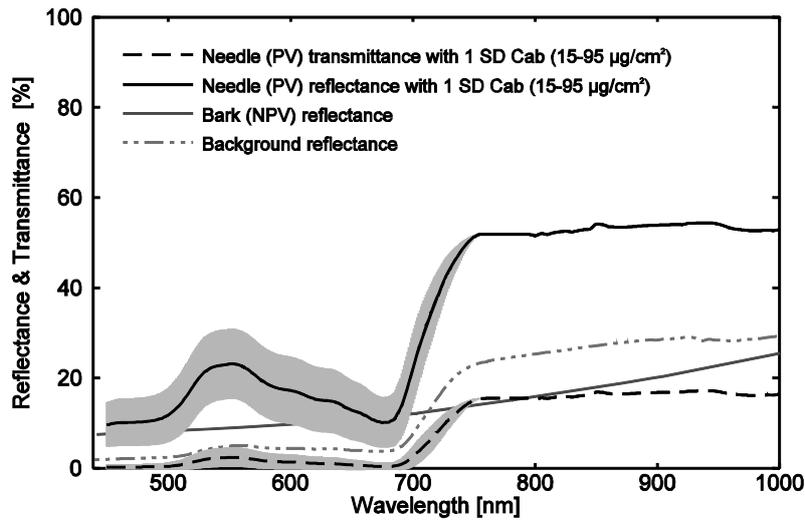
Figure 3.1: Averaged reflectance and transmittance of a PROSPECT-simulated needle, and reflectance of bark and background representing the spectral properties of PV, NPV, and background. The gray band represents the SD related to the *Cab* range of the needle.

Having introduced spectral variation at needle level, the analysis was shifted to canopy level, by inserting this spectral variation into FLIGHT. It is important to establish the relationship between confounding factors (e.g. structure, woody elements) and chlorophyll content for any given canopy structure or composition that may occur during forest aging. Key structural components that vary throughout stand development are stand LAI, canopy cover (CC), and the proportions of NPV and PV within the crown. In FLIGHT, LAI is defined as the one-sided total foliage area per unit covered scene area (North, 1996). This LAI represents the plant area index (PAI), i.e., including woody elements. Canopy (i.e. crown) cover is defined as the area of vertically projected tree crowns per total scene area. The optical properties of leaf/woody scattering elements in FLIGHT are randomly distributed within a tree crown. Hence, the model uses a parameter that describes the proportions of crown NPV and PV scattering elements, whereby NPV[%] = 100 – PV[%]. We used stand architecture data (e.g., trunk height, tree height, trunk radius, crown radius and leaf size) from the SPREAD campaign to parameterize FLIGHT. The major characteristics are summarized in Table 3.2. The simulated trees were horizontally distributed on a flat terrain according to a Poisson distribution and had crowns of irregular conical shape and cylindrical trunks. Within the individual crowns a spherical leaf angle distribution of the NPV and PV scattering elements was assumed.

BRFs were simulated in 18 spectral bands corresponding to the band settings of the Compact High Resolution Imaging Spectrometer (CHRIS) sensor in Mode 3 (land). CHRIS, on board European Space Agency's experimental satellite PROBA (Project for On-board Autonomy), is capable of providing combined spectral and directional sampling of selected terrestrial targets at high spatial resolution (~17 m) (Barnsley et al., 2004). One of CHRIS/PROBA's targeted test sites is the Swiss National Park. In the "land" mode, CHRIS

47

spectral bands are optimized to monitor vegetation cover. All spectral data were convolved to these spectral bands, using the CHRIS spectral bandpasses (Table 3.3). The solar zenith and azimuth angles were set to those during the Swiss National Park overpass on June 27, 2004 (θ_s: 24.0°, ϕ_s: 162.8°, see Verrelst et al., 2008b, for details), the view zenith angle was set at nadir (note that in principle, CHRIS/PROBA is able to observe at 5 nominal view zenith angles (0°, ±36°, ±55°)).

Table 3.3: Center wavelength (CHRIS$_{mid}$) and full-width-half-maximum (FWHM) for the CHRIS mode 3 "Land" band setting.

CHRIS$_{mid}$ (nm)	442	490	530	551	570	631	661	672	697	703	709	742	748
FWHM (nm)	9	9	9	10	8	9	11	11	6	6	6	7	7

781	872	895	905	1019
15	18	10	10	33

3.2.4. Sensitivity analysis

To ensure that we studied the relationships between reflectance spectra and chlorophyll content without influence from factors other than the variables of interest, the optical characteristics of the overstory canopy were simulated without the presence of an atmosphere. In addition to the canopy variables, the composition of the forest floor also affects the accuracy of chlorophyll content assessments (Zarco-Tejada et al., 2004; Zhang et al., 2008). Therefore, a background layer was included to mimic the optical properties of the understory at the Swiss National Park test site. A total of 7938 forest scene simulations (9 *Cab* × 14 LAI × 7 CC × 9 NPV) with PROFLIGHT provided the spectral sampling for the subsequent analysis of the contribution of woody elements and needle *Cab* content to the spectral signal at stand level. Once the initialization had been done, one million rays penetrated each experimental canopy. FLIGHT calculates directional reflectance by accumulating photons in predefined solid view angles. The theoretical accuracy of canopy reflectance approximated a relative standard error of 1.9% for the settings (1 million photons, 10 zenith and 36 azimuth angles), which is considered an appropriate level of accuracy (Kötz et al., 2004).

The idea underlying this modeling exercise is that the simulated stands might provide insights helpful for evaluating the suitability of imaging spectroscopy-based indicators for estimating chlorophyll content. The specific band configurations of CHRIS allow a number of chlorophyll sensitive indices to be calculated, as summarized in Table 3.4. Chlorophyll indices are assumed to outperform single wavelengths in predicting foliar chlorophyll content. However, their performance has not been systematically assessed in relation to woody canopies. To test which of the four studied input parameters (*Cab*, LAI, CC, and NPV) determines most of the variation in the forest scene simulations, we used analysis of variance (ANOVA) (Snedecor & Cochran, 1980) to decompose the total variance into terms related to the individual factors. The ANOVA partitions the sum of squares of the simulations into a

sum of squares related to the overall mean, a sum of squares related to treatment effects, and a residual sum of squares. Interactions among factors were found to be not important. In the ANOVA, the ratio of the mean square of an input parameter resulting from different levels of the input factor to the residual mean square, called the *F* statistic, can be tested for its significance (given by the critical level). If one band (or index) yields smaller critical levels than another one, then the former one has larger power. To test whether a specific band (or index) is sensitive for *Cab*, the *F* statistic for *Cab* was used. To test the sensitivity for *Cab* relative to the other factors (LAI, CC, and NPV) an *F* statistic was calculated by taking the ratio of the mean square related to *Cab* to the mean square related to one of the other factors and then testing its significance. The best spectral band (or index) for chlorophyll content estimation is the one that has the largest *F* value when the variance for chlorophyll effect is tested against the residual variance including all other confounding factors pooled. In addition, we calculated the *F* values for testing the *Cab* effect against LAI, CC and NPV effects, respectively.

Table 3.4: Overview of selected vegetation indices. *R* denotes reflectance. The wavelengths in the formula column represent the original proposed VI wavelengths, while the wavelengths in the columns headed formula CHRIS$_{mid}$ represent the center of the CHRIS bands that best approached the wavelengths proposed originally.

Index	Formula	Formula CHRISmid	Reference
Datt_98	R_{672} / R_{550}	R_{672} / R_{551}	Datt (1998)
Datt_99	$(R_{850} - R_{710}) / (R_{850} - R_{680})$	$(R_{872} - R_{709}) / (R_{872} - R_{672})$	Datt (1999)
GM_94a	R_{750} / R_{700}	R_{748} / R_{703}	Gitelson & Merzlyak (1994)
GM_94b	R_{750} / R_{550}	R_{748} / R_{551}	Gitelson & Merzlyak (1994)
Gitel_03a	$(R_{695-705})^{-1} - (R_{750-800})^{-1}$	$(R_{697-703})^{-1} - (R_{781})^{-1}$	Gitelson et al. (2003)
Gitel_03b	$R_{750-800} / (R_{695-705}) - 1$	$R_{781} / (R_{697-703}) - 1$	Gitelson et al. (2003)
Gitel_03c	$(R_{750-800} - R_{430-445}) / (R_{695-705} - R_{430-470}) - 1$	$(R_{781} - R_{442}) / (R_{697-703} - R_{442}) - 1$	Gitelson et al. (2003)
gNDVI	$(R_{780} - R_{550}) / (R_{780} + R_{550})$	$(R_{781} - R_{551}) / (R_{710} + R_{551})$	Smith et al. (1995)
Macc_01	$(R_{780} - R_{710}) / (R_{780} - R_{680})$	$(R_{781} - R_{709}) / (R_{781} - R_{672})$	Maccioni et al. (2001)
McM_94	R_{700} / R_{670}	R_{703} / R_{672}	McMurtey Iii et al. (1994)
mNDVI$_{705}$	$(R_{750} - R_{705}) / (R_{750} + R_{705} - 2R_{445})$	$(R_{748} - R_{703}) / (R_{748} + R_{703} - 2R_{442})$	Sims & Gamon (2002)
mSRI$_{705}$	$(R_{750} - R_{445}) / (R_{705} + R_{445})$	$(R_{748} - R_{442}) / (R_{703} + R_{442})$	Sims & Gamon (2002)
NDVI$_{705}$	$(R_{750} - R_{705}) / (R_{750} + R_{705})$	$(R_{748} - R_{703}) / (R_{748} + R_{703})$	Gitelson & Merzlyak (1994)
SIPI	$(R_{800} - R_{455}) / (R_{800} - R_{680})$	$(R_{781} - R_{442}) / (R_{781} - R_{672})$	Peñuelas et al. (1995)
TCARI/OSAVI	$3[(R_{700} - R_{670}) - 0.2(R_{700} - R_{550}) (R_{700} / R_{670})] / [(1 + 0.16)(R_{800} - R_{670}) / ((R_{800} + R_{670} + 0.16))]$	$3[(R_{703} - R_{672}) - 0.2(R_{703} - R_{551}) (R_{703} / R_{672})] / [(1+0.16)(R_{781} - R_{672}) / ((R_{781} + R_{672} + 0.16))]$	Haboudane et al. (2002)

The next step in the analysis was to study the chlorophyll effect on the best evaluated index in more detail for each combination of selected confounding canopy variables (LAI, CC, and NPV). From the set of PROFLIGHT-generated reflectance spectra, the derivative ($\partial y / \partial x$) of the relationship between *Cab* content (*x* variable) and vegetation index (*y* variable) was calculated over every *Cab* interval for every combination of confounding variables as a

measure of local sensitivity (Cacuci, 2003). The average slope was then calculated as the derivative averaged over all intervals for a stand-specific situation:

$$\Delta y / \Delta x = \frac{1}{n_{Cab}} \sum_{i=1}^{n_{Cab}} \frac{\partial y}{\partial x},$$
(3.1)

where n_{Cab} is the number of *Cab* intervals. Assuming that a steeper *Cab*-related slope ($\Delta y / \Delta x$) for a spectral band or vegetation index as measured by a space-borne optical sensor enables a more accurate detection and thus more accurate mapping of leaf chlorophyll content, then the slope ($\Delta y / \Delta x$) can be regarded as a stand-specific indicator of chlorophyll content detectability. For the best-performing index, confounding canopy variables (LAI, CC, and NPV) were paired up in different combinations: for each of the three possible combinations, the third variable was fixed according to the parameterization of the core test site in the Swiss National Park (Table 3.2). Plotting the slopes for each of these paired combinations yielded three templates of plausible canopies that might occur during forest aging. In these conceptual templates, each grid represents a unique, structurally-dependent forest type. The last step of the sensitivity analysis was to establish a link with the modeling results and structural information (LAI, CC, and NPV) derived from three distinct forest canopies.

3.3. Results

3.3.1. Chlorophyll-related spectral variation

Prior to analyzing the effects of the confounding canopy characteristics on the chlorophyll-related spectral response, the effects of scaling the needle optical properties to the canopy level were investigated. At needle level, PROSPECT reflectance and transmittance were simulated for a range of needle leaves with varying *Cab* contents. Their mean needle spectral signature and standard deviation (SD) are also displayed in Figure 3.1.

At canopy level, the solar radiant fluxes interact with the canopy foliage, the measured woody elements and the background layer. This was simulated by FLIGHT at wavelengths specific to the band settings of CHRIS. The average BRF and SD for each CHRIS band were calculated for the canopy configurations of the Swiss National Park test site (LAI: 2.5, CC: 60%, NPV: 30%) (Figure 3.2). The SD at canopy level is much smaller than the SD at leaf level because of the background contribution, stand configuration, and the contribution of NPV.
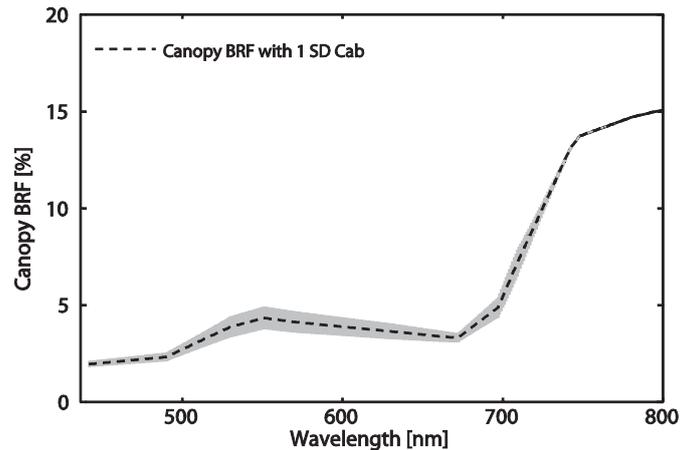
Figure 3.2: Average BRF with *Cab*-related SD (interpolated gray band) at canopy level as simulated by FLIGHT (Swiss National Park structural configurations: LAI: 2.5; CC: 60%; NPV: 30%, and Swiss National Park background).

The next step involved evaluating the sensitivity of specific CHRIS wavelengths for chlorophyll content at canopy level using the *F*-test. Table 3.5 gives an overview of the wavelengths, sorted according to the *F* values. The column headed *Cab* was used for the sorting: it presents the *F* value for testing the variance caused by chlorophyll content against the total variance of the confounding factors tested. A large value indicates that the confounding factors tested had a small influence on the total variation within the simulations. The column headed *Cab*/NPV depicts the *F* value for testing the variance caused by chlorophyll content against the *F* value caused by the NPV proportion. A large value indicates that the *Cab* effect is stronger than the NPV effect. Similarly, *Cab*/LAI and *Cab*/CC relate the chlorophyll variation to the variations caused by LAI and CC, respectively. It can be seen that the tested wavelength most sensitive to variation due to chlorophyll content relative to the confounding canopy variables is R_{490}, followed by R_{442}. The *F* values also show that at longer wavelengths the canopy structure variables exert more influence (smaller ratios). This is particularly noticeable for LAI. At canopy level, shorter wavelengths perform better than longer wavelengths because of the combined effects of low background and NPV reflectance (Figure 3.1) plus the relatively weak influence of canopy structure variables (LAI and CC). However, the use of shorter wavelengths for assessing chlorophyll content is usually not advocated for optical remote sensing data, because of the confounding atmospheric effects (Lillesand et al., 2004). Therefore, the third best performing wavelength, R_{631}, seems to be more suitable for satellite-based *Cab* retrieval approaches.

Table 3.5: ANOVA F values for single wavelengths found when testing Cab and Cab against NPV, LAI and CC, respectively.

Wavelength	$F_{8,7938}$ Cab	$F_{8,8}$ Cab/NPV	$F_{8,13}$ Cab/LAI	$F_{8,6}$ Cab/CC
R_{490}	1234.6***	23.6***	8.5***	2.8
R_{442}	1169.8***	39.7***	7.2**	2.5
R_{631}	932.8***	12.5***	6.5**	1.7
R_{570}	812.7***	2.7	7.7***	2.3
R_{530}	812.4***	2.3	9.1***	2.7
R_{661}	744.9***	270.1***	4.9**	1.1
R_{551}	712.2***	1.9	7.7***	2.3
R_{697}	673.4***	7.3**	4.7**	1.1
R_{672}	613.1***	555.9***	4.1*	0.8
R_{703}	526.8***	2.6	4.0*	1.0
R_{709}	377.0***	1.3	3.0*	0.8
R_{742}	12.2***	0.0	0.1	0.0
R_{748}	2.2*	0.0	0.0	0.0

*$p < 0.05$, **$p < 0.01$, ***$p < 0.001$.

3.3.2. Simulated chlorophyll indices at canopy level

The performance of chlorophyll indices at canopy level was evaluated similarly to the single wavelengths, using the F test. Table 3.6 gives an overview of the indices, sorted according to the F values found when testing the Cab effect. Of the indices tested, SIPI (Peñuelas et al., 1995), R_{672}/R_{550} ("Datt_98"; Datt, 1998) and R_{700}/R_{670} ("McM_94"; McMurtey lii et al., 1994) performed considerably worse than the single wavelengths (except for the reflectances at 742 and 748 nm where there was hardly any sensitivity to chlorophyll content). Their low sensitivity to chlorophyll content combined with a strong influence from NPV and CC reduces the applicability of the above-mentioned indices at canopy level. By contrast, all the other indices outperformed single wavelengths in maximizing sensitivity to chlorophyll content while minimizing undesired canopy effects. The $[R_{780}-R_{710}]/[R_{780}-R_{680}]$ index developed by Maccioni et al. (2001) ("Macc_01") produced the best results, followed by gNDVI (Smith et al., 1995), and R_{750}/R_{700} ("GM_94b"; Gitelson & Merzlyak, 1994). The reason the Maccioni index yielded the best results is because it is very sensitive to variation in chlorophyll content but is simultaneously poorly sensitive to CC, LAI, and, to a lesser extent, NPV. The superior performance of the Maccioni index corroborates the findings of Xue and Yang (2009). From a list of 40 chlorophyll indices, they concluded that this Maccioni index performed second best; only the normalized derivate difference ratio calibrated by le Maire et al. (2004) yielded a better relationship with leaf chlorophyll content. Overall, our results at canopy level show that, depending on the index, either CC or NPV mostly weaken the relationships with chlorophyll content. LAI influences the relationship with chlorophyll content the least.

Table 3.6: ANOVA *F* values for chlorophyll indices found when testing *Cab* and *Cab* against NPV, LAI and CC, respectively.

Index	$F_{8,7938}$ *Cab*	$F_{8,8}$ *Cab*/NPV	$F_{8,13}$ *Cab*/LAI	$F_{8,6}$ *Cab*/CC
Macc_01	4998.0***	29.0***	789.9***	358.9***
gNDVI	4106.7***	584.8***	2237.0***	14.4**
GM_94b	4017.3***	44.1***	1795.0***	19.7***
Datt_99	2772.5***	6.2**	662.5***	88.2***
Gitel_03c	2551.8***	10.7***	367.6***	17.7**
mNDVI705	2137.1***	5.6**	319.6***	9.1*
NDVI705	1864.2***	3.7*	449.8***	24.6***
GM_94a	1494.4***	3.1	366.1***	16.2**
Gitel_03b	1486.6***	3.1	370.7***	17.9**
TCARI/OSAVI	1464.8***	3.0	52.1***	10.3**
mSRI705	1291.8***	2.2	515.7***	111.0***
Gitel_03a	1189.5***	167.8***	9.6***	1.8
SIPI	160.9***	0.2	63.2***	0.5
Datt_98	69.1***	0.1	71.1***	0.2
McM_94	44.5***	0.1	79.6***	0.4

*p < 0.05, ** *p* < 0.01, ***p < 0.001.

3.3.3. Stand-specific relationships between Maccioni index and Cab content

Further analysis of the stand-specific relationships between *Cab* and the best performing index, the Maccioni index (Figure 3.3), revealed that variation in LAI has little influence on the relationship between *Cab* content and Maccioni index. Figure 3.3a shows that all LAI values changed at a similar rate along the *Cab* range (for CC: 60%, NPV: 30%). Only the relationship for an LAI of 1 indicates a somewhat less steep curve. Note that the quasi-linear relationships between the index and *Cab* content are due to the excellent performance of the index: the curves flattened off more at higher *Cab* content when they were plotted against single wavelengths (not shown here). By contrast, variation in CC has a greater influence on the relationship between the *Cab* content and Maccioni index (Figure 3.3b; for LAI: 2.5, NPV: 30%). The steepest curve occurs at a CC of 50%, meaning that for a relatively open crown cover, the canopy-leaving *Cab*-related spectral variation can be most accurately estimated from the chlorophyll index. Conversely, low CC values (e.g., < 30%) cause the spectrally distinct background to suppress the canopy-leaving *Cab*-related spectral variation as measured by the chlorophyll index. The variation in NPV is shown in Figure 3.3c (for LAI: 2.5, CC: 60%). This figure reveals that the slope declines with increasing contribution from woody elements. For instance, the angle of slope when 80% of the scattering elements consist of woody elements (and the other 20% of green foliage) is half the angle of slope for a completely green canopy (NPV of 0%), emphasizing the importance of woody elements as a perturbing factor. Overall, these modeling results suggest that two factors primarily determine the sensitivity of the Maccioni index to variation in *Cab* content: the composition of canopy-

scattering properties of foliage and woody elements, as expressed by NPV and PV, and the contribution of a spectrally distinct background.
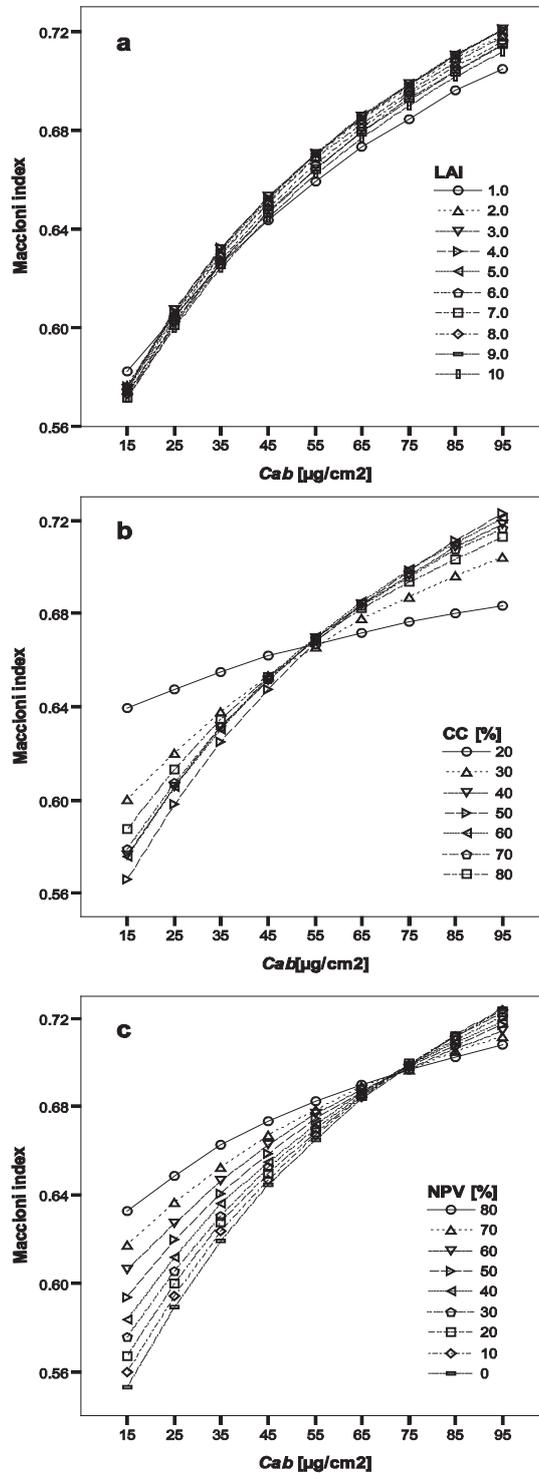
Figure 3.3: Relationships between *Cab* content (μg/cm^2) and the Maccioni index for a range of a: LAI, b: CC, and c: NPV; with fixed variables according to Swiss National Park: LAI: 2.5; CC: 60%; NPV: 30%, respectively).

3.3.4. Detectability of chlorophyll content: three forest canopy examples

Whereas in the former section the analysis was based solely on simulated data, here the slope results ($\Delta y / \Delta x$) for the Maccioni index are compared with structural information (LAI, CC, and NPV) derived from three selected examples of forest canopies. These are: 1) a young Norway spruce plantation stand in the Czech Republic, 2) an old-growth mixed pine stand in the Swiss National Park, and 3), an early mature Lodgepole pine stand in British Columbia, Canada (Table 3.1). Figures 3.4a, b and c present the 2D templates of Figure 3.3 by varying two confounding variables at a time instead of just one as in Figure 3.3. The same conclusions can be drawn as for Figure 3.3. Structural information derived from the three forest canopies are shown in figures 3.4a, b and c too. Interpretation of the $\Delta y / \Delta x$ figures suggests that in terms of CC and LAI each of the three coniferous stands has nearly optimal conditions for retrieving canopy chlorophyll content. They all have a CC above 50%, which implies a $\Delta y / \Delta x$ of at least 75% of the maximum $\Delta y / \Delta x$ (exemplified for an NPV of 0%). The modeling results suggest that a homogeneous, dense, young spruce stand like the example from the Czech Beskydy Mountains somewhat limits the detection of the *Cab*-related spectral variation (Figure 3.4d). This stand has a high LAI (about 8) and CC (on average 80%) (Homolová et al., 2007), which approaches a maximum $\Delta y / \Delta x$ in terms of LAI, but the *Cab*-related spectral variation is somewhat suppressed by the dense canopy and strong within-canopy mutual shading effects (Malenovský et al., 2008). The other two stands have a lower CC, which implies there is more opportunity for the *Cab*-related spectral variation to propagate outwards from the canopy, assuming no other factors perturb the *Cab*-index relationships.

Significant change in $\Delta y / \Delta x$ occurs, however, along the crown NPV gradient. In a dense young spruce stand, the woody surface is negligible in the upper canopy, which implies that the canopy reflectance signal is modulated mainly by the variation in foliar *Cab*. In contrast, the old-growth forest in the Swiss National Park (Figure 3.4e) represents an assembly of CWD, dead or partly defoliated trees, and trees with irregularly spaced branches with a lower LAI, where NPV cover may reach up to 40% at the CHRIS pixel resolution. The $\Delta y / \Delta x$ figures generated suggest that a woody contribution of this magnitude at the Swiss National Park test site may suppress the canopy-leaving *Cab*-related spectral variation by 27% compared to a full green canopy (NPV of 0%). Note that the Swiss National Park stand is more open, which implies that in reality the understory (essentially an NPV and PV mixture) contributes to the radiant flux as well.

Finally, the stand in British Columbia (Figure 3.4f), which is infested with bark beetles, has the largest proportion of woody material. The stand shows mixtures of green trees, red attack trees (the crowns turn red as a result of the lack of nutrients and water after pest infestation) and gray-attack trees (dead, gray tree skeletons; this occurs one year after red attack). Consequently, the spatial distribution of NPV scattering elements varies considerably. Such strong spatial variation in NPV and PV elements (figures 3.4b, 3.4c) implies that the

relationship between an index and the needle pigment contents of the remaining foliage is pixel-specific, which makes it difficult to accurately estimate chlorophyll content with a spectral index. Our modeling results suggest that for a forest stand composed of 50% NPV, an LAI of 4, and a CC of 70%, by comparison with a full green canopy (NPV of 0%), only 70% of the *Cab* variation will remain in a CHRIS pixel (size ~17 m).
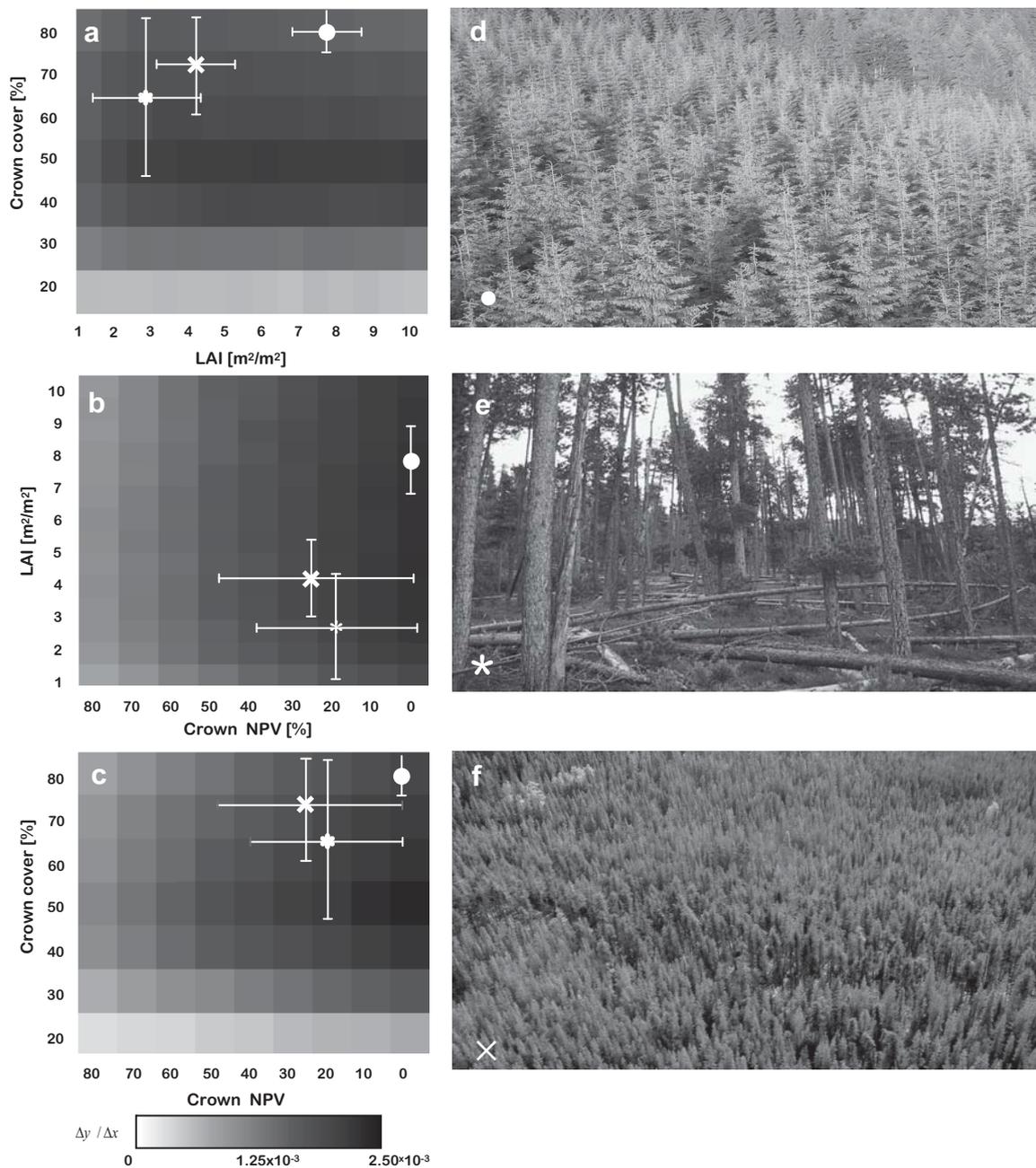
Figure 3.4: $\Delta y / \Delta x$ of the Maccioni index for three templates (a: CC − LAI; b: LAI − NPV; c: CC − NPV, with fixed variables according to Swiss National Park: LAI: 2.5; CC: 60%; NPV: 30%, respectively). Error bars per structural variable span the range of values specific for each site The three study sites used: d: ●) young Norway spruce stand, e: **x**) old-growth pine forest and, f: *) early mature beetle-infected lodgepole pine.

3.4. Discussion

The variability of forest canopy reflectance in the visible and red edge regions of the spectrum is driven mainly by variation in foliar pigment content, and also by the presence of forest background, canopy structure parameters, and woody elements. The importance of the latter factors increases with forest aging, particularly when the forest achieves the status of old-growth forest. The spectral response for development stages of production forests has been studied before and is reasonably well understood (e.g. Song & Woodcock, 2002; Roberts et al., 2004). Commonly, stand age and height are inversely related to the spectral response, due to increasing canopy closure and biomass accumulation. As young trees grow taller, the amount of foliage increases and extends over the understory and soil of the forest floor. In addition, the shadows cast by trees decrease the overall reflectance signal of the forest stand (Nilson & Peterson, 1994; Franklin et al., 2003). Although these earlier studies reported the spectral trajectories associated with forest growth development, they did not consider the encroachment of dead woody material and its consequences on foliage pigment retrieval. Once a forest stand reaches the old-growth state, woody elements also become part of the outer canopy, e.g., as dead tree tops and branches. Moreover, the woody elements in old-growth forests are not only part of living trees but are also distributed on the forest floor and in the space between living trees in the form of coarse woody debris (CWD) and also contribute to the reflectance signal.

Using spectral unmixing, Okin et al. (2001) demonstrated that the ability of imaging spectroscopy to provide a spectral vegetation signal is limited when the canopy cover is less than 30%. Our results support this finding but also suggest that above the same threshold the NPV cover (if present) starts to weaken the *Cab* signal appreciably. Data from the literature indicate that in coniferous canopies CC values typically range from 40–100%, LAI values range from 1 to above 8 (e.g., Chen et al., 2002), and woody cover rarely exceeds 40% (e.g. Radeloff et al., 1999; Fernandes et al., 2004; Jia et al., 2006). Given these figures, from the values shown in Figure 3.4 it can be calculated that as long as the proportion of crown NPV cover stays below 40% and the CC above 40%, the up-scaled Maccioni index data preserves at least 58% of the *Cab*-related spectral variation by comparison with an optimal $\Delta y / \Delta x$ (NPV of 0%, CC of 50%). Nevertheless, the contribution of background reflectance should be considered as well; its importance in the visible and red edge regions of the spectrum essentially depends on the overstory crown cover. In sparse stands (low CC or low LAI), the background reflectance of a coniferous forest may either contribute to the variation in *Cab*-related reflectance (if the forest floor is photosynthetically active), or act as an additional confounding factor (when the forest floor is e.g. litter, bare soil, CWD), or may be a dynamic mixture of both (common for old-growth forests).

In conclusion, our analysis confirms earlier studies (Demarez & Gastellu-Etchgorry, 2000; Zhang et al., 2008) that stated that an appropriate knowledge of background reflectance and forest structure parameters is important for the successful retrieval of leaf chlorophyll content from remote sensing imagery. Although, by comparison with single wavelengths, chlorophyll

indices correct for perturbing canopy factors, our results have demonstrated that some confounding effects of canopy heterogeneity remain. Specifically, it was found that in addition to structural parameters, NPV scattering elements also play an important role in the variation of TOC reflectance and derived indices, particularly in damaged and long-lived forest stands. Several studies have already attempted to include and parameterize woody material in advanced radiative transfer modeling, for instance by measuring the wood distribution with Light Detection and Ranging (LiDAR) techniques (e.g., Koetz et al., 2007; Côté et al., 2009; Morsdorf et al., 2009).

Finally, the proposed modeling design presents a simple theoretical sensitivity analysis for assessing the success of leaf chlorophyll pigment retrieval at canopy level from remotely sensed data at a spatial resolution suitable for the forest stand level. The advantage of using a modeling approach is the possibility of covering a wide range of scenarios while avoiding uncertainty related to measurement errors. Note that our study did not consider additional factors such as atmospheric effects, sun-viewing geometries, and sensor calibration errors, and that our findings may be biased by our choice of RT models and model input parameters. For example, we did not take account of variation in foliar chemicals other than chlorophyll content (e.g. anthocyanin and carotenoid foliar pigments) and variation in optical properties of woody parts, e.g. due to species composition or phenology. Since PROSPECT was essentially developed for broadleaves, the model may benefit from further improvement such as recalibration of the specific absorption coefficients (Malenovský et al., 2006) and refraction index (Feret et al., 2008) when used for narrow needle-shaped leaves. The LIBERTY model (Dawnson et al., 1998) designed specifically for such leaves may offer an appropriate alternative. Since in coniferous trees the woody parts and needles are hierarchically organized and highly clumped (Chen & Black, 1992), the random spherical distribution of NPV and PV scattering elements as defined in the ray-tracing FLIGHT model also deviates from the real forest situation. Aware of all these constraints, we exploited both models to their fullest capability, and addressed the role of variables that are regarded as key confounding factors in *Cab* content mapping, e.g., encroachment of woody materials, background contribution, and crown-scale clumping (Nichol et al., 2002; Kane et al., 2008; Ustin et al., 2009).

3.5. Conclusions and recommendation

Space-borne imaging spectrometers (e.g., CHRIS on board the PROBA spacecraft or Hyperion on board the Earth Observing-1 (EO-1) spacecraft; Pearlman et al., 2003) open up the possibility of monitoring the foliar pigment content of forest stands at scales ranging from regional (ecosystem) to global (biome) (Kokaly et al., 2009). A key element for the successful quantitative retrieval of foliar pigments from remote sensing data is information on the extent that confounding scattering elements contribute to photon–canopy interactions. The observation that a highly clumped and partially defoliated canopy of an old-growth forest exhibits noticeable mixtures of foliage and woody parts prompted us to investigate the

efficacy of estimating chlorophyll content in woody stands. The results obtained from PROFLIGHT suggest that if the crown cover is more than 30%, it should be possible to reliably estimate the variability of the chlorophyll content in a forest canopy. However, at this threshold, also crown NPV scattering elements – if present – start to weaken the *Cab* signal appreciably. Almost all the tested chlorophyll indices outperformed single wavelengths in minimizing undesired effects; the one that performed best at canopy scale was the Maccioni index ($[R_{780} - R_{710}] / [R_{780} - R_{680}]$), though the influence of NPV and CC remained. LAI only marginally influenced the ability of the index to assess *Cab*-related spectral variation. Our findings emphasize the role of woody elements when retrieving chlorophyll information from remotely sensed reflectance data of woody ecosystems. It can be concluded that ignoring the contribution of canopy woody components may lead to less accurate chlorophyll estimates. We recommend that future model refinement should focus not only on the photosynthetically active parts of the forest canopy, but also adequately take into account the woody elements as part of living and dead trees, as well as of forest understory.

Chapter 4

Spectrodirectional Minnaert-*k* retrieval using CHRIS/PROBA data

Jochem Verrelst, Michael E. Schaepman, Jan G.P.W. Clevers

Spectrodirectional Minnaert-K retrieval using CHRIS/PROBA data

Abstract

We studied the spectral information content related to the canopy structure embedded in the angular domain of imaging spectrometry data. CHRIS (Compact High Resolution Imaging Spectrometer) mounted onboard the PROBA (Project for On-board Autonomy) spacecraft is capable of sampling reflected radiation over the visible and near-infrared (NIR) region of the solar spectrum with high spatial resolution. The spectral anisotropic signature of an Alpine coniferous forest during winter in relation to canopy cover was investigated using the Minnaert-*k* parameter obtained by inverting the Rahman–Pinty–Verstraete (RPV) model against CHRIS data. Although earlier studies have demonstrated that Minnaert-*k* can be used to characterize surface heterogeneity at subpixel scale, its spectral dependency has not yet been fully assessed. Minnaert-*k* parameter retrievals across CHRIS bands revealed that a switch from bell-shaped to bowl-shaped anisotropic reflectance patterns occurs when comparing visible to NIR responses. Specifically, analysis of the underlying dynamics for pixels on the valley floor revealed that canopy cover and background brightness control were precisely in the spectral domain in which this anisotropy switch occurs. For a bright snow cover background, Minnaert-*k* values correlated best with canopy cover at the end of the red edge (e.g., around 735 nm). In this spectral region, pixels with medium canopy cover (40–70%) typically produced bell-shaped anisotropy patterns, while pixels with sparse (<30%) or dense (>80%) canopy covers typically produced bowl-shaped reflectance anisotropy patterns.

Keywords: Minnaert-*k*, imaging spectroscopy, reflectance anisotropy, forest heterogeneity, CHRIS

4.1. Introduction

The reflectance anisotropy of boreal and Alpine forests measured under winter conditions depends on the wavelength and the proportions of snow and plant cover that are recorded by a sensor (Vikhamer and Solberg, 2003; Nolin, 2004). These proportions depend on illumination and viewing angle, topography and structural canopy properties such as tree density, canopy geometry, and gap fraction. In the last twenty years, various studies have documented that anisotropic reflectance data encapsulate information about canopy structure at subpixel scale (e.g., Asner et al., 1998; Diner et al., 1999; Deering et al., 1999; Sandmeier & Deering, 1999). Yet, it was only with the development of surface reflectance models (e.g. Verhoef, 1984; Verstraete et al., 1990; Li et al., 1992) and the advent of multi-angular Earth observing sensors (e.g. Diner et al., 1998; Barnsley et al., 2004) that significant progress was made in the retrieval of canopy characteristics from multi-angular reflectance data (e.g., Diner et al., 2005; Schaepman et al., 2005; Chopping et al., 2003; Gao et al., 2003; Canisius & Chen, 2007; Schaepman, 2007).

Among the surface reflectance models, the Rahman–Pinty–Verstraete (RPV) parametric model (Rahman et al., 1993) is particularly suitable for estimating reflectance anisotropy because it simulates the bidirectional reflectance distribution function (BRDF) of an arbitrary land surface on the basis of three (optionally four) parameters. Of these parameters, the Minnaert-*k* parameter is specifically of interest as it describes most of the angular variation related to surface reflectance anisotropy. Pinty et al. (2002) and Widlowski et al. (2001, 2004) have theoretically demonstrated that the Minnaert-*k* parameter contains information on subpixel heterogeneity. Specifically, the *k* parameter has been shown to better identify canopy structure and heterogeneity at the subpixel scale than what is feasible on the basis of spectral measurements only (Gobron et al., 2000b; Gobron & Lajas, 2002; Pinty et al., 2002; Widlowski et al., 2001, 2004).

Several studies have been performed to map Minnaert-*k* as a proxy for vegetation structure and density at the subpixel scale for various landscapes such as a prairie, woodlands and forests (Pinty et al., 2002; Nolin, 2004; Lavergne et al., 2007; Sedano et al., 2008). All these studies used Multiangle Imaging SpectroRadiometer (MISR) satellite data, or its airborne variant: AirMISR. MISR, on board the NASA EOS Terra platform, is configured with 9 cameras, each of which observes the Earth in four spectral bands. In the global data acquisition mode, eight oblique cameras observe the Earth's surface at a resolution of 1100 m in blue, green, and near-infrared bands and at a resolution of 275 m in the red domain. In addition, all four bands of the nadir-observing camera have a spatial resolution of 275 m (Diner et al., 1991). Pinty et al. (2002) reported that the availability of sufficient brightness contrast between overstory and background in conjunction with a relatively high sun position (sun zenith < 60°) is critical for detecting maximal variability in reflectance anisotropy, and thus in Minnaert-*k*. They also demonstrated that the potential to detect canopy structural information from multi-angular measurements depends on the sensor's spatial resolution.

Typically, the higher the spatial resolution, the more opportunities exist to detect reflectance anisotropy at stand or tree scale.

In 2001, two years after the launch of Terra, the European Space Agency (ESA) launched the experimental satellite sensor CHRIS (Compact High Resolution Imaging Spectrometer) onboard the PROBA (Project for On-board Autonomy) spacecraft. The imaging spectrometer acquires a series of five angular images of a terrestrial surface at a high spatial resolution (~17 m) during the same orbit. Depending on its operating mode, CHRIS is capable of sampling the anisotropic behavior of the reflected solar radiation in up to 62 narrow spectral bands covering the visible and near-infrared (VNIR) region of the solar spectrum.

A set of concurrent multi-angular CHRIS images of an old-growth alpine forest stand was acquired during winter in order to characterize the structural properties of the observed forest using the Minnaert-*k* parameter. Using the CHRIS observations at high spatial and spectral resolution and the spectrally distinct snow vegetation signal it is possible to explore the spatial and spectral dynamics of Minnaert-*k* at the forest stand scale. Though Koetz et al. (2005) have also demonstrated that structural parameters can be related to the *k* parameter at the CHRIS subpixel scale, the spectral dependency of these relationships has not yet received full attention. We therefore formulated two research objectives: 1) to evaluate the spectral dependency of the Minnaert-*k* parameter retrieved from coniferous stands during winter, and 2) to interpret the parameter's underlying wavelength-dependent biophysical meaning. Both objectives were intended to elucidate the anisotropic reflectance properties of forested surfaces recorded with a high spatial resolution sensor like CHRIS. This improved understanding is useful, for example, to serve as a benchmark for interpreting spectrodirectional (combined spectral and multi-angular) data and to trigger new methods that exploit the angular domain in a more physically-based way.

4.2. Biophysical interpretation of Minnaert-*k*

The RPV model provides a phenomenological description of the target's anisotropy, without attempting to assign it to specific physical causes or processes. As such, it is an empirical and efficient parametric representation of that surface property. The RPV model splits the BRF field for a given wavelength (λ) into a scalar amplitude component (ρ_0) and an associated directional component describing the anisotropy of the surface (Rahman et al., 1993; Pinty et al., 2002). The directional component is expressed as the product of three functions, each dependent on a single parameter: 1) the modified Minnaert function (k) that controls the curvature of the scattering regime, 2) the Henyey-Greenstein function (Θ) that controls the degree of forward and backward scattering regimes, and 3) an optional hotspot descriptor function (ρ_c). The algorithms underlying each of the parameters are documented in the above-mentioned publications. The empirical parameter k of the Minnaert's function (Minnaert, 1941) is particularly interesting, since it quantifies the extent to which the angular variations in the BRF pattern resemble a "bell-shaped" or "bowl-shaped" pattern. It has been proven that

under favorable illumination conditions and large background brightness, the angular pattern is largely controlled by the physical properties and geometric arrangements of the plant elements (Widlowski et al., 2001; Pinty et al., 2002). This means that the angular signature for a single wavelength of a pixel as measured by a multi-angular sensor can be diagnostic for the assessment of subpixel structural surface properties, if there is sufficient contrast between the darker overstory and brighter background.

Coniferous forests commonly appear darker in the VIS region than deciduous forests, due to the strong internal shadowing caused by clumping effects and the relatively high light absorption capacity of needles (Smolander & Stenberg, 2003). In open canopies composed of tall trees in conjunction with a bright snow background mean that boreal or alpine winter landscapes offer ideal conditions for Minnaert-*k* analysis. Given a sufficiently low solar zenith angle (i.e. < 60°; Koetz et al., 2006) and no snow cover on tree branches, the following situations can occur in coniferous stands during winter:

- Surfaces that are brighter at large oblique viewing angles in forward and backward scattering directions lead to a bowl-shaped reflectance anisotropy pattern. Enhanced scattering towards larger zenith angles typically occurs in case of closed and structurally homogeneous forests or in case of single-layer surfaces, such as bare soil or snow cover. Bowl-shaped anisotropy patterns result in *k* values smaller than 1.

- Conversely, surfaces that are brighter at nadir viewing angle than at oblique viewing angles lead to the inverse pattern: a bell-shaped reflectance anisotropy pattern. In open, vertically elongated canopies, the contribution of uncollided radiation to the total signal (i.e. the fraction of radiation that has travelled through the gaps of the canopy layer and has been scattered by the background only; Pinty et al., 2004), is maximized at nadir viewing angle, while at greater zenith angles it is intercepted by the tall trees. Bell-shaped anisotropy patterns result in *k* values larger than 1.

- Surfaces that exhibit Lambertian reflectance, i.e. the amount of scattered radiation is the same in all directions, result in a *k* value of 1.

The Minnaert-*k* value can thus essentially be used as a proxy for canopy heterogeneity simply based on canopy closure and fluctuations in the amount of scattering and absorbing material at one specific wavelength. It has been shown to be successful for characterizing structural heterogeneity of canopies over snow (Nolin, 2004). In this paper we evaluate the Minnaert-*k* parameter in relation to canopy structure in the whole VNIR spectral domain.

4.3. Test site

The chosen test site is located in an Alpine valley, the Ofenpass valley, in the Swiss National Park in the Engadine region, south-east Switzerland (10°13′48″E/ 46°39′45″N). The Ofenpass represents a dry inner-alpine valley with limited precipitation (900–1100 mm/year) at an average altitude of about 1900 m asl. Two subalpine ecosystems – a coniferous old-growth forest and a meadow – cover the south-facing slope. The forest is dominated by mountain pine (*Pinus Montana* spp. *arborea*) and some stone pine (*Pinus cembra*) tree species. The forest can be classified as woodland associations of the *Erico-Pinetum mugo* type, typified by relatively open discontinuous stands. The forests vary in topography, openness, tree clumping, leaf area index (LAI) and woodiness (Kötz et al., 2004; Verrelst et al., 2008b). The south-facing valley floor of the Ofenpass valley was considered to be the core test site. Stand variables of the core test site are provided in Table 4.1.

Table 4.1: Stand variables for the core "Ofenpass" test site (south-facing valley floor). Data were collected during the SPREAD field campaign (Kötz et al., 2004; Morsdorf et al., 2004).

Variable	Unit	Generic field observations
Stand structure		
Stand age	years	165−200
Tree height	m	11.93 ± 2.9
Crown radius	m	0.88
Crown base	m	7.0
Stand density	trees/ha	790±250 (>12 cm DBH)
Within-crown structure		
Crown LAI	m^2/m^2	1.5−4.5
Crown photosynthetic vegetation	%	60−90

4.4. CHRIS data

PROBA is an experimental ESA platform that enables CHRIS to capture near-concurrent multiple views of a surface in a short period of time. CHRIS uses the satellite's tilting and pointing capabilities in along-track and across-track directions, allowing the acquisition of up to five images during a few minutes (Barnsley et al., 2004). CHRIS can be operated in five different modes, with different combinations of band configuration (number, center location and width) and spatial resolution for specific applications (e.g. aerosols, land or water).

A set of CHRIS mode 5 "land" images were acquired over the Swiss National Park site on March 17, 2007, near noon local time (11:34h local time) under cloud-free conditions. Mode 5 is configured in CHRIS's best spatial resolution (nominally ~17 m) and spectral resolution (37 narrow spectral bands with bandwidths of 6–33 nm located between 438 nm and 1036 nm). Its specifications are summarized in Table 4.2. The large number of spectral

bands enables, among other things, the anisotropic spectral behavior to be examined in the transition zone between the visible and near infrared, the "red edge", as there are eight CHRIS bands in the spectral domain ranging from 700–750 nm. Several mono-angular nadir studies have shown that measurements based on the red edge position correlated well with biophysical variables at canopy scale, such as LAI (e.g. Clevers et al., 2002). However, only scant attention has been paid to what goes on in the directional domain of the red edge, i.e. how the curvature of the anisotropic reflectance responds to canopy structure.

The acquisition date was chosen to ensure that a snow carpet was still present while the sun position was already acceptably high at noon (sun zenith 50°, azimuth 161°). The solar position can be regarded as constant for all five CHRIS fly-by zenith angles, since the time elapsed between the first and last recordings during the satellite overpass was less than two minutes. In the current along-track pointing configuration, the fly-by zenith angles are equivalent to the nominal viewing zenith angles (VZA: 0°, ±36°, ±55°). Due to its narrow field of view (FOV), however, CHRIS is only occasionally able to acquire a target at nominal view angle. PROBA must be tilted so that the target area falls within the sensor's FOV (Barnsley et al., 2004). This means that the actual observation angles at which the images are acquired may deviate from the nominal view angles. For example, the nominal nadir camera position happened to be pointed in a forward VZA of +21°.

The exact viewing geometries of all five CHRIS view angles and the sun position are shown in the polar plot of Figure 4.1. The CHRIS images were captured near the principal plane; the forward-pointing +36° view zenith angle happened to be positioned right within the solar principal plane. A subset of the near-nadir image of the Ofenpass valley overpass is depicted in Figure 4.2. The dark parts in the figure are the forest vegetation; the white patch within the dark forest represents a snow-covered meadow. Note that snow quality also influences the shape of the reflectance anisotropy patterns (Warren et al., 1998; Painter and Dozier, 2004). From snow and weather information provided by the Swiss Federal Institute for Snow and Avalanche Research (SLF) we know there was no snowfall that week in the Engadine region (14.03.2007–17.03.2007: no snowfall, cloud-free). This was also noted during a field visit to the region during the CHRIS/PROBA overflight. Snow on the branches of the trees had melted, which means that strictly speaking the "snow-covered forest" had snow on the ground, but not on the trees. Following a comparison of CHRIS spectral signatures with those the John Hopkins spectral library. (Salisbury et al., 1994) the snow grain size diameter was assessed as medium. Hardly any spatial variation in snow grain size was noted.

Table 4.2: CHRIS specifications for Land Mode 5.

Sampling	Image area	View angles	Spectral bands	Spectral range
~17 m @ 556 km altitude	13 x 13 km (766 x 748 pixels)	5 nominal angles @ 0°, ±36°, ±55°	37 bands of 6−33nm width	438−1036 nm
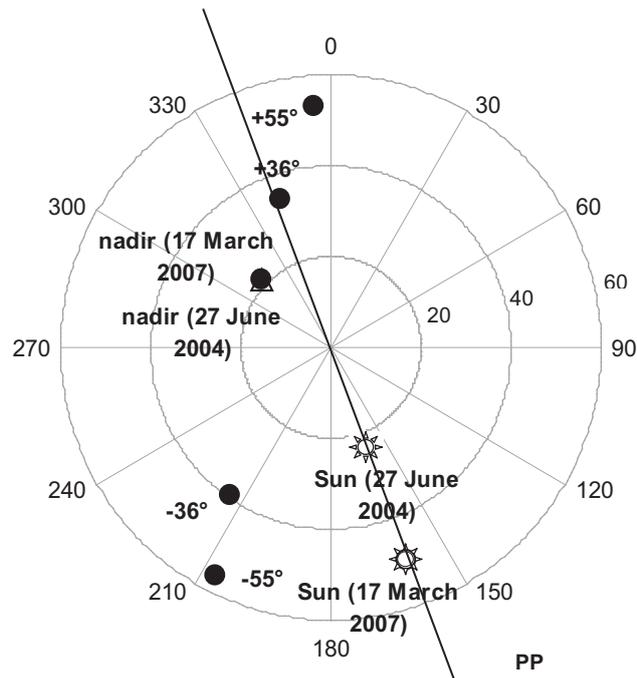
Figure 4.1: Polar plot of illumination geometry (Sun:☼) and CHRIS image acquisition as of March 17, 2007 (●), and nadir acquisition geometry as of June 27, 2004 (Δ). The nominal −55° view zenith angle missed the test site. PP: Principal Plane.
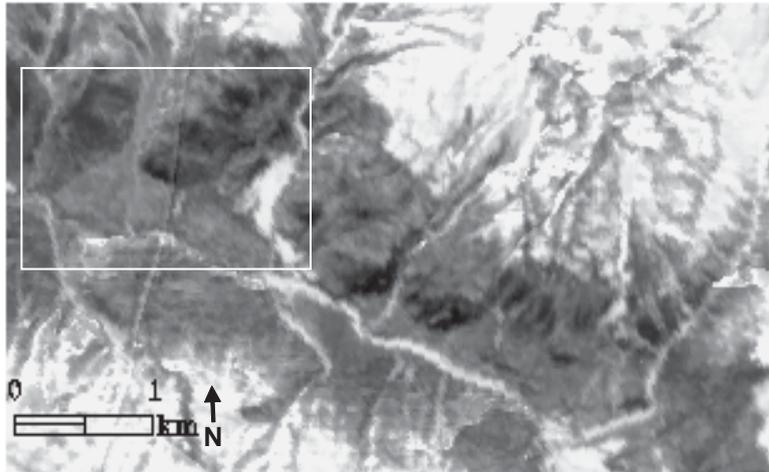
Figure 4.2: RGB subset of the geometrically and atmospherically corrected CHRIS/PROBA nadir scene acquired over the Swiss National Park study site on March 17, 2007. The Ofenpass valley stretches from upper left to below right of the image. The square indicates the core test site. The white part within the square is the snow-covered meadow. The pink color on the mountain tops is saturation effect. R: 631 nm, G: 550 nm, B: 442 nm.

4.5. Methods of data analysis

The CHRIS scenes acquired at various angles were corrected to account for the topographic effect of rugged, mountainous terrain, following the approach developed by (Kneubühler et al., 2005). A parametric approach for geometric correction of each CHRIS acquisition (up to 5 viewing angles) was applied; it was based on a 3D physical model (Toutin, 2004). The method allowed us to achieve high geometric accuracy with a geolocation uncertainty of about half a pixel across and along track when using a digital terrain model (DTM; Swisstopo) with 2 m resolution (Schläpfer et al., 2003). Regrettably, as a consequence of the reduced spatial footprint, the backward-pointing −55° view zenith angle just missed the test site. The remaining four images were atmospherically corrected using a freely available MODTRAN-based atmospheric correction module (Guanter et al., 2005a) implemented in the Basic ERS & Envisat (A)ATSR and Meris (BEAM) Toolbox (http://www.brockmann-consult.de/beam) that has been specifically developed for correcting CHRIS images (Guanter et al., 2007). The method is designed to automatically derive aerosol loading, columnar water vapor and surface reflectance from CHRIS data, as well as to update CHRIS's spectral and radiometric calibration parameters when necessary (Guanter et al., 2005a). The preprocessing efforts resulted in geometrically corrected images of hemispherical-directional-reflectance-factor (HDRF) data (Schaepman-Strub et al., 2006) at a spatial resolution of 18 m. The observations at 442 and 489 nm were removed from the analysis, because of significant atmospheric scattering in the blue bands of CHRIS (Guanter et al., 2004). Moreover, bands close to the atmospheric water vapor absorption band at 940 nm (CHRIS bands at 925, 940 and 955 nm) were also omitted from further analysis. For all remaining 32 bands the Minnaert-*k* parameter was calculated.

4.5.1. Minnaert-k retrieval

For each pixel, the Minnaert-*k* parameter was retrieved by inverting the Rahman–Pinty–Verstraete (RPV) model by using the RPVinversion-3 software package (Lavergne et al., 2007). The inversion method is documented in Gobron and Lajas (2002). The package offers a number of features, including the complete assessment of the measurement-model mismatch covariance matrix and the option of operating adjoint software codes derived from automatic differentiation techniques. This allowed us to perform the inversion of the nonlinear RPV model under the classical Bayesian approach in a numerically and computationally efficient manner, while at the same time generating an unbiased estimation of the Probability Density Functions (PDFs) for the parameters retrieved. The package implements the inverse model for two versions of the model: the standard version using 3 parameters and an extra version with the hot spot parameter in addition. The hotspot parameter is only required to improve the representation of the hotspot when illumination and observation geometries close to the hotspot are present. In the observed winter scene of CHRIS, this configuration was not of importance. The RPVinversion-3 procedure thus resulted in sets of RPV parameters (ρ_0, k, and Θ) and additional information on the accuracy of the fit expressed by the χ^2-value. Measured and modeled data were compared using the χ^2 test (for a significance level $\alpha = 0.05$) to evaluate the performance and the fit of the model parameters. The smaller the value of χ^2, the better is the correspondence between the CHRIS HDRF data and RPV-reconstructed HDRF data, and thus the model performance.

4.5.2. Reference map

Simultaneous exploitation of the spectral and directional behavior of vegetation canopies allows canopy biophysical and biochemical properties to be assessed on the basis of subtle variations in the reflectance signatures, and at the same time provides additional information on canopy structure based on subtle variations in the angular signatures. Regarding the angular signatures, it is of interest to identify the structural parameter that has most influence on the reflectance anisotropy, so that the resulting map can be used as reference for evaluating the Minnaert-*k* parameter. Widlowski et al. (2001) and Pinty et al. (2002) have already reported the importance of the background contribution. Kayitakire and Defourny (2004) concluded that in forested landscapes, the horizontal arrangement of the trees and the stand density influence the anisotropy of the canopy reflectance more than tree height and diameter. Koetz et al. (2007) used LiDAR data to try to establish a relationship between the Minnaert-k parameter and forest structure, but that approach does not provide information about the background brightness. It therefore seems more logical to use an independent spectrally derived forest cover map to assess the relationship of the Minnaert-*k* parameter. Since illuminated snow and coniferous tree crowns are spectrally highly distinct (Vikhamar and Solberg, 2003), a canopy cover map was generated from the near-nadir CHRIS image by applying linear spectral unmixing (LSU). LSU is a technique commonly applied to derive canopy cover maps, including from high resolution spatial data (Sabol et al., 2002; Chen et al.,

2004). Canopy cover is defined as the percentage (from 0–100%) of a grid cell that is covered by plant canopy when imaged from above. LSU analysis was developed to decompose image pixels into their pure constituents (Settle & Drake, 1993; Adams et al., 1995), which under winter conditions means vegetation and snow cover. LSU assumes that the reflectance at pixel scale can be described by a spectral mixture model in which a mixed spectrum is represented as a linear combination of spectral endmembers (Eq. 4.1):

$$R_i = f_{\text{vegetation}} \cdot R_{i,vegetation} + f_{\text{snow}} \cdot R_{i,snow} + \varepsilon_i \qquad (4.1)$$

under constraint $\quad f_{\text{vegetation}} + f_{\text{snow}} = 1$ and $\quad f > 0,$ $\qquad\qquad\qquad$ (4.2)

where $f_{\text{vegetation}}$ and f_{snow} are the fractions of vegetation and snow in the pixel studied, R_i the reflectance of a pixel in band i, $R_{i,\ \text{vegetation}}$ ($R_{i,\ \text{snow}}$) the reflectance of the vegetation (snow) endmember in band i, and ε_i the residual error associated with band i. The unmixing was forced to be fully constrained (Eq. 4.2). This guaranteed a physical interpretation of the results, since the fractions sum to 1 and all the fractions are positive (Zurita-Milla et al., 2007). The fit of the model can be assessed by the root mean square error (RMSE):

$$\text{RMSE} = \sqrt{\frac{\sum_{b=1}^{i} \varepsilon_b^{\,2}}{i}}\ , \qquad\qquad\qquad\qquad (4.3)$$

where i is the number of bands used in the spectral unmixing. The full spectral domain (excluding the bands we had removed) was used to unmix the near-nadir image into these two endmembers. The endmembers are depicted in Figure 4.3. The snow endmember was extracted from 16 fully snow-covered central meadow pixels of the near-nadir CHRIS data. Hardly any spectral variation was noted. The vegetation endmember was extracted from 94 dense, fully vegetated forest cover pixels of the core test site, using summer near-nadir CHRIS data (June 27, 2004; see Verrelst et al., 2008b for more information) to avoid contamination from snow cover underneath the canopy layer. As during summer the forest is characterized by a vegetated understory (rejuvenates, shrubs), more spectral variation was noted. Hence the averaged spectral variation resembles a generic, photosynthetically active vegetation signature. The CHRIS near-nadir viewing geometry of the summer acquisition precisely matched the CHRIS near-nadir viewing geometry of the winter acquisition (Figure 4.1). We know of no events (e.g. storms) that may have significantly altered the forest structure in the last few years. While recognizing the limitations of applying LSU at high spatial resolution data due to multiple scattering from the targets (Borel & Gerstl, 1994), the advantage lies in the technique's fast calculation and compatibility. The unmixing quantified the subpixel spectral contributions of overstory canopy cover and underlying snow cover proportions on the basis of the spectral dimension of mono-angular, near-nadir CHRIS measurements, thereby minimizing uncertainties related to geolocation and spatial resampling.

The unmixing approach for the forest site was tested pixelwise on its uncertainty as expressed by the RMSE. As there were only two endmembers, the RMSE values were consistently low (around 0.016). The results were compared with ground reference data collected for four plots (20 x 20 m) according to the VALERI protocol during the Fire Spread and Mitigation (SPREAD) campaign (Kötz et al. 2004; Morsdorf et al., 2004). Consistent results were obtained, with a slight overestimation of canopy cover of about 8% when compared with the ground reference data.
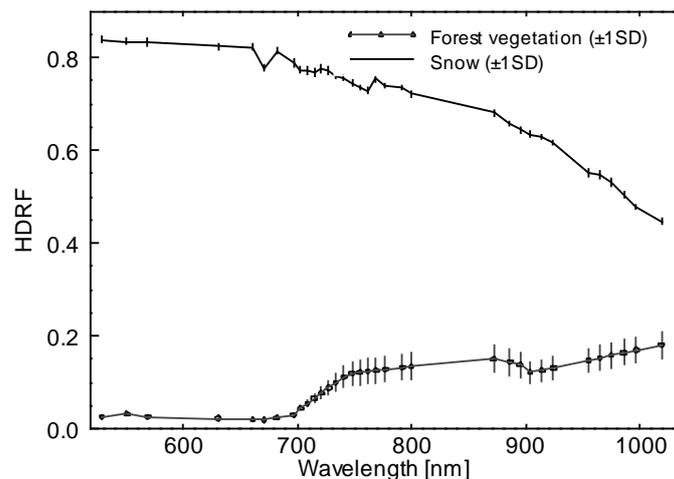
Figure 4.3: Snow and forest vegetation endmembers extracted from near-nadir CHRIS images (average and standard deviation). The small spikes in the snow endmember are artifacts of the atmospheric correction (pers. comm. L. Guanter, 2009).

4.6. Results and discussion
4.6.1. Spectral maps of the Minnaert-k parameter

Minnaert-k maps were generated on a pixel-by-pixel basis across all the used CHRIS wavelengths. The wavelengths ranged from the green (530 nm) to the NIR (1019 nm). Six of these maps are shown in Figure 4.4. The accuracy of the retrieval for each pixel was calculated using the χ^2 test. Despite the limited number of angular observations, the RPV model was able to fit the CHRIS angular signatures for the Ofenpass valley with high accuracy for most of the pixels. The best χ^2 results were for the forest vegetation at the valley floor. Misfits at the 5% significance level typically occurred along the forest edges, riverbeds and along steep slopes, and in some bands over snow-covered regions. In particular, the sudden change in volumetric structure on the forest–meadow interface led to unexpected shapes of anisotropy. All pixels with a bad fit were filtered out in further analysis. Considering the Minnaert-*k* retrievals, systematic and pronounced patterns emerged in both the spatial and spectral dimensions. The excessive blue coloring at the shorter wavelengths indicates an enhanced near-nadir scattering, while excessive red coloring at the longer wavelengths indicates a bowl-shaped anisotropy. The series of Minnaert-*k* maps show that

anisotropy patterns shift from predominantly bell-shaped patterns ($k > 1.0$; in blue color tones) at the shorter wavelengths towards predominantly bowl-shaped patterns ($k < 1.0$; in red color tones) at the longer wavelengths. These maps also suggest that the largest variability of bell and bowl shapes is located around the red edge region. For instance, in the 770 nm map, patches of bell-shaped and bowl-shaped anisotropy patterns emerged that seem to be related to subpixel surface cover. The homogeneous non-forested pixels (meadow) exhibit pronounced bowl-shaped reflectance patterns, while there is a fair amount of variability in Minnaert-k parameter over the forest vegetation, suggesting a relationship with forest structure at subpixel scale.
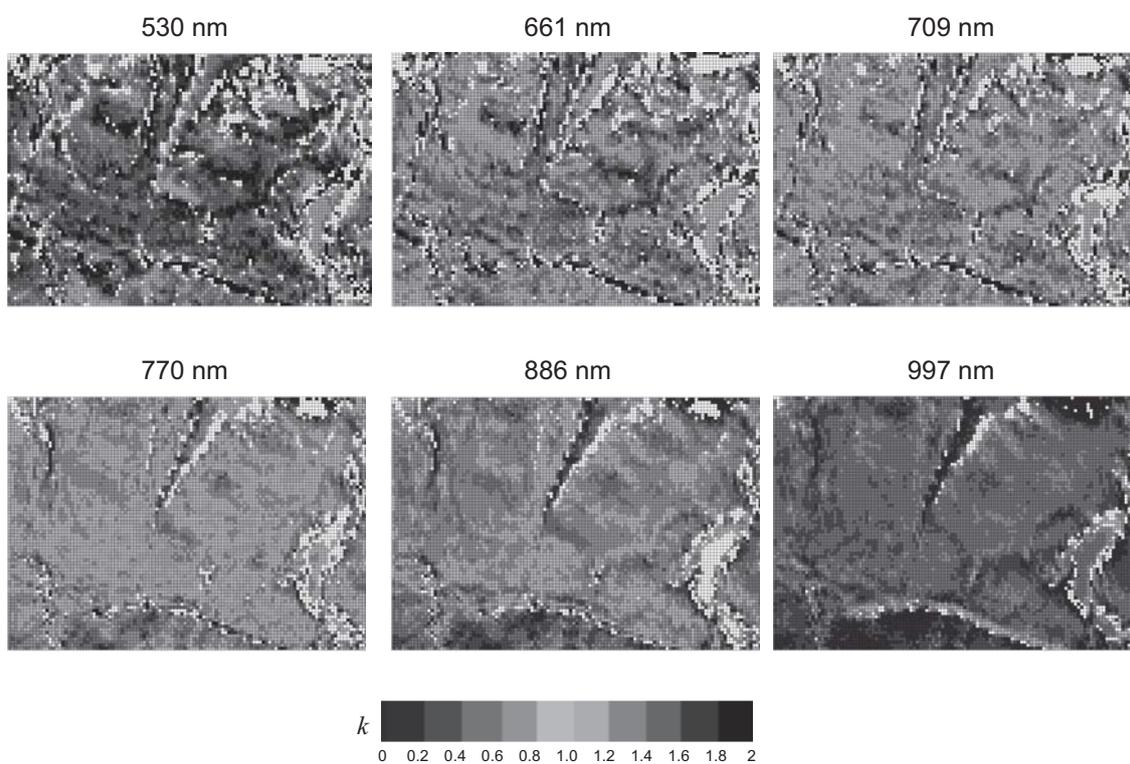
Figure 4.4: Minnaert-k maps for various CHRIS wavelengths. The white pixels are those in which the reflectance anisotropy of the CHRIS-HDRF data and the RPV-reconstructed HDRF data was significantly different.

A more systematic overview of the Minnaert-k dynamics along the spectral range of CHRIS is provided in Figure 4.5. The figure presents the spectral dependency of the k values averaged for the study site in conjunction with their standard deviations: it can be seen that these values decreased progressively towards longer wavelengths. This trend underlines the strong spectral dependency of the Minnaert-k parameter. In the visible region, bell-shaped reflectance anisotropy patterns dominate ($k > 1.0$); the bright background controls the reflectance of the entire scene at smaller zenith angles (e.g. near-nadir), while at larger zenith angles the absorbing properties of the coniferous trees control the reflectance. Conversely, in

the NIR spectral region, bowl-shaped reflectance anisotropy patterns dominate ($k < 1.0$) due to enhanced transmission and multiple scattering processes of NIR radiation throughout the canopy (Sandmeier & Deering, 1999). As a consequence of these multiple scattering processes, the brightness contrast between canopy components and background diminishes, particularly further into the NIR. This leads to lower k values that vary within a limited numerical range in the NIR, which hampers the separation of different canopy structures, although some spatially distinct features remain visible. For instance, the riverbed (centre, below) and the edges of the homogeneous snow-covered meadow exhibit a pronounced bell-shape up to the 886 nm map, while at 997 nm the spatial patterns remain visible but k values hardly reach 1. The spatial patterns of contrasting low and high k values can be explained by extreme topographic features, i.e. by slope and aspect effects, or by subpixel landscape features with extreme spectral contrast, such as roads or riverbeds transecting the area of vertically elongated coniferous trees.
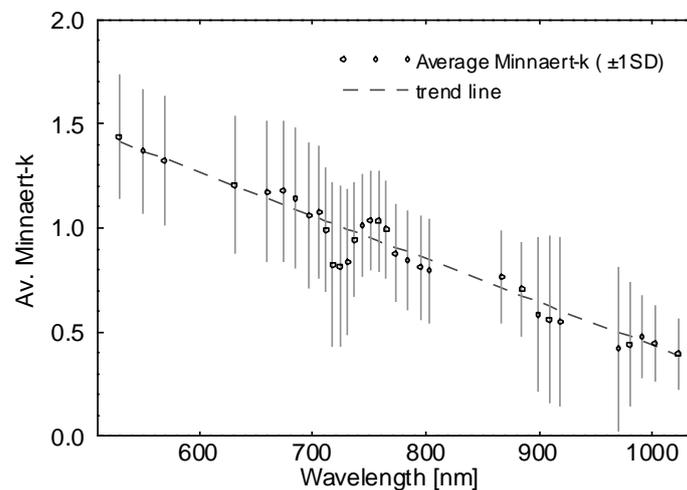
Figure 4.5: Average Minnaert-k and standard deviation as a function of wavelength. A linear trend line has been added.

4.6.2. Biophysical interpretation Minnaert-k maps

As it became evident that the Minnaert-k parameter is influenced by wavelength, our next step was to analyze the parameter's underlying physical meaning. For this analysis we used CHRIS data on the forest on the south-facing valley floor. Although most of the erratic, mountainous terrain was excluded from the analysis, subtle variations in topography may still lead to target occlusions or larger degrees of anisotropy and thus affect the inversion results. Further interpretations of the retrieved model parameters were therefore restricted to forested areas on south-facing slopes with a maximum steepness of 7°. In an earlier study, tests on the influence of topographic variables using multiple regressions revealed that this approach would sufficiently decouple the topographic effects (Verrelst et al., 2008b). We are therefore

justified in assuming that remaining surface anisotropy is controlled predominantly by canopy structure and density.

Since the curvature of the angular signature strongly depends on the relative proportion of scattering from the overstory and the background, the independently derived canopy cover map was used as a base map for the biophysical evaluation. The canopy cover map was stratified into seven canopy cover classes, starting with 20% and with subsequent increments of 10%. Canopy cover classes lower than 40% are referred to as "sparse", canopy cover classes above 80% are referred to as "dense", and all the intervening canopy cover classes are referred to as "medium dense". No pixels in the 0–20% canopy cover class were included, as most of them occurred along meadow and river edges. The abrupt transition from flat, homogeneous land cover types to more volumetric land cover types is known to significantly impact the horizontal radiation fluxes (e.g. Widlowski et al., 2006). Hence, only pixels within the continuous forest were used for further analysis. As an example, the performance of the RPV inversion using the four viewing angles at 631 nm for these canopy cover classes and the snow covered meadow is shown in Figure 4.6. This figure shows the relationship between the measured CHRIS-HDRF data, the RPV-reconstructed HDRF data, and the canopy cover classes and pure snow pixels taken from the snow-covered meadow field. For the majority of angular measurements a one-to-one relation was found, which emphasizes the good performance of the inversion. The angular measurements that deviated from the one-to-one line tended to be the mid-angular measurements (near-nadir and +34° VZA). This is because not all pixels showed an unambiguous bell or bowl shape, but instead tended to show an irregular curvature, for which the RPV-reconstructed HDRF values optimized a smoother curvature in between the irregular values observed.
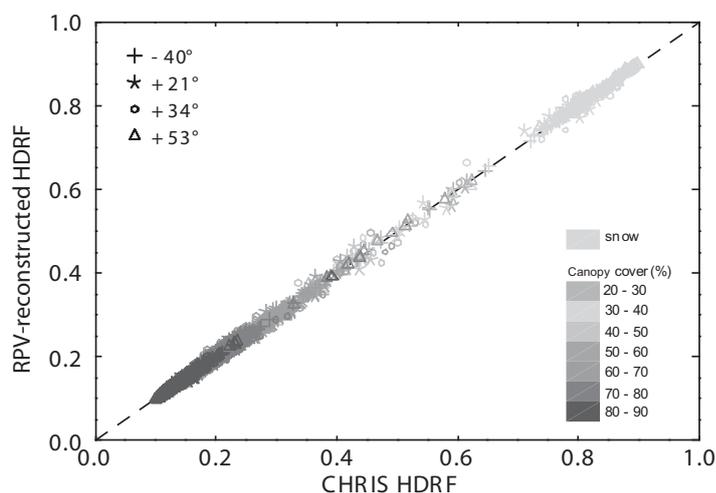
Figure 4.6: Comparison of CHRIS–HDRF and RPV-reconstructed HDRF at 631 nm for various canopy cover classes.

Using canopy cover as a spatial mask, the averaged Minnaert-*k* value was calculated for each wavelength and canopy cover class (Figure 4.7). The figure shows a systematic, gridded

overview of Minnaert-k values plotted for the wavelengths recorded by CHRIS along the x-axis and the canopy cover along the y-axis. Each grid cell represents the averaged Minnaert-k value for a specific cover class and wavelength. For a few grid cells its associated averaged angular signature is illustrated. The column of numbers immediately to the right of the central panel shows the number of pixels in each canopy cover class. Note that 94% of the pixels have a canopy cover of 60% or more. Only very few pixels with low canopy cover ($< 40\%$) are available, potentially weakening the robustness of the results in this range; nevertheless, the dynamics detected are sufficiently comprehensive in this figure.

Figure 4.7 illustrates that the anisotropic spectral behavior is controlled by the interactions between canopy cover and wavelength. The underlying radiative transfer dynamics that control the variations of the gridded Minnaert-k results are further explained with the help of the example figures illustrated in the four panels of Figure 4.8. These figures display the spectral trajectories of the averaged anisotropic reflectance signatures for sparse (*i*: 20–30%), medium dense (*ii*: 40–50% and *iii*: 70–80%) and dense (*iv*: 80–90%) canopy cover classes. As can be observed from figures 4.7 and 4.8, canopy cover essentially determines the importance of vegetated overstory and snow cover relative to the total top of canopy reflectance, and determines the curvature of the angular signature. For example, it controls whether stand HDRFs peak at near-nadir zenith angles (e.g. in case of open canopies) or at higher zenith angles (e.g. in case of closed canopies). Not only the canopy density but also wavelength controls the curvature of the angular signature, and thus the value of the k parameter. This will be demonstrated in the next section.

For almost all canopy cover classes, the signatures at shorter wavelengths are characterized by bell-shaped patterns. Only the sparse canopy cover (see Figure 4.8a: 20–30%) gave rise to bowl-shaped anisotropy patterns. The absorptive properties of the sparse tree cover did not exert sufficient influence to alter the surface-leaving bowl-shaped reflectance field into a bell-shaped field. Instead, this bowl-shape remained unchanged throughout the spectral domain. The uncollided forward scattering of snow cover and – from the red edge onwards – some contribution of multiple scattering due to sparse tree cover led solely to enhanced HDRF values at greater zenith angles. Because of the low amount of pixels, this class should nevertheless be interpreted with caution.
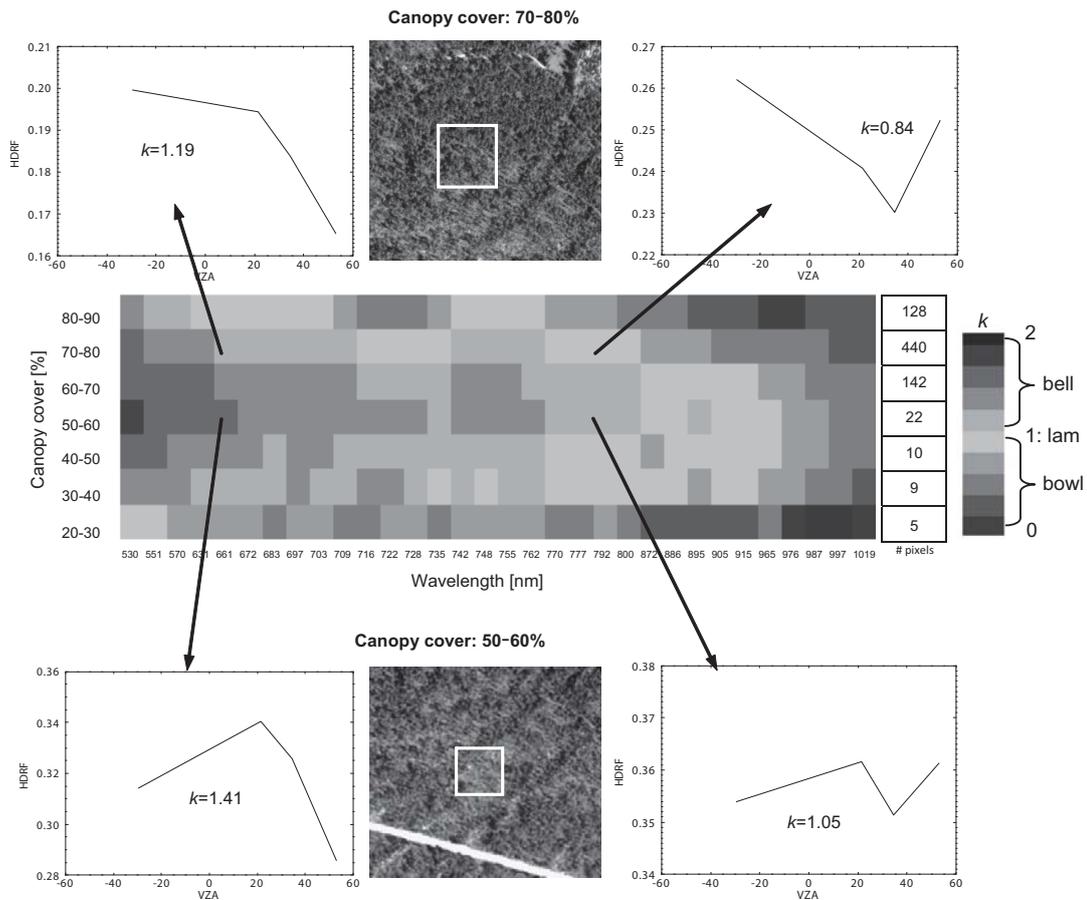
Figure 4.7: Averaged Minnaert-*k* values as a function of canopy cover and wavelength. The number of pixels per canopy cover class is given and some examples of the original angular signatures are shown. The RGB snapshots for a given canopy cover (white square) are derived from an HRSC (High Resolution Stereo Camera) acquisition in summer 2003. (lam= Lambertian)

At denser canopy cover the contribution of uncollided radiation scattered from the bright snow background to the total reflectance is greatest at near-nadir viewing angle and decreases at larger zenith angles as it becomes obscured by the vertical trees, and therefore a bell-shaped reflectance pattern results. Subsequently, when the red edge region is entered, a combination of two independent processes at subpixel level affect the top of canopy reflectance anisotropy: (*i*) a systematic decrease of scattered radiation that exits the snow background, due to increased absorption by snow grains, and (*ii*) an increase in multiple scattering processes that govern the dispersion processes of radiation exiting throughout the canopy. Both processes tend to reduce the bell-shaped pattern: a more absorbing background starts to mimic the reflectance pattern of vegetation, and a high scattering of the foliage will enhance the bowl-shaped pattern. In addition, the degree of canopy openness and background brightness will determine where in the spectral domain a bell-shaped pattern will turn into a bowl-shaped pattern.

These dynamics are clearly illustrated for canopy covers of 40–50% (Figure 4.8b) and 70–80% (Figure 4.8c). Bell-shaped anisotropy signatures are prominently present in the visible spectral region of both cover classes, and even enter the red edge. At a certain wavelength, the bright snow reflectance diminishing due to increasing absorption at longer wavelengths is however no longer able to provide maximum values at smaller zenith angles. Induced by the enhanced multiple scattering processes throughout the canopy, which start to be important from the red edge onwards, high reflectance values at larger zenith angles become dominant: a transition into a bowl shape takes place. This transition will occur quicker at greater tree cover, as then the influence of uncollided radiation from the bright snow background is diminished while the multiple scattering effects are further enhanced. At 40–50% canopy cover a bell-shape holds until the early NIR (762 nm); thereafter, enhanced scattering at larger zenith angles starts to lead to a bowl shape. At denser canopy cover (70–80%), the shift from a bell shape into a bowl shape happens more rapidly, i.e. already at the beginning of the red edge (at 716 nm).

Also, it is noteworthy that, despite the influence of a medium dense canopy cover, the contributing snow reflectance still exerts a strong influence on the spectral anisotropic behavior. This is especially notable for the near-nadir data in the 900 nm region, where reflectance values continue to drop.

At even denser canopy cover (between 80–90%; Figure 4.8d), the tree crowns are so densely packed that the remaining uncollided radiation from the snow background is hardly able to produce a bell-shaped pattern. Only in the green spectral range does sufficient brightness contrast remain between the dark canopy and the bright background. Yet, once the red edge has been entered, the predominantly multiple scattering processes throughout the canopy directly outperform the influence of single scattering from the snow layer and cause a shift to a bowl-shaped pattern.
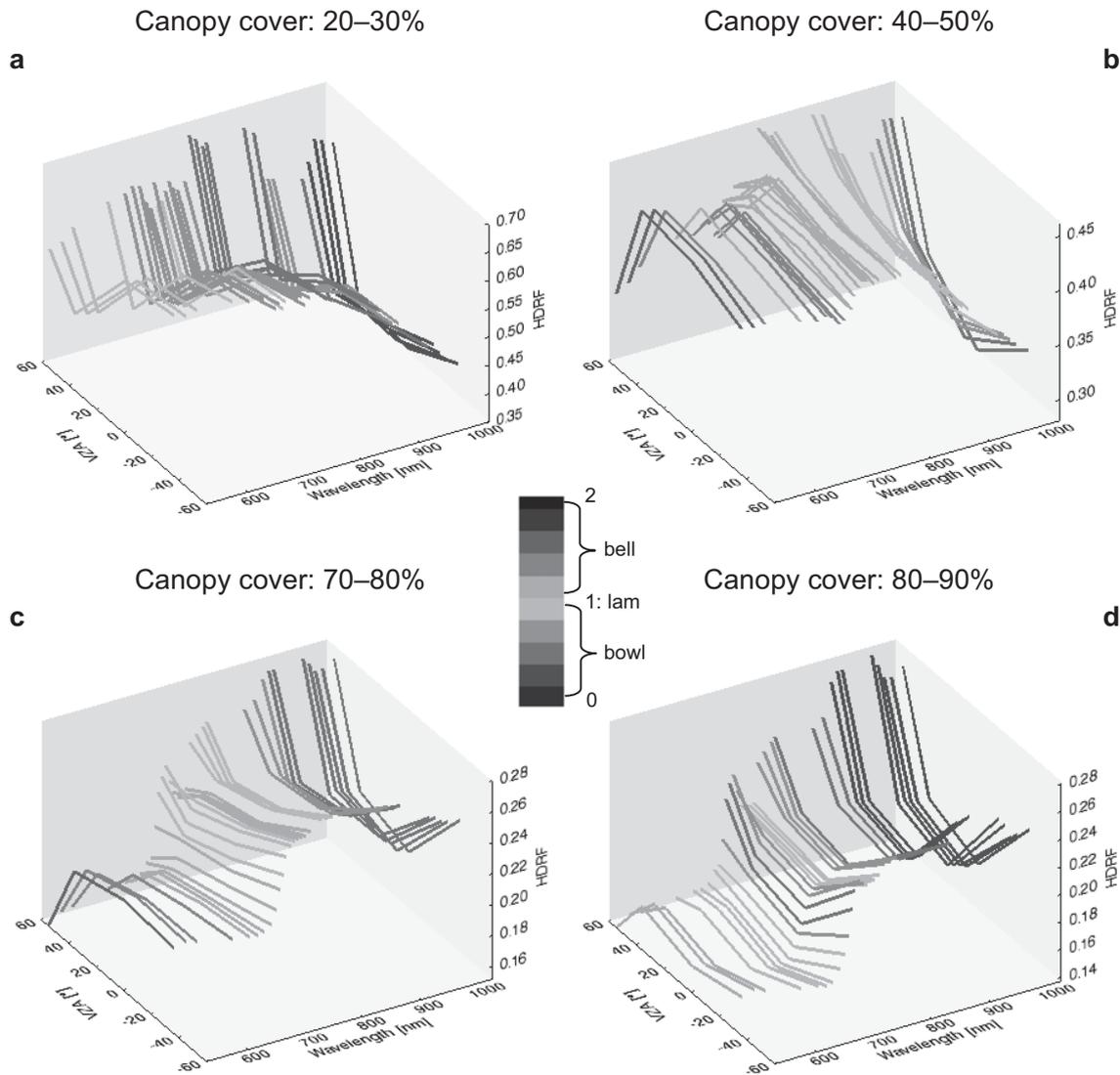
Canopy cover: 20–30%   Canopy cover: 40–50%

Canopy cover: 70–80%   Canopy cover: 80–90%

Figure 4.8: Averaged angular HDRF signatures for 4 canopy cover classes (a: 20−30%; b: 40−50%; c: 70−80%; d: 80−90%) with a color depending on the Minnaert-*k* value. Negative View Zenith Angles (VZA) represent the backscattering directions, positive VZAs represent forward scattering directions (lam= Lambertian).

4.6.3. Applications of Minnaert-k

Many studies have reported that the use of multi-angular data improves assessments of land cover classes and canopy characteristics such as crown cover, tree height, and LAI (Abuelgasim et al., 1996; Bicheron et al., 1997; Braswell et al., 2003; Sandmeier & Deering, 1999; Heiskanen, 2006; Liesenberg et al., 2006; Vuolo et al., 2008). They have also amply demonstrated that multi-angular data provide additional information; however, all these studies are based on a series of angular data and statistical approaches without explicitly separating the directional information content from the spectral information content. The RPV

model is particularly useful for exploring and elucidating the independent contribution of the angular domain. It is a simple model that allows fast decomposition of the scattered radiation into three parameters, of which the Minnaert-*k* parameter relies solely on the curvature of the reflectance anisotropy at a single wavelength. Our work links the RPV's Minnaert-*k* parameter with a subpixel structural heterogeneity variable (canopy cover) at the scale of the CHRIS subpixel resolution over the full VNIR region including the critical red edge region.

In the initial work by Pinty et al. (2002) the use of measurements in the red spectral region was advocated, on the grounds that this is where the subpixel reflectance contrast between the vertical, photosynthetically active coniferous trees and the underlying soil cover is maximized. But this assumes summer conditions, where maximum brightness contrast with vegetation is given by a bright bare soil. In a winter landscape, the influence of the underlying bright snow cover is considerably larger, i.e. significant brightness contrast continues throughout the red edge. This greater brightness contrast led to the transition from bell to bowl shapes moving throughout the red edge towards the early NIR. Our work used multi-angular CHRIS data to bring the findings of earlier theoretical and broadband studies (e.g. Gobron & Lajas, 2002; Pinty et al., 2002; Nolin 2004; Widlowski et al., 2001, 2004) into the field of imaging spectrometry. Given the local character of the data set, the results might be subject to uncertainties related to the atmospheric correction procedure, the generation of the base canopy cover map, and the solar zenith angle. Nevertheless, for a set of χ^2-filtered pixels on the valley floor it has been demonstrated that the bell and bowl shapes of reflectance anisotropy as expressed by the Minnaert-*k* parameter is bounded by physical limitations, both by wavelength as well as by canopy cover. For instance, the bell-shaped patterns dominate throughout the visible region and narrows down to medium canopy cover densities throughout the red edge. Identification of such bell-shaped trajectory for a given overstory canopy and background type along the spectral range may lead to the selection of the most appropriate wavelength for Minnaert-*k* mapping.

As a shift from bell to bowl shape takes place in the red edge and early NIR regions as a function of canopy cover, this is the critical region for characterizing forest heterogeneity under winter conditions. Inspection of Figure 4.7 reveals that for the given conditions, promising results appeared at the end of the red edge (e.g. 735 nm). In this region, blue color tones typically indicate the presence of a heterogeneous surface type such as a forest cover between 40–70%. Red color tones typically indicate the presence of a structurally homogeneous surface, such as either a sparse tree cover up to 40% or a dense tree cover with a canopy cover over 70%. Moreover, as well as indicating canopy cover, the Minnaert-*k* parameter may also act as vertical profiling proxy within a canopy: high k values (>1.0, bell-shaped) indicate the occurrence not only of gap effects, but also of vertical structures within a pixel. For instance, the depth of the bell-shaped curvature for a given canopy cover is additionally controlled by tree height; i.e. tall coniferous trees will result in a more pronounced bell-shaped curvature compared to low-growing plants (e.g. shrubs), because the vertically elongated foliage clumps already obscure the background-leaving radiation at

smaller zenith angles. Conversely, low k values (<1.0, bowl-shaped) characterize pixels in which a vertical profile at the subpixel scale is less marked. This notion of vertical profiling makes the Minnaert-k parameter more distinctive than a canopy cover map; it provides a quantitative indicator of vertical and horizontal heterogeneity at the subpixel scale. Research in this direction was initiated by Widlowski et al. (2001, 2004). Using a ray-tracing radiative transfer model they attempted to relate the Minnaert-k parameter to tree density and height. The relationships found were subsequently tested in a real forest stand using a LiDAR dataset (Koetz et al., 2005). Although multiple solutions did occur for a single k value (an example of the well-known ill-posed problem), canopies with heterogeneity in either horizontal or vertical dimension were successfully discriminated from homogeneous canopies.

Our results coincide with the work of Kayitakire and Defourny (2004) that reflectance anisotropy in the red edge and early NIR region is critical for canopy characterization. These authors reported that the angular signatures of winter temperate forest types not under snow were significantly different at the red edge and NIR wavelengths of CHRIS. They concluded that canopy structure caused these spectral differences, but did not quantify the underlying radiative transfer mechanisms. Progress in this direction was recently made by Rautiainen et al. (2008) by using a radiative transfer model and CHRIS acquisitions during summer. Their modeling results did identify the red edge domain as receiving the largest contribution from forest understory, and revealed that the more oblique the view angle, the smaller the direct contribution from the understory. Our work provides an explanation of the underlying mechanisms, e.g. why a shift in the curvatures of the anisotropy field occurs.

When the brightness contrast between overstory and background is small (e.g. due to understory) variations in angular signatures will nevertheless be more subtle. What will then cause the main differences in reflectance anisotropy is the fraction of sensed shadow cast on the background (Kayitakire & Defourny, 2004). Regardless of the type of background, these studies all suggest that the red edge region has strong potential for linking reflectance anisotropy with subpixel surface heterogeneity (e.g. canopy cover, vertical profiling). Further research needs to be done on the anisotropic behavior of the red edge spectra in relation to biophysical information content. Such research will be of interest for the design of future airborne and space-borne multi-angular sensors.

Despite the good correlations found over flat, forested surfaces, it should be taken into account that several additional factors other than canopy closure are important in shaping the reflectance anisotropy and hence in determining the k parameter. The following potential factors can be identified: (*i*) influence of solar zenith angle (Pinty et al., 2002); (*ii*) multiple targets contributing to a pixel's angular signature, i.e. background other than snow cover beneath the vegetation canopy (e.g. rock outcrops, understory) or snow on trees; (*iii*) snow quality affecting anisotropy patterns (Warren et al., 1998); (*iv*) influence of horizontal radiation fluxes due to the high spatial resolution of CHRIS (Widlowski et al., 2006); (*v*) reduced co-registration quality at greater zenith angles; and, (*vi*) topographic effects, which, although largely decoupled, may still occur (Koetz et al., 2005; Kneubühler et al., 2008). The

topographic effects in particular may complicate the robustness of using the Minnaert-*k* parameter as a bio-indicator, because the presence of topography can lead to enhancement or attenuation of reflectance anisotropy patterns (Schaaf et al., 1994).

To overcome the influence of the horizontal radiation fluxes, an alternative may be to coarse-grain the observations from stand to landscape scale, i.e. by using data from coarser spatial resolution multi-angular sensors such as MISR (275 m in red). With the use of MISR data the influence of horizontal radiation fluxes will be exceeded by the influence of the vertical fluxes of the larger surface covered by a pixel (Widlowski et al., 2006). However, with MISR data not only variation in canopy cover but also variation in topography and additional land cover types (e.g. rocks, roads, rivers) governs reflectance anisotropy at the sensor subpixel scale. Then the subtle variations in anisotropy patterns invoked by vegetation structure tend to be outperformed by the landscape-scale variations in reflectance anisotropy (e.g. due to riverbeds) (Pinty et al., 2002).

The fact that the red color tones in Figure 4.7 (bowl-shaped anisotropy patterns; $k < 1.0$) either represent an open snow-covered surface or a dense canopy cover poses another constraint to the interpretation of *k* values. To overcome this constraint, an option would be to combine the Minnaert-*k* map with the spectral dimension of the RPV model (e.g. the amplitude parameter) so that vegetation spectra can easily be discriminated from the snow spectra. Another option is to combine the Minnaert-*k* map with an independently derived canopy cover map. Spectrodirectional CHRIS data are particularly useful for generating both kinds of maps, e.g. by applying LSU in the spectral domain and Minnaert-*k* retrieval in the directional domain. Merging both products may yield subpixel information beyond what is possible from single-source datasets.

4.7. Conclusions

So far, there has been no widespread development of applications making use of both the angular and spectral domains. This paper links anisotropic reflectance signatures of a forested surface as observed from space with forest 3D-heterogeneity at subpixel scale in the spectral domain. We used spectrodirectional CHRIS data to elaborate the exploitation of reflectance anisotropy and more specifically addressed the spectral dependency of the Minnaert-*k* parameter as measured over a coniferous forest. CHRIS images of a coniferous forest acquired during winter were found particularly useful for evaluating the underlying biophysical information content embedded in the angular domain. The Minnaert-*k* parameter pixelwise mapped variation in anisotropic reflectance of the forest vegetation across the CHRIS bands. For the set of pixels analyzed, a spectrally-driven transition in reflectance anisotropy emerged: from predominantly bell-shaped anisotropy patterns in the visible spectral region towards predominantly bowl-shaped anisotropy patterns in the NIR spectral region. Due to the underlying bright snow cover, the transition from bell to bowl shape for heterogeneous canopies with a canopy cover between 30–80% was found somewhere in the

red edge region: the exact spectral position of the switch from bell to bowl shape was controlled by canopy cover. At 735 nm, medium canopy cover (40–70%) typically led to bell-shaped anisotropy patterns, while canopy covers that were sparse or dense typically led to bowl-shaped reflectance anisotropy patterns. In turn, when the background is less bright than snow cover, then the switch from bell to bowl shape is expected to occur earlier in the spectral domain due to a reduced brightness contrast. Further research is required to evaluate the inherently embedded biophysical information content of reflectance anisotropy in the full spectral domain under non-snow conditions, e.g. during summer. In addition, further attempts should be made to link subtle variations in canopy reflectance anisotropy with more specific structural parameters, such as crown diameter and tree height.

Acknowledgements

Chapter 5

Merging the Minnaert-*k* parameter with spectral unmixing to map forest heterogeneity with CHRIS/PROBA data

Jochem Verrelst, Jan G.P.W. Clevers, Michael E. Schaepman

Merging the Minnaert-*k* parameter with spectral unmixing to map forest heterogeneity with CHRIS/PROBA data

Abstract

CHRIS (Compact High Resolution Imaging Spectrometer) mounted onboard the PROBA (Project for On-board Autonomy) spacecraft is capable of sampling reflected radiation at five viewing angles over the visible and near-infrared regions of the solar spectrum with high spatial resolution. We combined the spectral domain with the angular domain of CHRIS data in order to map the surface heterogeneity of an Alpine coniferous forest during winter. In the spectral domain, linear spectral unmixing of the nadir image resulted in a canopy cover map. In the angular domain, pixelwise inversion of the Rahman–Pinty–Verstraete (RPV) model at a single wavelength at the red edge (722 nm) yielded a map of the Minnaert-*k* parameter that provided information on surface heterogeneity at subpixel scale. However, the interpretation of the Minnaert-*k* parameter is not always straightforward, because fully vegetated targets typically produce the same type of reflectance anisotropy as non-vegetated targets. Merging both maps resulted in a forest cover heterogeneity map, which contains more detailed information on canopy heterogeneity at the CHRIS subpixel scale than is possible to realize from a single-source data set.

Keywords*: hyperspectral, multi-angular, CHRIS, reflectance anisotropy, forest heterogeneity mapping

5.1. Introduction

The measured reflected solar radiation of boreal and Alpine forests under winter conditions depends on the wavelength and the proportions of snow cover and plant canopy cover detected by a sensor (Vikhamar and Solberg, 2003). These proportions depend on illumination and viewing angle, topography, and structural canopy properties such as tree density, canopy geometry, and gap fraction. Consequently, the reflected radiation can be sampled by a space-borne optical sensor either in the spectral domain, i.e. at multiple wavelengths, or in the angular domain, i.e. at various viewing angles, or as a combination of both. Though the inferring of information on the terrestrial surface from reflectance data sampled in the spectral domain has been extensively studied in the last forty years, e.g. through image classification (Lu and Weng, 2007; Muñoz-Marí et al., 2007), spectral vegetation indices (Glenn et al., 2008; Haboudane et al., 2008), surface reflectance models (e.g. Verhoef, 1984; Verstraete et al., 1993), or spectral mixture analysis (e.g. Roberts et al., 1993), considerably less research has been done on exploiting reflectance data sampled in the angular domain for mapping applications (Diner et al., 2005; Schaepman, 2007; Chopping et al., 2008).

With the advent of multi-angular Earth observing sensors (Diner et al., 1999; Barnsley et al., 2004) and the development of surface reflectance models (e.g. Verhoef, 1984; Verstraete et al., 1993), physically-based attempts were undertaken to retrieve canopy characteristics from multi-angular reflectance data. Among the surface reflectance models, the Rahman–Pinty–Verstraete (RPV) parametric model (Rahman et al., 1993) is particularly suitable for estimating reflectance anisotropy, because it simulates the bidirectional reflectance distribution function (BRDF) of an arbitrary land surface on the basis of three parameters. Of these parameters, the k parameter is of particular interest as it describes most of the angular variation related to surface reflectance anisotropy (Pinty et al., 2002). Pinty et al. (2002) theoretically demonstrated that the Minnaert-k parameter contains information on subpixel heterogeneity, particularly when a low solar zenith angle is present in combination with a bright background. Their work has been corroborated by other studies, e.g. on forest areas underlain by a snowpack (Nolin et al., 2004; Koetz et al., 2005; Verrelst et al., 2010b).

In 2001, the European Space Agency (ESA) launched the experimental satellite sensor CHRIS (Compact High Resolution Imaging Spectrometer) onboard the PROBA (Project for On-board Autonomy) spacecraft. The imaging spectrometer captures quasi-instantaneously a series of five angular images of a terrestrial surface at a high spatial resolution (~17 m) during the same orbit. CHRIS is capable of sampling the anisotropic behavior of the reflected solar radiation in up to 62 narrow spectral bands over the visible and near-infrared (VNIR) regions of the electromagnetic spectrum (400–1050 nm) (Barnsley et al., 2004; Duca & Del Frate, 2008).

To ascertain the capability of CHRIS for measuring reflectance anisotropy in the VNIR, an old-growth alpine forest stand in the Swiss Alps was chosen as a test site (Schaepman et al.,

2004). It was overflown by CHRIS/PROBA on March 17, 2007. On this day, the snow had melted from the tree canopy but the forest floor was still covered by a thick pack of snow, which spectrally simplified the image: dark overstory vegetation underlain by a bright snow-covered background. The concurrent spectrodirectional (combined spectral and multi-angular) observations of a spectrally simplified landscape at a high spatial and spectral resolution makes it possible to explore the spatial, spectral and angular information content of spectrodirectional measurements to the fullest.

In the spectral domain, a widely applied technique is linear spectral unmixing (Plaza et al., 2004). It works particularly well in discriminating vegetation from snow cover, thereby generating a canopy cover map (Verrelst et al., 2010b). Canopy cover is defined as the percentage (from 0–100%) of a grid cell that is covered by a vegetation canopy. Linear unmixing techniques, however, are unable to provide information on the vertical distribution or 3D distribution of canopy cover, so cannot reveal whether the canopy cover is of tall trees or short vegetation.

In the angular domain, a simple technique for obtaining information on surface reflectance anisotropy is retrieval of the Minnaert-k parameter from the RPV model. Although the Minnaert-k parameter makes it possible to map variations in subpixel heterogeneity, the interpretation of the parameter is limited by various factors, such as the parameter's dependence on solar zenith angle, background brightness, and topography (Pinty et al., 2002; Koetz et al., 2005). Further, the practical applicability of the Minnaert-k parameter is not always straightforward. Surfaces that behave radiatively like turbid media (typically they are homogeneous surfaces, either fully vegetated or non-vegetated surfaces) result in a bowl-shaped reflectance anisotropy pattern (Pinty et al., 2002), and thus cannot be directly discriminated from each other. A possible way to overcome this and to improve forest heterogeneity mapping is to merge Minnaert-k information with the information content obtained from the spectral domain. The two aims of the study we describe here were therefore 1) to merge the Minnaert-k map with a spectrally-derived canopy cover map, and 2) to ascertain whether the resulting map contains more valuable information related to canopy structure at the CHRIS subpixel scale than the single-source maps.

5.2. Biophysical interpretation of Minnaert-*k*

The RPV model provides a description of the target's reflectance anisotropy, without attempting to assign it to specific physical causes or processes. As such, it is an empirical and efficient parametric representation of that surface property (Rahman et al., 1993; Pinty et al., 2002). The RPV model splits the scattered radiation field for a given wavelength into a scalar amplitude component and an associated directional component describing the anisotropy of the surface (Rahman et al., 1993; Pinty et al., 2002). The directional component of the reflectance function is expressed as the product of three functions: (*i*) the modified Minnaert function k that controls the curvature (e.g. the degree of convexity or concavity), (*ii*) a

parameter that controls the degree of forward and backward scattering regimes, and (*iii*) an optional hotspot descriptor function. The underlying algorithms for each of the parameters are documented in (Rahman et al., 1993; Pinty et al., 2002).

Under favorable conditions of illumination and background brightness, the angular pattern is largely controlled by the physical properties and geometrical arrangements of the plant elements that constitute the terrestrial surfaces (Pinty et al., 2002). This means that the angular signature of a pixel at a single wavelength as measured by a multi-angular sensor can be diagnostic for the assessment of subpixel structural surface properties when there is sufficient difference in brightness between the overstory and background.

Coniferous forests commonly appear darker than deciduous forests, due to the strong internal shadowing caused by clumping effects and the relatively high light absorption capacity of needle foliage (Smolander & Stenberg, 2003). In coniferous stands in winter the following situations can occur: a surface that is brighter at large oblique viewing angles in forward and backward scattering directions leads to a "bowl-shaped" reflectance anisotropy pattern. A bowl-shaped anisotropy pattern results in a k value smaller than 1. This is a common situation for more homogeneous surface covers. Conversely, a surface that is brighter at nadir viewing angle than at oblique viewing angles leads to the inverse pattern: a "bell-shaped" reflectance anisotropy pattern. A bell-shaped anisotropy pattern results in a k value larger than 1. This is a common situation for open, vertically elongated canopies with a bright background. Finally, a surface that exhibits Lambertian reflectance, i.e. the amount of scattered radiation is the same in all directions, results in a k value of 1 (Pinty et al., 2002).

The Minnaert-k parameter can thus be used as a bio-indicator for canopy heterogeneity simply on the basis of canopy closure and fluctuations in the amount of scattering and absorbing material at one specific wavelength (Pinty et al., 2002; Nolin, 2004; Verrelst et al., 2010b). While k values in excess of 1 are generated by targets that exhibit vertical structures and 3D effects, k values less than 1 are typically associated with targets that behave radiatively like turbid media. As a result, the k parameter is of limited use for discriminating homogeneous surface covers (e.g., it may characterize either very sparse or very dense canopy covers).

To overcome this limitation and to improve subpixel heterogeneity mapping, we proposed to combine the Minnaert-k parameter to canopy cover derived from the spectral domain. Kayitakire and Defourny (2004) concluded that in forested landscapes, the horizontal arrangement of the trees and the stand density influence the angular component of the reflectance more than tree height and diameter. The contribution of the background brightness is another crucial factor in governing the shape of reflectance anisotropy (Pinty et al., 2002). It therefore seems logical to derive a canopy cover map and combine that with the Minnaert-k map. Since illuminated snow and conifer tree crowns are spectrally highly separable, we used linear spectral unmixing (LSU) of the spectral dimension of the nadir CHRIS data for this purpose.

5.3. Methodology

5.3.1. Test site and CHRIS data

An Alpine valley, the Ofenpass valley, located in the Swiss National Park, South East Switzerland (10°13′48″E/ 46°39′45″N), was chosen as test site. The valley is characterized by a coniferous old-growth forest and patches of Alpine meadow. The forest can be classified as woodland associations of the *Erico-Pinetum mugo* type typified by relatively open and discontinuous stands. The forests vary in topography, openness, tree clumping, leaf area index (LAI) and woodiness. The south-facing valley floor of the Ofenpass valley was considered to be the core test site (Figure 5.1).
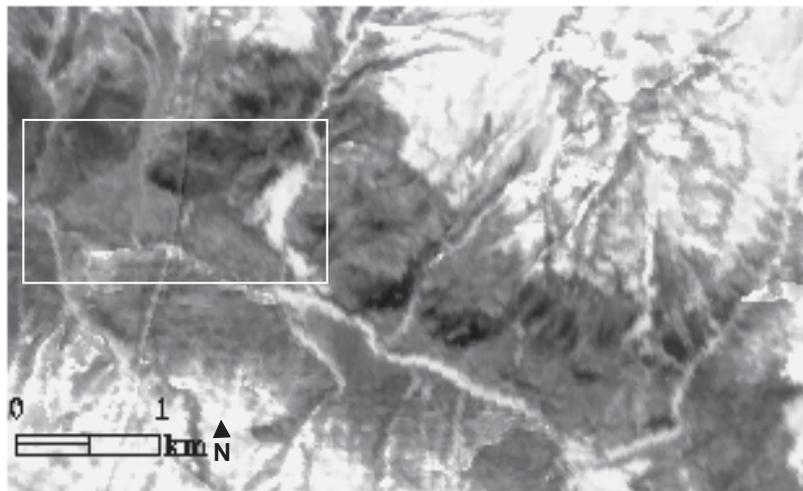
Figure 5.1: Subset of the geometrically and atmospherically corrected CHRIS nadir scene acquired over the Swiss National Park study site on March 17, 2007. The Ofenpass valley stretches from top left to bottom right of the image. The whitish parts are snow-covered meadow fields or mountaintops. The square marks the core test site.

A series of CHRIS mode 5 "land" images was acquired over the Swiss National Park on March 17, 2007, near noon local time (11:34h local time; sun zenith: 50°, azimuth: 161°) under cloud-free conditions. Mode 5 is configured in CHRIS's best spatial resolution (nominally ~17 m) and spectral resolution (37 narrow bands with bandwidths of 6–33 nm located between 438 nm and 1036 nm). The acquisition date was chosen to ensure that a carpet of snow was still present while the sun position was already acceptably high at noon for the purpose of Minnaert-*k* retrievals. The solar position can be regarded as constant for all five CHRIS Fly-by Zenith Angles (FZA), since the images are instantly recorded during the satellite overpass. In the current along-track pointing configuration, the FZA is equivalent to the nominal viewing angles (0°, ±36°, ±55°). Due to its narrow field of view (FOV), however, CHRIS is only occasionally able to acquire a target at nominal viewing angle. PROBA must be tilted so that the target area falls within the sensor FOV. This means that the actual observation angles at which the images are acquired may deviate from the nominal viewing angles. For example, the nominal nadir camera position appeared to be pointing in a forward

view zenith angle of +21°. A subset of the near-nadir image of the Ofenpass valley overpass is depicted in Figure 5.1. The dark areas in the figure are the forest vegetation; the white patch within the dark forest represents a snow-covered meadow. Snow on the branches of the trees had melted, so in this case, "snow-covered forest" refers to snow covering the ground but not the trees.

Unfortunately the backward-pointing –55° view zenith angle just missed the test site. The angular CHRIS scenes of the remaining four images were geometrically corrected following an approach for rugged, mountainous terrain (Kneubühler et al., 2005) and were subsequently atmospherically corrected using a freely available MODTRAN-based procedure implemented in the BEAM toolbox (http://www.brockmann-consult.de/beam) that has been specifically developed for correcting CHRIS images (Guanter et al., 2005a). The end-to-end module simultaneously derives a set of calibration coefficients and an estimation of water vapor content and aerosol optical thickness from the data themselves. The preprocessing efforts resulted in geometrically corrected images of hemispherical-directional-reflectance-factor (HDRF, see Schaepman-Strub et al., 2006 for terminology used) data at a spatial resolution of 18 m. We did not include the bands in the blue part of the spectrum (442 and 489 nm) in our analysis, because of significant atmospheric scattering in the blue bands of CHRIS (Guanter et al., 2004). The bands close to the atmospheric water vapor absorption band at 940 nm (CHRIS bands at 925, 940 and 955 nm) were also omitted from further analysis.

5.3.2. Spectral and angular information

In the spectral domain, the reflectance of a pixel can be described by a spectral mixture model in which a mixed spectrum is represented as a linear combination of pure vegetation and snow spectra (Eq. 5.1 & 5.2):

$$R_i = f_{vegetation} \cdot R_{i,vegetation} + f_{snow} \cdot R_{i,snow} + \varepsilon_i \tag{5.1}$$

under the constraint $f_{vegetation} + f_{snow} = 1$ and $f > 0,$ (5.2)

where $f_{vegetation}$ and f_{snow} are the fractions of vegetation and snow in the pixel studied, R_i the reflectance of a pixel in band i, $R_{i, vegetation}$ ($R_{i, snow}$) the reflectance of the vegetation (snow) endmember in band i, and ε_i the residual error associated with band i. The full spectral domain (excluding the bands we had removed) was used to decompose the near-nadir image into fractions of these two endmembers. Hence the LSU quantified the subpixel spectral contributions of canopy and underlying snow solely on the basis of mono-angular, near-nadir spectral measurements. The unmixing approach for the forest site was accompanied by uncertainty, expressed by the root mean square error (RMSE). Due to the spectrally simplified landscape the RMSE values were consistently low (around 0.016). The results of the unmixing were compared with ground reference data collected following the VALERI

protocol during the Fire Spread and Mitigation (SPREAD) campaign (Kötz et al., 2004; Morsdorf et al., 2004). Consistent results were obtained by LSU, though the canopy cover was systematically overestimated by about 8% by comparison with the ground reference data. The canopy cover map was subsequently stratified into canopy cover classes with increments of 10%, starting from 0% (full snow cover).

In the angular domain, reflectance anisotropy was quantified by means of the Minnaert-k parameter. Pixelwise retrieval of the Minnaert-k parameter through RPV model inversion was achieved using the RPVinversion-3 software package (Lavergne et al., 2007). The inversion method is documented in (Gobron & Lajas, 2002). The inversion method is documented in [31]. The package offers a number of features, including the complete assessment of the measurement-model mismatch covariance matrix and the option of operating adjoint software codes derived from automatic differentiation techniques. This allowed us to perform the inversion of the nonlinear RPV model under the classical Bayesian approach in a numerically and computationally efficient manner, while at the same time generating an unbiased estimation of the probability density functions for the parameters retrieved. The package implements the inverse model for two versions of the model, with or without the hotspot parameter. The hotspot parameter is only required to improve the representation of the hotspot when illumination and observation geometries close to the hotspot are present. In the observed winter scene of CHRIS, this configuration was not of importance. The RPV inversion-3 package thus resulted in sets of RPV parameters and additional information on the accuracy of the fit expressed by the χ^2-statistic. Minnaert-k maps were generated on a pixel-by-pixel basis across all the used CHRIS wavelengths. Using canopy cover classes as a spatial mask, averaged Minnaert-k values were calculated per class across the CHRIS bands. In this way the Minnaert-k parameter can be systematically related to wavelength and canopy cover.

The Minnaert-k maps across the CHRIS bands and the canopy cover map were subsequently used to select the wavelength at which the best relationship between both data sources can be established. Given that low Minnaert-k values ($k < 1$) are expected at both very sparse and dense canopy covers (homogeneous surface covers), and high values ($k > 1$) at medium dense covers (heterogeneous surface covers), we expected a quadratic trend. It has been demonstrated that given a bright background, a switch from bell to bowl shape is most likely to occur somewhere in the red edge (Verrelst et al., 2010b). CHRIS in mode 5, with its eight bands in the red edge, provides an excellent basis for selecting an appropriate wavelength. We based the selection of the wavelength at which the best relationship between canopy cover map and Minnaert-k map occurred on the Pearson's squared correlation coefficient of the quadratic-polynomial fit and an F-test to test the significance of the relationships.

The advantage of CHRIS is that its multidimensionality can be exploited to map forest cover heterogeneity at the CHRIS subpixel scale. Spectrodirectional CHRIS data are particularly useful for generating two kinds of maps: in the angular domain the data allow Minnaert-k retrieval to be applied for a given wavelength by inverting the RPV model,

whereas in the spectral domain the data allow LSU to be applied for a given viewing angle. We then merged both independently-derived maps (LSU$_{RGB}$ + Minnaert_k_{RGB}) / 2, to create a new data layer. In addition, the original horizontal and vertical color bars associated with the canopy cover and Minnaert-k maps were likewise converted to an RGB representation and merged to a 2D legend with canopy cover in the *x* direction and Minnaert-k in the *y* direction (cf., Figure 5.8B).

5.4. Results and discussion

5.4.1. Linear umixing

The canopy cover map generated from the nadir spectral domain is displayed in Figure 5.2. Its frequency distribution is displayed in Figure 5.3. The white spot on the right represents a snow-covered meadow. The histogram shows that only a few pixels with low densities ($< 40\%$) were present, usually at the edge of the meadow and as gaps within the forest. The histogram also indicates that the canopy cover in most of the pixels is between 60 and 90%, which is typical for an Alpine forest stand (see Figure 5.3). About 14% of the pixels represent other situations: a snow-covered meadow (middle right in Figure 5.2), riverbeds (striped patterns), and gaps within the forest. However, whereas the canopy cover map shows spatial variations in proportion of tree cover, the map is unable to indicate the surface heterogeneity at subpixel level.
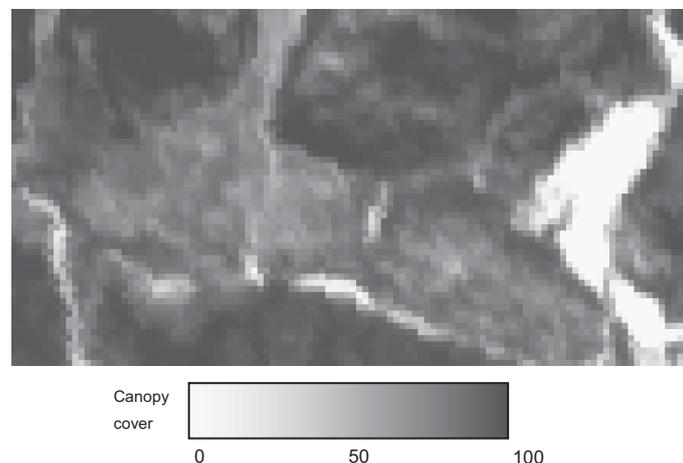
Figure 5.2: Map of canopy cover based on constrained LSU of the nadir CHRIS image of March 17, 2007.
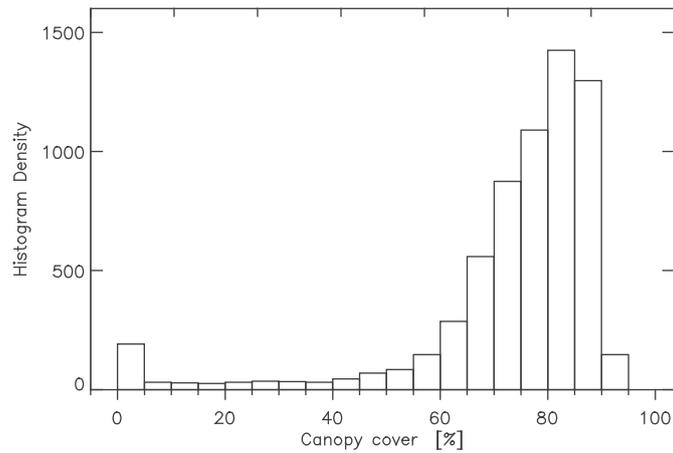
Figure 5.3: Histogram of the canopy cover map based on constrained LSU of the nadir CHRIS data.

5.4.2. Minnaert-k retrieval

Pixelwise inversion of the RPV model generated maps of Minnaert-*k* values across the CHRIS bands. In an earlier paper (Verrelst et al., 2010b) we demonstrated some relationships between Minnaert-*k*, wavelength and canopy cover for the forest stands for a limited number of pixels on the valley floor (slope < 7°). These relationships were again tested, but now for the whole region (Figure 5.4). This figure shows a systematic, gridded overview of averaged Minnaert-*k* values for the wavelengths recorded by CHRIS along the *x*-axis and the canopy cover classes along the *y*-axis. This overview enables us to track the specific spectral trajectory of the Minnaert-*k* parameter for each canopy cover class.
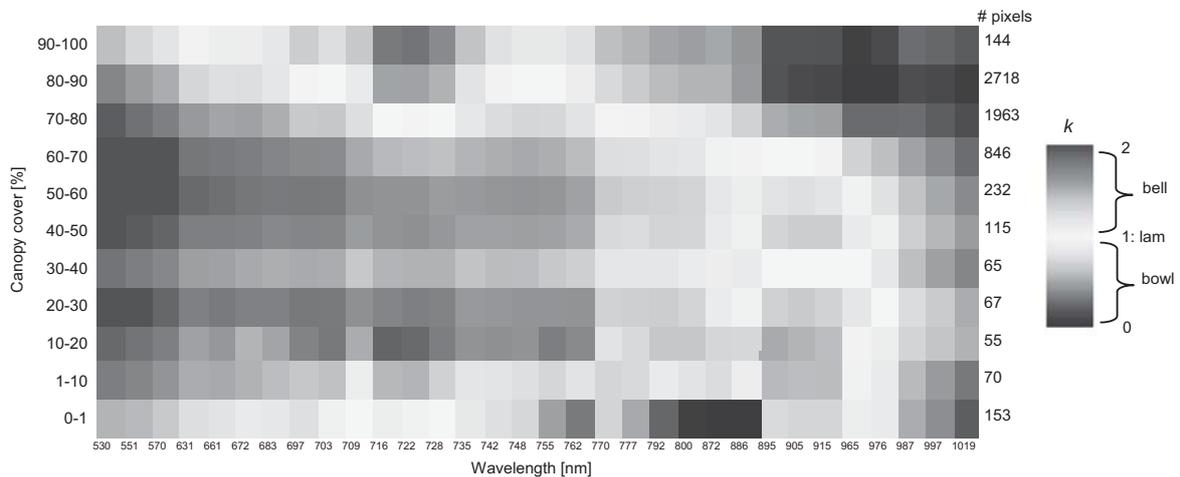
Figure 5.4: Averaged Minnaert-k values as a function of canopy cover and wavelength. The numbers on the right represent the number of pixels for each class (lam= Lambertian).

Although the Minnaert-*k* parameter is a semi-empirical parameter, Figure 5.4 shows that the bell-shaped and bowl-shaped reflectance anisotropies depend on both canopy cover and wavelength. For instance, the bell-shaped domain dominates throughout the visible region and

narrows down to medium canopy cover densities throughout the red edge and early NIR. Since reflectance anisotropy switches from bell shape to bowl shape in the red edge and early NIR as a function of canopy cover, it provides the critical spectral region for characterizing stand heterogeneity under winter conditions. The white color tones indicate the turning point from bell to bowl shape. For an exhaustive description of the underlying wavelength-dependent mechanisms related to land cover and sun-target-sensor geometry, see (Verrelst et al., 2010b). The R^2 results of the quadratic regression model between canopy cover and Minnaert-k across the CHRIS bands for the complete data set yielded a best correlation at 722 nm (R^2 of 0.43). The relationship between the canopy cover map and the Minnaert-k map at 722 nm is shown in the scatter plot of Figure 5.5. Although the relationship was significant ($F_{2,6433} = 2405$, $p < 0.0001$), the low R^2 indicates that canopy cover is not the only variable determining reflectance anisotropy. This is particularly the case for pixels with canopy covers less than 60%, where no clear pattern can be observed. Most of these pixels with sparse forest cover are found at the interface between forest cover and snow-covered meadow or on the riverbeds. At these locations, edge effects and the position of the edge in relation to the sun may yield varying anisotropy effects. Another explanation for the low R^2 is the influence of topographic effects. For pixels with > 60% canopy cover the relationship between Minnaert-k and canopy cover is more obvious.
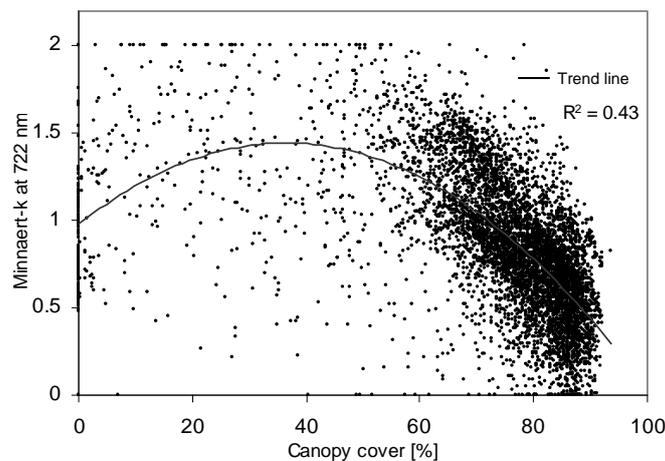
Figure 5.5: Scatter plot of canopy cover against Minnaert-k at 722 nm. Trend line: $p < 0.0001$.

The Minnaert-k map at this wavelength is shown in Figure 5.6. Whitish-blue color tones indicate the presence of a heterogeneous surface type such as open to medium dense forest stands with a cover density of up to 70%. Reddish-white color tones indicate the presence of a structurally homogeneous target such as a dense tree cover or a snow-covered meadow. Reddish-white patterns are to be found over the forest stands (e.g. the middle of the figure) but also over the snow-covered meadow (to the right). Such ambiguity of bowl-shaped patterns makes it hard to interpret this map for forest monitoring applications. Although forest cover predominantly exhibited enhanced reflectance patterns in backscattering direction (with maximal backscatter at -36° zenith angle, which approaches closest the hot spot) and snow

cover predominantly exhibited enhanced reflectance patterns in the forward scattering direction (due to its specular component), both land cover types yielded a bowl-shaped reflectance anisotropy pattern ($k<1$). Therefore, from the generated Minnaert-k map it is impossible to discern forest cover from non-forest cover. In addition, at a pixel size of 18 m, pixels with sparse forest cover at near-nadir may either lead to low k values (e.g. at the meadow) or high k values (e.g. at the riverbed). In the latter locations, reflectance anisotropy is strongly influenced by the volumetric contribution of the adjacent pixels, e.g. if adjacent pixels represent a dense forest cover then lower reflectance values at larger viewing angles are observed due to a partly pixel overlapping in comparison to the near-nadir observation and so leading to a bell-shaped curvature (high k values). In case an irregular curvature is observed, the RPV inversion-3 package has been optimized to fit a smoother curvature in between the irregular values. The provided χ^2-statistics provide information how close the fit matches the observations of the four CHRIS viewing angles. At 722 nm 7.3% of the pixels led to a mismatch at a significance level of 0.05, mainly due to irregular reflectance anisotropy curvatures occurring on the meadow and riverbeds.

Figure 5.6: Minnaert-k parameter obtained by RPV model inversion at 722 nm (lam= Lambertian).

From Figure 5.6 it is obvious that apart from vegetation structure two spatial factors affect reflectance anisotropy at the CHRIS subpixel scale: (*i*) interfaces between land covers of contrasting volumetric compositions (e.g. forest–meadow interface, riverbeds, road intersections); and (*ii*) topography: variation in slope gradient and aspect, and the related variation in topographic shadowing. Both factors lead to the enhancement or attenuation of reflectance anisotropy patterns. The histogram related to the data in Figure 5.6 has a normal distribution (Figure 5.7), with a peak towards Minnaert-k values of 0.8 (small bowl-shaped pattern). Compared with the histogram of the canopy cover map (Figure 5.3), the pattern is very different: the distribution has a wider spread, underlining that the spectral and angular domains are to a great extent independent of each other.
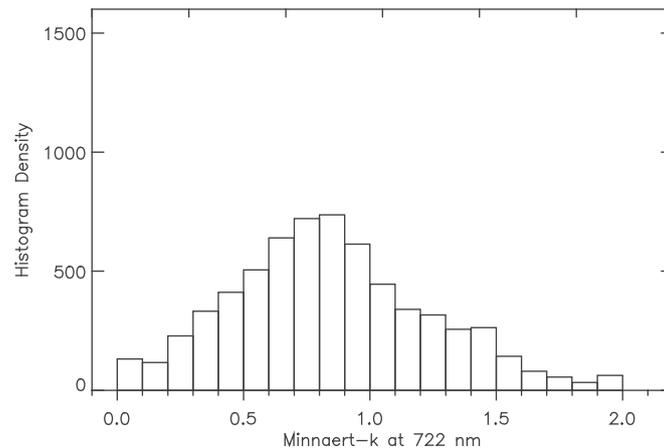
Figure 5.7: Histogram of the Minnaert-*k* map inferred from the RPV model and angular CHRIS data at 722 nm.

5.4.3. Merging

The merging of the canopy cover map with the Minnaert-*k* map is displayed in panel A of Figure 5.8. In this merged map not only is the snow-covered meadow (whitish color tones) clearly separated from the forest cover (greenish color tones), but also subtle color tones related to subpixel heterogeneity appear. The biophysical meaning of these color tones is explained in the 2D color chart of panel B in Figure 5.8.

In the 2D color chart all possible color tone combinations of Minnaert-*k* and canopy cover are displayed: canopy cover along the *x*-axis (generated from the spectral domain), Minnaert-*k* along the *y*-axis (generated from the angular domain). In the RGB color scheme, the green color represents the degree of canopy cover. The red color represents the degree of bowl-shaped reflectance anisotropy, whereas the blue color represents the degree of bell-shaped reflectance anisotropy. A pixel can either exhibit a degree of bowl-shape (red) or of bell-shape (blue). Briefly, the four corners of the 2D color legend, representing the extreme situations that may theoretically occur, are:

I.   *Pale blue color tones:* no canopy cover and maximal bell-shaped reflectance anisotropy. This is an unusual situation, since subpixel heterogeneity is required to obtain a high Minnaert-*k* value, i.e. there must be some vegetation cover. However, some pixels at the meadow–forest interface approximate this situation due to the abrupt cessation of the vertically-elongated canopy. For instance, while from the nadir viewing angle on a meadow edge no more forest cover is observed, it may happen that at a larger view zenith angle some forest cover can still be observed.

II. *Dark bluish–green color tones:* maximal canopy cover and maximal bell-shaped reflectance anisotropy. This is also an unusual situation, since a full cover behaves radiatively like turbid media, i.e. the canopy is so densely packed that no uncollided radiation exits the background snow cover to create a bell-shaped pattern. However, as soon as gaps appear in the cover (canopy cover < 100%), bell-shaped patterns occur.

This situation is observable for the pixels with the bluish-green color tones in Figure 5.8 (panels A and C).

III. *Dark reddish–green color tones:* maximal canopy cover and maximal bowl-shaped anisotropy. This is a typical situation due to the homogeneous character of the dense canopy. Patches of dense forest cover are observable in Figure 5.8 (panels A and C).

IV. *Pale reddish color tones:* No canopy cover and maximal bowl-shaped anisotropy. This typically occurs on non-vegetated surfaces such as the snow-covered meadow.
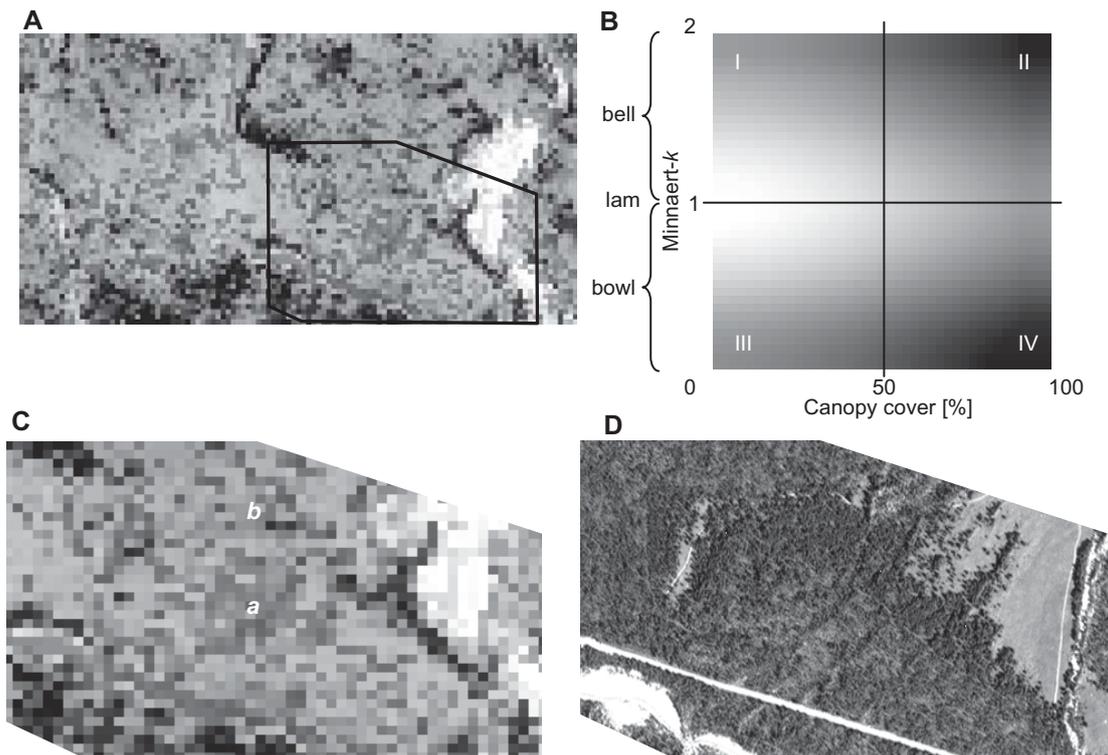
Figure 5.8: A) The RGB result of merging the Minnaert-*k* map with the canopy cover map. B) 2D color chart based on the color bar of the canopy cover map (*x*-axis) and the color bar of the Minnaert-*k* map (*y*-axis) (lam=Lambertian). C) Zoom-in of the merged map as presented in panel A. D) The reference image as derived from a high resolution stereo camera (HRSC) acquisition in summer 2003 (true color).

As the canopy cover map solely provides fractions but no information about heterogeneity and the Minnaert-*k* map provides information on subpixel surface heterogeneity, the merged map provides information on both these attributes. The map shows that most of the pixels are situated between canopy covers of 60% and 90% and a Minnaert-*k* fluctuating between 0.3 and 1.5. Consequently, the pixels with bluish-green color tones refer to medium to dense forest cover with large subpixel heterogeneity ($k > 1$). See, for instance, region *a* in panel C of Figure 5.8: here more subtle variation in color tones is observable than in the canopy cover map of Figure 5.2. The spatial pattern observed is thus not only due to variation in canopy cover but also to variation in other parameters impacting reflectance anisotropy, such as tree height. Although tree height may be a less influential factor than canopy cover (Kayitakire &

Defourny, 2004), note that if the canopy cover consists of low-growing shrubs, then the variation in anisotropy would be smaller (Koetz et al., 2005; Widlowski et al., 2004), leading to paler bluish color tones. The pixels with dark bluish–green color tones typically represent areas with large, dark vertical structures (trees) in conjunction with open targets (i.e. gaps). Conversely, the pixels with dark reddish–green color tones ($k < 1$) refer to dense forest covers that behave radiatively like turbid media and thus lack subpixel heterogeneity. That is for instance the case for region *b* in panel C of Figure 5.8. This region shows a canopy cover in which the canopy is so dense that it imposes a typical bowl-shaped anisotropy pattern. Tree height does not play a role here; the same type of bowl-shaped pattern occurs over homogeneous, flat targets (i.e. snow-covered meadow). Also of interest are the pale color tones ($k \approx 1$). These pixels represent surfaces that exhibit Lambertian reflectance without vegetation cover. They are to be found over the snow-covered meadow. Other snow-covered meadow pixels showed a typical bowl-shaped anisotropy behavior.

Our study has demonstrated that CHRIS data can be decomposed into its spectral and angular components by using linear unmixing and by deriving the Minnaert-*k* parameter. Both maps are useful for describing forest structure but have their specific advantages and limitations due to their single-source nature. Merging them to produce a combined map leads to an improved characterization of forest heterogeneity at subpixel scale that can be used for monitoring forest development or for parameterizing canopy reflectance models, enabling proper retrieval of biophysical (e.g. biomass) or biochemical (e.g. chlorophyll content) parameters (Verrelst et al., 2008b; Kooistra et al., 2008).

When interpreting the merged map it should be noted that solar zenith angle, background brightness and the position of the angular sampling in relation to the principal plane also exert influence on the spectrodirectional response. In addition, variations in topography and the spectral and anisotropy characteristics of land cover features other than snow and vegetation cover (e.g. sharp land cover edges, rock outcrops, water bodies) may affect the spectrodirectional response and thus the results of the merged map as well. These site-specific influences are nevertheless strongly related to pixel size. At a relatively high spatial resolution of 18 m and trees that may reach up to 18 m, scattered radiation is influenced not only by variation in the horizontal plane (e.g. tree density) but also by variation in the vertical plane (e.g. variation in tree height). This implies that the pixel's reflectance at such a high spatial resolution is considerably impacted by radiation fluxes in the horizontal plane (Widlowski et al., 2006). This impact is typically observable for pixels located at the forest–meadow interfaces where the radiation fluxes shift from a volumetric medium (pixel size approximately equal to stand height) to a flat medium (pixel size largely exceeding stand height). For further application purposes it might be therefore advisable to validate the inversion performance, e.g., by analyzing the fit of the original CHRIS measurements with the RPV-reconstructed measurements (Verrelst et al., 2010b; Lavergne et al., 2007). By contrast, at coarser pixel size (e.g. MISR at 275 m in red) tree-level anisotropy effects and edge effects tend to be smoothed, yielding more accurate fits but less detailed maps (Pinty et al., 2002).

Alternatively, the use of LiDAR data may be an option to validate the informative value of reflectance anisotropy (e.g. see Koetz et al., 2005); however, note that apart from the structural configuration also the spectral influence of background has to be accounted for (e.g. see Pisek et al., 2010).

Regardless of the above-mentioned limitations, because the angular and spectral domain originated from the same data source (CHRIS), problems related to co-registration and spatial resampling are minimized, and processing can be fast and quasi-automatic. The RPV inversion-3 package retrieves Minnaert-*k* fast and can easily be automated (Lavergne et al., 2007). Additionally, provided χ^2 uncertainty measures can filter out poorly inverted pixels, wavelength selection can be resolved on the basis of statistical or physical indicators. The automatic identification of endmembers still has to be resolved, but numerous methods are available to do this automatically (e.g. Martínez et al., 2006; Zurita-Milla et al., 2008). Once this has been addressed, mapping forest heterogeneity can be further automated by combining information from the spectral and angular domains. Having the methods available, however, more research may be necessary on the robustness of the method. For instance, it remains to be investigated how successfully forest cover heterogeneity can be mapped during summer conditions when the spectral contrast between canopy and background is reduced due to the green-up of the undergrowth.

5.4. Conclusions

The European Space Agency's small PROBA satellite carries the only imaging spectrometer in space (CHRIS) that provides multi-angular measurements of the reflected solar radiation from the Earth's surface at a high spatial resolution. This paper has demonstrated that combining canopy cover information derived from the spectral domain at one single viewing angle (nadir) with heterogeneity information derived from the angular domain at one single wavelength in the red edge (722 nm) generates spatially explicit information about forest cover heterogeneity at the CHRIS subpixel scale. The generated map included information on surface heterogeneity that was much more detailed than the information that can be derived from single-source optical datasets.

Chapter 6

Synthesis

6.1. Main results

This research has been motivated by the need to improve our knowledge of the potentials of space-borne spectrodirectional (combined multi-angular and spectroscopy) data for forest monitoring applications from space. More precisely, the main objective of this thesis is to exploit spectrodirectional data for the quantification of biochemical and structural canopy properties of forested ecosystems. The thesis has been divided into 5 separate chapters. The first chapter is used to establish the environment in which the work is framed. The other four chapters (2–5) address different approaches that pursue the use of spectrodirectional data to quantify forest canopy parameters. Each of these four chapters concentrates on one of the research questions presented in section 1.7, which are answered and synthesized below (questions A–D).

A: To what extent does the anisotropic reflectance of vegetated surfaces as measured by CHRIS influence the performance of vegetation indices, and what are the underlying mechanisms?

In chapter 2, the effects of reflectance anisotropy as measured by CHRIS were assessed for a set of vegetation indices. Angular effects due to anisotropy of vegetation canopy reflectance are typically treated either as superfluous information or as a source of additional information, but in either case the magnitude and significance of the angular variability needs to be assessed, quantified, and included in the interpretation of the data. The angular response for a wide variety of broadband and narrowband vegetation indices was assessed for two contrasting structural vegetation types: an Alpine old-growth coniferous forest and a meadow. Not only the conventional broadband greenness indices (e.g. SRI, NDVI) but also narrowband greenness indices (e.g. $NDVI_{705,}$) as well as light use efficiency and leaf pigment indices (e.g. SIPI, PRI, and ARI) were subject to canopy anisotropy effects. All indices showed larger angular response over the forest area than over the meadow area, with largest magnitudes obtained by PRI and ARI (Verrelst et al., 2006a; 2006b).

Two physical-based radiative transfer models, one at leaf-level (PROSPECT) and one at canopy-level (FLIGHT), were coupled to quantify and substantiate the findings beyond an incidental case study. It is hypothesized that in a relatively open, heterogeneous old-growth forest the observed proportions of photosynthetic vegetation (PV) and non-photosynthetic vegetation (NPV) are of critical importance shaping the angular response of the studied VIs. The model-based quantification of anisotropy effects on VIs showed that angularity of leaf pigment indices (e.g. PRI) can be partly explained by the angular-dependent variation in observed PV and NPV proportions (Verrelst et al., 2007; 2008b). Further, given the structural and compositional heterogeneity of an old-growth forest it is noted that not only viewing geometry but also canopy structural variables play a role in accurate assessment of foliar

biochemistry. Since canopy structural variables have not been assessed in detail, it led to the following question.

B: Can foliar chlorophyll content be reliably estimated in woody, heterogeneous forest types using vegetation indices?

Chapter 3 builds further on the findings of chapter 2 by assessing the influence of structural and compositional variables on the performance of vegetation indices. Questions that emerged in the former chapter about the role of structural variables and canopy composition demanded a more exhaustive analysis to obtain insight in their mechanisms. Old-growth forests challenge the interpretation of EO data due to their structural heterogeneity together with significant fractions of standing and fallen dead woody material. For instance, the large variability in structural and compositional parameters, which affects significantly the EO signal, is perturbing the accurate assessment of foliar chemistry. To assess the role of structural variables on the estimation of biochemistry, a sensitivity study was employed whereby the detectability of chlorophyll (*Cab*) content was analyzed on the basis of modeled reflectance data. The same coupled radiative transfer model as in chapter two (PROSPECT/FLIGHT) was used to generate top-of-canopy bidirectional reflectance data wherefrom vegetation indices sensitive to *Cab* were calculated (Verrelst et al., 2008a). The contributions of canopy scattering elements (PV and NPV), leaf area index (LAI) and crown cover on the retrieval of *Cab* content were statistically analyzed. The performance of single wavelengths and chlorophyll indices was compared on their capacity of estimating *Cab* content given the wide variation in stand structure. Statistical analysis revealed that most of the chlorophyll indices outperform single wavelengths, with best results obtained by the Maccioni index ($[R_{780} - R_{710}] / [R_{780} - R_{680}]$). The Maccioni index responded highly sensitive to variations in *Cab* content but relatively insensitive to variations in LAI and to a lesser extent to CC and NPV. A stand-specific sensitivity analysis using the Maccioni index suggested that variations in *Cab* content can be best estimated on stands with medium dense canopies. However, the relationship weakens with increasing contribution of crown NPV scattering elements. It can be concluded that the spectral influence of woody elements plays an important role in the estimation of foliar pigments in heterogeneous stands, particularly if the stands are partly defoliated or long-lived (Verrelst et al., 2010c).

Moving further along on the above topic was to investigate if the spectral dependency of anisotropy can be used to retrieve information on forest stands. Since in classical inverse problems ill-conditioned and ill-posed situations are predominant (and inversion following the Hadamard criteria not usable), an intermediate inversion was chosen. This led to the following question.

C: How does reflectance anisotropy of a heterogeneous forest behave across the spectral VNIR domain as measured by CHRIS?

Whereas the former chapter shed some light on the underlying contributors to the anisotropic properties of on old-growth forest as measured by CHRIS, chapter 4 explores the unique information content that is embedded in it. In this chapter the focus shifted to a wintertime image. The spectral anisotropic behavior of an Alpine coniferous forest in relation to canopy cover was investigated using the Minnaert-k parameter obtained through inversion of the parametric Rahman–Pinty–Verstraete (RPV) model. Although earlier studies have demonstrated that the Minnaert-k parameter can be related to canopy heterogeneity at the subpixel scale, its spectral dependency has not yet been fully assessed (Verrelst et al., 2009b).

Minnaert-k parameter retrievals across the CHRIS bands revealed that for a forest underlain by snow cover a switch from bell-shaped to bowl-shaped anisotropic reflectance patterns occurs when moving to NIR wavelengths. Specifically, analysis of the underlying dynamics for pixels on the valley floor revealed that canopy cover and background brightness controls at which wavelength this switch takes place. While having a bright, snow-covered background, Minnaert-k values in the red edge region were best related to canopy cover. In this spectral region, pixels with medium canopy cover densities typically led to bell-shaped anisotropy patterns, whereas pixels with either sparse or dense canopy covers typically led to bowl-shaped reflectance anisotropy patterns. The underlying mechanisms that cause the observed anisotropy switch can be found in the increase of multiple scattering and the decrease of background reflectance due to increasing absorbance by snow grains at longer wavelengths. It results in that the uncollided radiation exiting the snow-covered background in near-nadir direction is no longer able to outperform the scattered radiation exiting to off-nadir directions (Verrelst et al., 2010b). It should nevertheless be noted that the location of the anisotropy switch in the spectral domain is dependent on illumination conditions and the degree of brightness contrast. Given the same illumination conditions, in less bright background situations (e.g. bare soil) the switch from bell to bowl shape is expected to occur at lower wavelengths due to the reduced spectral contrast between background and overstory.

Having uncovered some spectrally-dependent anisotropy mechanisms, ultimately the goal is to derive a measure for physical forest heterogeneity information using space-borne spectrodirectional observations at the subpixel scale. This let to the final question, namely:

D: Can spectrodirectional CHRIS data be applied for forest heterogeneity mapping?

Chapter 5 presents a mapping application based on the uniqueness of multi-angular CHRIS data. CHRIS data sampled in the spectral domain were combined with CHRIS data sampled in the angular domain with the purpose of mapping the 3D heterogeneity of an Alpine coniferous forest during winter. Such a mapping application is of interest for the forest manager, e.g. to monitor forest change. In the spectral domain, near-nadir CHRIS data were

spectrally unmixed to generate a canopy cover map. However, such a map lacks notion of the 3D distribution of the cover. In the angular domain, inversion of the RPV model against angular CHRIS data led to the Minnaert-*k* parameter that provided information on surface heterogeneity at the subpixel scale. Quadratic regression between canopy cover and Minnaert-*k* maps across the CHRIS bands was applied to select the wavelength where both parameters are best related. Comparison of correlation coefficients (R^2) revealed that best relationship occurred in the red edge, at 722 nm (R^2 of 0.43). The relatively low R^2 nevertheless suggests that there is still a considerable portion of unexplained variation present, e.g. due to topography and tree height. Another constraint is that the interpretation of the Minnaert-*k* is not always obvious, e.g. fully vegetated pixels typically produce the same anisotropy patterns as non-vegetated pixels. Both maps were merged to overcome the map-specific limitations (Verrelst et al., 2009a). The merging resulted in a forest cover heterogeneity map that includes information on 3D canopy heterogeneity at the CHRIS subpixel scale at a level beyond what is possible to realize from single-source optical data sets (Verrelst et al., 2010a). Since both maps originated from the same sensor (CHRIS), the merged map can be generated in a quasi-automatic way.

6.2. General conclusions

Within the context of exploring space-borne sprectrodirectional data for forest monitoring applications, the main contribution of this work is (*i*) the improved knowledge of terrestrial reflectance anisotropy that play a role in the performance of broadband and narrowband vegetation indices, (*ii*) the assessment of canopy reflectance perturbing factors such as LAI, canopy cover and woody elements (NPV) when assessing chlorophyll content from reflected radiation and derived vegetation indices, (*iii*) the quantification and interpretation of anisotropy patterns across the visible and NIR (VNIR) wavelengths, and (*iv*) the development of an application that quantifies forest cover heterogeneity at the sensor subpixel scale by combining the spectral domain with the angular domain.

Summarizing, based on the studies of this thesis it can be concluded that:

- Radiative transfer models, both 1D and 3D models, are becoming widely implemented in retrieval schemes for forest properties mapping based on spectrodirectional data. Old-growth forests, however, are quite challenging for the modeler because of its large heterogeneity, both in composition and structure.

- While vegetation indices have proven their use for mapping biochemical properties of terrestrial vegetation, uncertainties related to anisotropic effects are for the majority of indices still to be resolved. For a set of narrowband and broadband indices their response to canopy reflectance anisotropy was quantified using multi-angular CHRIS measurements. The light use efficiency index PRI and the pigment index ARI were most affected by reflectance anisotropy.

- Not only anisotropic effects but also the canopy structure plays a role in perturbing the assessments of foliar pigments. Using radiative transfer models it was evaluated that the scattering and absorption properties of woody elements and background play the most perturbing role when estimating chlorophyll content from space-borne spectrodirectional data. The Maccioni index revealed to be the most robust chlorophyll index.

- The shape of reflectance anisotropy can be quantified and linked to canopy structure with the Minnaert-*k* parameter at one single wavelength. Analysis across the CHRIS spectral bands revealed the spectral dependency of the *k* parameter. Results indicate that for a forested ecosystem with a bright underlying snow-covered background a switch from bell-shaped ($k > 1$) to bowl-shaped ($k < 1$) reflectance anisotropy patterns takes place in the red edge to early NIR. Canopy cover plays an important role in determining at which wavelength this anisotropy switch takes place.

- The Minnaert-*k* parameter (angular domain) can be combined with a canopy cover map (spectral domain) to derive information about forest cover heterogeneity at the sensor subpixel scale. The multi-angular CHRIS imaging spectrometer is particularly useful for such combined spectrodirectional mapping. This creates new opportunities to monitor heterogeneous ecosystems such as forests, woodlands and shrublands at a local-to-regional scale.

6.3. Reflection

Most importantly, this thesis brought earlier findings of terrestrial reflectance anisotropy into the field of imaging spectroscopy. Earlier studies showed with the use of a few broad bands (red, NIR) that the anisotropic properties of a canopy can be related to canopy structure. With the use of CHRIS data, these findings have been systematically expanded and refined over the VNIR part of the spectrum (from 530 to 1019 nm) with a spatial resolution at the tree level. A strong spectral dependency of canopy reflectance anisotropy has been demonstrated. Based on this thesis a few lessons have been learned:

- Most of the vegetation indices are too much affected by reflectance anisotropy for robust canopy properties estimations when calculated from HDRF data. Multi-angular data allow to assess anisotropic effects and eventually to correct for it.

- The main canopy scatterers at canopy level (PV and NPV) and to lesser extent soil scatterers determine the anisotropic reflectance properties of a canopy. A proper assessment of the biochemical constituents from canopy PV scatterers (e.g. chlorophyll content) is only possible if they can be separated from canopy NPV scatterers and soil scatterers. A challenge remains to separate the contribution from a spectrally distinct understory (likewise mixture of PV and NPV scatterers) as well.

- The occurrence of ill-conditioned and ill-posed situations in model inversion remains problematic for realizing operational canopy parameter retrieval. An intermediate solution offered by semi-empirical models (e.g. RPV inversion) is an appropriate compromise. For spectrodirectional data the RPV model can be used to further limit ill-conditioned problems of canopy properties retrieval. For instance, if the anisotropy is bowl-shaped then a 1D model suffices for the inversion, if the anisotropy is bell-shaped a 3D model is required.

- The anisotropic reflectance of a canopy is particularly to be exploited in the red edge region, because in this part of the spectrum the curvature of the reflectance anisotropy is best related with canopy structure. Yet this anisotropy also depends on background brightness and illumination conditions. For operational retrievals of canopy structure it implies that information of the surface spectral characteristics is required. Such information can be derived from the spectral domain of spectrodirectional data.

- Topography remains nevertheless a problem in the linkage between reflectance anisotropy and structural canopy properties. In mountainous regions, additional efforts may be required to decouple reflectance anisotropy invoked by the canopy from the reflectance anisotropy invoked by topography (e.g. by using a 3D model). Alternatively, adding a data layer with DEM-based reliability flags may be an option.

From all the above, it can be concluded that multi-angular spectroscopy can capture a data richness that cannot be reached by any mono-angular optical sensor. Spectrodirectional data has the unique capability to simultaneously retrieve structural canopy properties (predominantly based on information from the angular domain), and canopy biochemical properties (predominantly based on information from the spectral domain). Moreover, both domains can complement each other. In this way, information from the angular domain can facilitate narrowing down ill-conditioned situations when retrieving biochemistry, while information from the spectral domain can complement the retrieval of structural properties from the angular domain. This grounds the argument that spectrodirectional data can pursue critical value-adding mapping applications for forest monitoring; e.g., as has been shown with the developed forest cover heterogeneity map (chapter 5). Therefore, up-to-date availability of combined spectrodirectional mapping products increases opportunities for adequate monitoring of forest development and forest cover change (e.g. due to storms, fires, forest logging, deforestation, pest infestations, environmental changes). Coupling these mapping products with existing monitoring programs (e.g. GOFC, GEOSS) and in situ measurements should lead to an improved monitoring service on how our forests respond to a changing world and to climate change impacts.

In preparation to the United Nations Climate Change Conference held in Copenhagen (COP15; 7–18 December 2009), in October 2009 the world forestry congress (WFC) demanded for urgent action to active forest monitoring and assessment to fully achieve forests' potential in addressing the challenges of climate change (http://www.cfm2009.org/

en/index.asp). Given that forests contribute positively to the global carbon balance, harbor two thirds of all land-based biodiversity, and generate critical ecosystem goods and services (http://www.fao.org/forestry/en/), an accurate monitoring system is becoming a critical necessity. In this respect, a next step would be to elaborate how multi-angular imaging spectroscopy can deliver forest monitoring services in an operational way.

6.4. Outlook

Although this thesis investigated the possibilities of spectrodirectional CHRIS data for forest properties monitoring, it should not be forgotten that CHRIS/PROBA was designed as a technology demonstrator. In fact CHRIS was initially intended as a one year mission, but both the satellite and the CHRIS instrument continue to function well at the time of writing (December 2009), making this sensor very successful. Yet, some signs of detector anomalies already started to appear (e.g. striping effects), which indicates that the sensor will not much longer be able to provide angular images. This implies that CHRIS/PROBA is incompetent to operate as a forest monitoring Earth observer, which, after all, has never been its mission. Nevertheless, the recent burst of knowledge on terrestrial reflectance anisotropy and derived mapping applications based on CHRIS data (e.g., Kayitakire & Derfourny, 2004; Guanter et al., 2005; Rautiainen et al., 2008; Vuolo et al., 2008; Barducci et al., 2009; Galvão et al., 2009; Kneubühler et al., 2009; Mõttus et al., 2009 to name a few) emphasizes the need for continuity in spectrodirectional data for Earth observation. This thesis contributed to expanding this field of knowledge, specifically on the side of exploiting reflectance anisotropy of forested targets. Capitalizing on the unique and valuable features of space-borne spectrodirectional data, a logical following step would be to implement such a technology into an instrument dedicated to forest monitoring, i.e. as an extension of the sentinel fleet.

Despite the potential of spectrodirectional data for operational use, some points in this respect have been left aside in this thesis, while other points require further research. These points are of importance for deriving maximum benefits out of spectrodirectional data, as well as for the development of novel spectrodirectional-based forest monitoring applications. The next sections discuss these points that have been grouped according to the following domains:

- angular

- spatial

- temporal

- spectral

Angular domain

Currently, CHRIS on board PROBA-1 is the only imaging spectrometer in space that is able to re-orient itself in order to acquire multiple looks. PROBA-1 is able to be tilted in the across-track direction so that the target area is viewed. While this opens opportunities for anisotropy-based applications, knowledge of the geometry of the viewing cameras is mandatory for proper interpretation. PROBA-1 is configured with five nominal viewing angles, which samples only a fraction of the reflected radiation. Whether the viewing geometry of the five angular sampling points is optimized to characterize the dominant anisotropic pattern of a terrestrial target remains nevertheless questionable. For instance, it may well happen that when sampling a terrestrial target with five viewing angles along the principal plane a pronounced bell-shaped curvature occurs, but when sampling the same target away from the principal plane, the curvature may rather look like a bowl-shaped pattern. For future multi-angular imaging spectroscopy missions it is therefore advisable to configure the angular sampling as close as possible within the principal plane, to keep consistency and to measure the maximal variation in reflectance anisotropy.

Sun-synchronicity of the instrument's orbital path is required to approach principal plane sampling. Experience from CHRIS/PROBA indicates that sun-synchronicity alone, however, is not enough to reach sampling right within the principal plane. CHRIS/PROBA is not able to sample with all viewing angles within the principal plane due to the pointing to specific targets along the orbital path. The inability of consistent sampling within the principal plane means that maximal variation in reflectance anisotropy is not measured. Theoretical studies have argued to invest in platform steerability in order to sample a maximal anisotropy in the hot spot and dark spot of the principal plane for optimized vegetation structure mapping (e.g. Simic & Chen, 2008; Simic et al., 2009). A future mission with improved steerability may enable to sample right within the principal plane, yet it remains questionable whether the gain in data richness for operational applications is large enough to overcome the technical constraints that go along with it.

Increasing the number of viewing angles is another option to clarify the shape of the anisotropic pattern. For instance, MISR has 9 viewing angles, reaching forward and backward zenith angles up to 70.5°. An observed problem with the use of nine viewing cameras is nevertheless that they may not always lead to an unambiguous angular signature. Often angular measurements lead to an angular signature that may considerably deviate from a smooth bell or bowl shape, i.e. due to the geometry of the angular sampling and/or the scattering regime of the observed target (e.g. see Nolin, 2004). This makes it hard for a semi-empirical parametric model (such as RPV) to invert angular data into a small number of parameters (such as Minnaert-*k*). Consequently, in order to realize a robust inversion it may be more adequate to rely on a smaller number of viewing angles (i.e. 5 to 7) along or close to the principal plane that produces a rather simplified but meaningful angular signature.

Regardless of the number of viewing angles, space-borne multi-angular EO instruments are however unable to measure the total amount of terrestrial reflected radiation. Linking angular measurements with a physically-based RT model may clarify the full hemispherical cover of the reflected radiation, which is of interest e.g. for robust canopy parameter or albedo retrievals (e.g. bihemispherical reflectance (BHR) or directional-hemispherical reflectance (DHR) products) (Chen et al., 2008).

Spatial domain

Although in this thesis emphasis was laid on linking reflectance anisotropy with canopy heterogeneity at the CHRIS subpixel scale by means of the Minnaert-*k* parameter, it remains questionable whether CHRIS' relatively high spatial resolution (~17 m) is the best spatial resolution for robust quantitative forest heterogeneity mapping.

In chapter 4 it was argued that with such a high spatial resolution most of the measured anisotropic reflectance is related to canopy heterogeneity at the tree level. Nevertheless, this resolution may also have its drawbacks, especially in the case of discontinuous forest covers. In a forest stand, lateral radiation fluxes considerably contribute to the surface-leaving radiation (e.g. Widlowski et al., 2006), thereby creating difficulty in establishing a quantitative link between reflectance anisotropy (Minnaert-*k*) and a structural canopy parameter like canopy cover. Linking the Minnaert-*k* parameter with a canopy parameter at such a high spatial resolution, can therefore only work if the adjacent pixels are volumetrically continuous (e.g. as is the case in chapter 4).

In order to reduce the influence of horizontal radiation fluxes, alternatively, the use of a coarser pixel size may be advocated, thereby increasing the importance of the vertical radiation fluxes relative to the contribution of the horizontal radiation fluxes. The other multi-angular instrument currently in space, MISR, is nevertheless unable to quantify heterogeneity at the tree level. Its spatial resolution is too coarse to measure anisotropic properties of the single trees (275 m in red).

What would be required to achieve operational multi-angular based applications in the near-future, is the development of a multi-angular imaging spectrometer with a spatial resolution that is on one hand fine enough to measure stand-related variations in reflectance anisotropy, but on the other hand coarse enough to overcome the influence of horizontal radiation fluxes. In this respect, it was recently theoretically assessed that a pixel size of 30 m^2 may be an appropriate threshold, thereby significantly reducing the impact of the horizontal fluxes from the adjacent pixels (Widlowski et al., 2008). This pixel size seems suitable for operationally delivering forest heterogeneity products, as it is still able to capture anisotropic properties at the tree level.

Further, along with the topic of pixel size, the topic of spatial extent is important. Pointing to a limited number of specific targets, as is currently the case for CHRIS, does not fulfil the

requirement to cover all the forests across the globe. An operational multi-angular instrument requires being equipped with a flexible and fast pointability, a large data storage capacity, and a rapid data transfer.

Temporal domain

While in this thesis the possibility of mapping and monitoring forest properties based on multi-angular imaging spectroscopy has been investigated, the development of multi-angular based applications dedicated to seasonal forest monitoring has been left aside. It is now increasingly understood that multi-angular sensors possess a unique potential to improve detection of forest canopy heterogeneity (e.g. Verrelst et al., 2010b) and understory vegetation (e.g. Canisius & Chen, 2007; Pocewicz et al., 2007; Hilker et al., 2009). Consequently, exploiting the seasonal reflectance anisotropy of a forest stand can pursue new ways of space-based forest monitoring applications, particularly with respect to the mapping of seasonal changes of canopy and understory structure and composition.

Among others, an appealing topic for further research is studying the seasonal dynamics of the Minnaert-k parameter. Verrelst et al. (2009a) documented that for open Alpine forests during winter a bell-shaped anisotropy pattern dominates throughout the visible and red edge parts of the spectrum. In this spectral region, the pronounced brightness contrast between the elongated crowns and the underlying bright snow pack leads to a maximized background-leaving uncollided radiation flux into nadir direction. Into the direction of more oblique angles a large portion of the background-leaving radiation is intercepted by the elongated crowns, thereby forming a bell-shaped reflectance anisotropy pattern ($k > 1$).

When a boreal or Alpine forest subsequently evolves from winter to spring and summer, the underlying snow pack melts and a photosynthetically active understory vegetation cover emerges: the background transforms into a more absorptive (darker) medium. The pronounced brightness contrast with the overstory will reduce, and – in case of a densely vegetated understory – eventually disappear. The anisotropic properties of the forest will therefore change over time: due to the snow melting the bell-shaped reflectance anisotropy pattern ($k > 1$) will shift into a bowl-shaped anisotropy pattern ($k < 1$). Such a seasonal Minnaert-k trend can be useful for seasonal forest monitoring applications. For instance, the availability of repetitive data streams of the Minnaert-k parameter over boreal or Alpine forests would not only be able to deliver information related to the forest cover heterogeneity (Verrelst et al., 2010c) but may also be related to the seasonal melting of the underlying snow pack.

Conversely, in non-snow covered forested regions the seasonal reflectance anisotropy trajectory from winter to summer will be determined by the growth and greening of overstory and understory vegetation. Because of the smaller spectral contrast between canopy and background, the seasonal variations in canopy reflectance anisotropy will be more subtle. It is

left to be studied how these subtle variations can be correctly understood with respect to structural canopy properties.

Spectral domain

Currently, CHRIS on board PROBA-1 and the Hyperion on Earth Observing-1 (EO-1) developed by NASA (Ungar et al., 2003) are the only truly imaging spectrometers operative in space. Nevertheless, contrary to Hyperion, CHRIS particularly lacks bands in the SWIR. Due to the limited range of CHRIS' spectral coverage it misses opportunities related to land and forest mapping applications, such as inferring canopy water content (Clevers et al., 2008) or snow cover features (e.g. grain size, water content; Li et al., 2001; Mishra et al., 2009). Furthermore, research on the anisotropic properties of canopy cover in the SWIR part of the spectrum as measured from space is non-existent at the moment.

In the race of developing new space-borne imaging spectrometers empowered with more and finer spectral bands, new initiatives are underway that cover both VNIR and SWIR at a relatively high spatial resolution (30 m), e.g. EnMAP (Environmental Mapping and Analysis Program) (Stuffler et al., 2009) and PRISMA (PRecursore IperSpettrale della Missione Applicativa) (Labate et al., 2009). These emerging technologies will soon outdate the spectral performance of the CHRIS instrument; however when another *multi-angular* imaging spectrometer will be launched is left to be awaited.

Given the above points are sufficiently understood, it is without doubt that data from multi-angular imaging spectrometers, with sufficient bands in the main pigment absorption regions and red edge and an angular sampling approaching the principal plane, encapsulate an unprecedented information richness related to canopy structure and biochemistry. This thesis opens avenues for future work, namely for the development of a standardized protocol for quantitatively monitoring forest changes based on space-borne spectrodirectional data, which eventually could become part of national and international forest inventory and monitoring services. In this respect the development of a new imaging spectrometer with the possibility to routinely acquire multiple angular images of terrestrial targets across the globe is strongly encouraged.

References

Abdou, W.A., Pilorz, S.H., Helmlinger, M.C., Conel, J.E., Diner, D.J., Bruegge, C.J., Martonchik, J.V., Gatebe, C.K., King, M.D., & Hobbs, P.V. (2006). Sua pan surface bidirectional reflectance: A case study to evaluate the effect of atmospheric correction on the surface products of the Multi-angle Imaging SpectroRadiometer (MISR) during SAFARI 2000. *IEEE Transactions on Geoscience and Remote Sensing, 44*, 1699-1706.

Abuelgasim, A.A., Gopal, S., Irons, J.R., & Strahler, A.H. (1996). Classification of ASAS multiangle and multispectral measurements using artificial neural networks. *Remote Sensing of Environment, 57*, 79-87.

Adams, J.B., Sabol, D.E., Kapos, V., Filho, R.A., Roberts, D.A., Smith, M.O., & Gillespie, A.R. (1995). Classification of multispectral images based on fractions of endmembers: Application to land-cover change in the Brazilian Amazon. *Remote Sensing of Environment, 52*, 137-154

Asner, G.P. (1998). Biophysical and biochemical sources of variability in canopy reflectance. *Remote Sensing of Environment, 64,* 234-253.

Asner, G.P., Borghi, C.E., & Ojeda, R.A. (2003). Desertification in Central Argentina: Changes in ecosystem carbon and nitrogen from imaging spectroscopy. *Ecological Applications, 13*, 629-648.

Asner, G.P., Nepstad, D., Cardinot, G., & Ray, D. (2004). Drought stress and carbon uptake in an Amazon forest measured with spaceborne imaging spectroscopy. *Proceedings of the National Academy of Sciences of the United States of America, 101*, 6039-6044.

Asner, G.P., Braswell, B.H., Schimel, D.S., & Wessman, C.A. (1998). Ecological research needs from multiangle remote sensing data. *Remote Sensing of Environment, 63,* 155-165.

Asrar, G., Myneni, R.B., & Choudhury, B.J. (1992). Spatial heterogeneity in vegetation canopies and remote sensing of absorbed photosynthetically active radiation: a modeling study. *Remote Sensing of Environment, 41*, 85-103.

Atzberger, C. (2004). Object-based retrieval of biophysical canopy variables using artificial neural nets and radiative transfer models. *Remote Sensing of Environment, 93*, 53-67.

Bacour, C., Bréon, F.M., & Maignan, F. (2006). Normalization of the directional effects in NOAA-AVHRR reflectance measurements for an improved monitoring of vegetation cycles. *Remote Sensing of Environment, 102*, 402-413.

Baret, F., & Guyot, G. (1991). Potentials and limits of vegetation indices for LAI and APAR assessment. *Remote Sensing of Environment, 35*, 161-173.

Barnsley, M.J., Allison, D., & Lewis, P. (1997). On the information content of multiple view angle (MVA) images. *International Journal of Remote Sensing, 18*, 1937-1960.

Barnsley, M.J., Settle, J.J., Cutter, M.A., Lobb, D.R., & Teston, F. (2004). The PROBA/CHRIS mission: A low-cost smallsat for hyperspectral multiangle observations of the earth surface and atmosphere. *IEEE Transactions on Geoscience and Remote Sensing, 42*, 1512-1520.

Barton, C.V.M., & North, P.R.J. (2001). Remote sensing of canopy light use efficiency using the photochemical reflectance index: Model and sensitivity analysis. *Remote Sensing of Environment, 78*, 264-273.

Beck, P.S.A., Atzberger, C., Høgda, K.A., Johansen, B., & Skidmore, A.K. (2006). Improved monitoring of vegetation dynamics at very high latitudes: A new method using MODIS NDVI. *Remote Sensing of Environment, 100*, 321-334.

Belanger, M.J., Miller, J.R., & Boyer, M.G. (1995). Comparative relationships between some red edge parameters and seasonal leaf chlorophyll concentrations. *Canadian Journal of Remote Sensing, 21*, 16-21.

Bicheron, P., Leroy, M., Hautecoeur, O., & Bréon, F.M. (1997). Enhanced discrimination of boreal forest covers with directional reflectances from the airborne polarization and directionality of Earth reflectances (POLDER) instrument. *Journal of Geophysical Research D: Atmospheres, 102*, 29517-29528.

Blackburn, G.A., & Steele, C.M. (1999). Towards the remote sensing of matorral vegetation physiology: Relationships between spectral reflectance, pigment, and biophysical characteristics of semiarid bushland canopies. *Remote Sensing of Environment, 70*, 278-292.

Borel, C.C., & Gerstl, S.A.W. (1994). Nonlinear spectral mixing models for vegetative and soil surfaces. *Remote Sensing of Environment, 47*, 403-416.

Bousquet, L., Lachérade, S., Jacquemoud, S., & Moya, I. (2005). Leaf BRDF measurements and model for specular and diffuse components differentiation. *Remote Sensing of Environment, 98*, 201-211.

Braswell, B.H., Hagen, S.C., Frolking, S.E., & Salas, W.A. (2003). A multivariable approach for mapping sub-pixel land cover distributions using MISR and MODIS: Application in the Brazilian Amazon region. *Remote Sensing of Environment, 87*, 243-256.

Brown, L., Chen, J.M., Leblanc, S.G., & Cihlar, J. (2000). A shortwave infrared modification to the simple ratio for LAI retrieval in boreal forests: An image and model analysis. *Remote Sensing of Environment, 71*, 16-25.

Brown, M.J., & Parker, G.G. (1994). Canopy light transmittance in a chronosequence of mixed-species deciduous forests. *Canadian Journal of Forest Research, 24*, 1694-1703.

Bruniquel-Pinel, V., & Gastellu-Etchegorry, J.P. (1998). Sensitivity of texture of high resolution images of forest to biophysical and acquisition parameters. *Remote Sensing of Environment, 65*, 61-85.

Cacuci, D.G. (2003). Sensitivity and Uncertainty Analysis: Theory, Volume 1, Chapman & Hall/CRC, Boca Raton.

Canisius, F., & Chen, J.M. (2007). Retrieving forest background reflectance in a boreal region from Multi-angle Imaging SpectroRadiometer (MISR) data. *Remote Sensing of Environment, 107*, 312-321.

Carter, G.A., & Knapp, A.K. (2001). Leaf optical properties in higher plants: Linking spectral characteristics to stress and chlorophyll concentration. *Am. J. Bot., 88*, 677-684.

Chapin Iii, F.S., Sturm, M., Serreze, M.C., McFadden, J.P., Key, J.R., Lloyd, A.H., McGuire, A.D., Rupp, T.S., Lynch, A.H., Schimel, J.P., Beringer, J., Chapman, W.L., Epstein, H.E., Euskirchen, E.S., Hinzman, L.D., Jia, G., Ping, C.L., Tape, K.D., Thompson, C.D.C., Walker, D.A., & Welker, J.M. (2005). Role of land-surface changes in arctic summer warming. *Science, 310*, 657-660.

Chen, J.M., & Black, T.A. (1992). Defining leaf area index for non-flat leaves. *Plant, Cell & Environment, 15*, 421-429.

Chen, J.M., & Cihlar, J. (1996). Retrieving leaf area index of boreal conifer forests using Landsat TM images. *Remote Sensing of Environment, 55*, 153-162.

Chen, J.M., Li, X., Nilson, T., & Strahler, A. (2000). Recent advances in geometrical optical modelling and its applications. *Remote Sensing Reviews, 18*, 227-262.

Chen, J.M., Menges, C.H., & Leblanc, S.G. (2005). Global mapping of foliage clumping index using multi-angular satellite data. *Remote Sensing of Environment, 97*, 447-457.

Chen, J.M., Pavlic, G., Brown, L., Cihlar, J., Leblanc, S.G., White, H.P., Hall, R.J., Peddle, D.R., King, D.J., Trofymow, J.A., Swift, E., Van Der Sanden, J., & Pellikka, P.K.E. (2002). Derivation and validation of Canada-wide coarse-resolution leaf area index maps using high-resolution satellite imagery and ground measurements. *Remote Sensing of Environment, 80*, 165-184.

Chen, X., Vierling, L., & Deering, D. (2005). A simple and effective radiometric correction method to improve landscape change detection across sensors and across time. *Remote Sensing of Environment, 98*, 63-79.

Chen, X., Vierling, L., Rowell, E., & DeFelice, T. (2004). Using lidar and effective LAI data to evaluate IKONOS and Landsat 7 ETM+ vegetation cover estimates in a ponderosa pine forest. *Remote Sensing of Environment*, 91, 14-26.

Chen, Y.M., Liang, S., Wang, J., Kim, H.Y., & Martonchik, J.V. (2008). Validation of MISR land surface broadband albedo. *International Journal of Remote Sensing, 29*, 6971-6983.

References

Cheng, Y.B., Zarco-Tejada, P.J., Riano, D., Rueda, C.A., & Ustin, S.L. (2006). Estimating vegetation water content with hyperspectral data for different canopy scenarios: Relationships between AVIRIS and MODIS indexes. *Remote Sensing of Environment, 105*, 354-366.

Chopping, M. (2008). Terrestrial applications of mulitangle remote sensing. In S. Liang (ed.), Advances in land remote sensing: system, modeling, inversion and application, Chapter 5. New York: Springer.

Chopping, M., Moisen, G.G., Su, L., Laliberte, A., Rango, A., Martonchik, J.V., & Peters, D.P.C. (2008). Large area mapping of southwestern forest crown cover, canopy height, and biomass using the NASA Multiangle Imaging Spectro-Radiometer. *Remote Sensing of Environment, 112*, 2051-2063.

Chopping, M., Nolin, A., Moisen, G.G., Martonchik, J.V., & Bull, M. (2009). Forest canopy height from the Multiangle Imaging SpectroRadiometer (MISR) assessed with high resolution discrete return lidar. *Remote Sensing of Environment, 113*, 2172-2185.

Chopping, M., Su, L., Laliberte, A., Rango, A., Peters, D.P.C., & Kollikkathara, N. (2006). Mapping shrub abundance in desert grasslands using geometric-optical modeling and multi-angle remote sensing with CHRIS/Proba. *Remote Sensing of Environment, 104*, 62-73.

Chopping, M., Su, L., Rango, A., Martonchik, J.V., Peters, D.P.C., & Laliberte, A. (2008). Remote sensing of woody shrub cover in desert grasslands using MISR with a geometric-optical canopy reflectance model. *Remote Sensing of Environment, 112*, 19-34.

Chopping, M.J., Rango, A., Havstad, K.M., Schiebe, F.R., Ritchie, J.C., Schmugge, T.J., French, A.N., Su, L., McKee, L., & Davis, M.R. (2003). Canopy attributes of desert grassland and transition communities derived from multiangular airborne imagery. *Remote Sensing of Environment, 85*, 339-354.

Clevers, J.G.P.W., De Jong, S.M., Epema, G.F., Van der Meer, F.D., Bakker, W.H., Skidmore, A.K., & Scholte, K.H. (2002). Derivation of the red edge index using the MERIS standard band setting. *International Journal of Remote Sensing, 23*, 3169-3184.

Clevers, J.G.P.W., Kooistra, L., & Schaepman, M.E. (2008). Using spectral information from the NIR water absorption features for the retrieval of canopy water content. *International Journal of Applied Earth Observation and Geoinformation, 10*, 388-397.

Colombo, R., Meroni, M., Marchesi, A., Busetto, L., Rossini, M., Giardino, C., & Panigada, C. (2008). Estimation of leaf and canopy water content in poplar plantations by means of hyperspectral indices and inverse modeling. *Remote Sensing of Environment, 112*, 1820-1834.

Combal, B., Baret, F., Weiss, M., Trubuil, A., Mace, D., Pragnere, A., Myneni, R., Knyazikhin, Y., & Wang, L. (2003). Retrieval of canopy biophysical variables from bidirectional reflectance - Using prior information to solve the ill-posed inverse problem. *Remote Sensing of Environment, 84*, 1-15.

Côté, J.F., Widlowski, J.L., Fournier, R.A., & Verstraete, M.M. (2009). The structural and radiative consistency of three-dimensional tree reconstructions from terrestrial lidar. *Remote Sensing of Environment, 113*, 1067-1081.

Csiszar, I., Gutman, G., Romanov, P., Leroy, M., & Hautecoeur, O. (2001). Using ADEOS/POLDER data to reduce angular variability of NOAA/AVHRR reflectances. *Remote Sensing of Environment, 76*, 399-409.

Curran, P.J. (1989). Remote sensing of foliar chemistry. *Remote Sensing of Environment, 30*, 271-278

Datt, B. (1998). Remote sensing of chlorophyll a, chlorophyll b, chlorophyll a+b, and total carotenoid content in eucalyptus leaves. *Remote Sensing of Environment, 66*, 111-121.

Datt, B. (1999). Visible/near infrared reflectance and chlorophyll content in Eucalyptus leaves. *International Journal of Remote Sensing, 20*, 2741-2759.

Dawson, T.P., Curran, P.J., & Plummer, S.E. (1998). LIBERTY - Modeling the effects of Leaf Biochemical Concentration on Reflectance Spectra. *Remote Sensing of Environment, 65*, 50-60.

Dawson, T.P., Curran, P.J., North, P.R.J., & Plummer, S.E. (1999). The propagation of foliar biochemical absorption features in forest canopy reflectance: A theoretical analysis. *Remote Sensing of Environment, 67*, 147-159.

Deering, D.W., Eck, T.F., & Banerjee, B. (1999). Characterization of the reflectance anisotropy of three boreal forest canopies in spring-summer. *Remote Sensing of Environment, 67*, 205-229.

Demarez, V., & Gastellu-Etchegorry, J.P. (2000). A modeling approach for studying forest chlorophyll content. *Remote Sensing of Environment, 71*, 226-238.

Diner, D.J., Asner, G.P., Davies, R., Knyazikhin, Y., Schaaf, C.B., Muller, J.P., Nolin, A.W., Stroeve, J., & Pinty, B. (1999). New directions in Earth observing: scientific applications of multiangle remote sensing. *Bulletin of the American Meteorological Society, 80*, 2209-2228.

Diner, D.J., Beckert, J.C., Reilly, T.H., Bruegge, C.J., Conel, J.E., Kahn, R.A., Martonchik, J.V., Ackerman, T.P., Davies, R., Gerstl, S.A.W., Gordon, H.R., Muller, J.P., Myneni, R.B., Sellers, P.J., Pinty, B., & Verstraete, M.M. (1998). Multi-angle imaging spectroradiometer (MISR) instrument description and experiment overview. *IEEE Transactions on Geoscience and Remote Sensing, 36*, 1072-1087.

Diner, D.J., Braswell, B.H., Davies, R., Gobron, N., Hu, J., Jin, Y., Kahn, R.A., Knyazikhin, Y., Loeb, N., Muller, J.P., Nolin, A.W., Pinty, B., Schaaf, C.B., Seiz, G., & Stroeve, J. (2005). The value of multiangle measurements for retrieving structurally and radiatively consistent properties of clouds, aerosols, and surfaces. *Remote Sensing of Environment, 97*, 495-518.

Disney, M., Lewis, P., & Saich, P. (2006). 3D modelling of forest canopy structure for remote sensing simulations in the optical and microwave domains. *Remote Sensing of Environment, 100*, 114-132

Disney, M.I., Lewis, P., & North, P.R.J. (2000). Monte Carlo ray tracing in optical canopy reflectance modelling. *Remote Sensing Reviews, 18*, 163-196.

Dobbertin, M., & Brang, P. (2001). Crown defoliation improves tree mortality models. *Forest Ecology and Management, 141*, 271-284.

Duca, R., & Del Frate, F. (2008). Hyperspectral and multiangle CHRIS-PROBA images for the generation of land cover maps. *IEEE Transactions on Geoscience and Remote Sensing, 46,* 2857-2866.

Eklundh, L., Harrie, L., & Kuusk, A. (2001). Investigating relationships between landsat ETM+ sensor data and leaf area index in a boreal conifer forest. *Remote Sensing of Environment, 78*, 239-251

Eriksson, H.M., Eklundh, L., Kuusk, A., & Nilson, T. (2006). Impact of understory vegetation on forest canopy reflectance and remotely sensed LAI estimates. *Remote Sensing of Environment, 103*, 408-418.

Fang, H., Liang, S., & Kuusk, A. (2003). Retrieving leaf area index using a genetic algorithm with a canopy radiative transfer model. *Remote Sensing of Environment, 85*, 257-270.

Feret, J.B., François, C., Asner, G.P., Gitelson, A.A., Martin, R.E., Bidel, L.P.R., Ustin, S.L., le Maire, G., & Jacquemoud, S. (2008). PROSPECT-4 and 5: Advances in the leaf optical properties model separating photosynthetic pigments. *Remote Sensing of Environment, 112,* 3030-3043.

Fernandes, R., Fraser, R., Latifovic, R., Cihlar, J., Beaubien, J., & Du, Y. (2004). Approaches to fractional land cover and continuous field mapping: A comparative assessment over the BOREAS study region. *Remote Sensing of Environment, 89*, 234-251.

Fernandes, R.A., Miller, J.R., Chen, J.M., & Rubinstein, I.G. (2004). Evaluating image-based estimates of leaf area index in boreal conifer stands over a range of scales using high-resolution CASI imagery. *Remote Sensing of Environment, 89*, 200.

Ferreira, L.G., Yoshioka, H., Huete, A., & Sano, E.E. (2003). Seasonal landscape and spectral vegetation index dynamics in the Brazilian Cerrado: An analysis within the Large-Scale Biosphere-Atmosphere Experiment in Amazonia (LBA). *Remote Sensing of Environment, 87*, 534-550.

Fourty, T., Baret, F., Jacquemoud, S., Schmuck, G., & Verdebout, J. (1996). Leaf optical properties with explicit description of its biochemical composition: Direct and inverse problems. *Remote Sensing of Environment, 56*, 104-117.

Franklin, J.F., & Van Pelt, R. (2004). Spatial aspects of structural complexity in old-growth forests. *Journal of Forestry, 102*, 22-29.

Franklin, J.F., Spies, T.A., Pelt, R.V., Carey, A.B., Thornburgh, D.A., Berg, D.R., Lindenmayer, D.B., Harmon, M.E., Keeton, W.S., Shaw, D.C., Bible, K., & Chen, J. (2002). Disturbances and

structural development of natural forest ecosystems with silvicultural implications, using Douglas-fir forests as an example. *Forest Ecology and Management, 155*, 399-423.

Franklin, S.E., Hall, R.J., Smith, L., & Gerylo, G.R. (2003). Discrimination of conifer height, age and crown closure classes using Landsat-5 TM imagery in the Canadian Northwest Territories. *International Journal of Remote Sensing, 24*, 1823-1834.

Galvão, L.S., Ponzoni, F.J., Epiphanio, J.C.N., Rudorff, B.F.T., & Formaggio, A.R. (2004). Sun and view angle effects on NDVI determination of land cover types in the Brazilian Amazon region with hyperspectral data. *International Journal of Remote Sensing, 25*, 1861-1879.

Galvão, L.S., Ponzoni, F.J., Liesenberg, V., & Santos, J.R.d. (2009). Possibilities of discriminating tropical secondary succession in Amazonia using hyperspectral and multiangular CHRIS/PROBA data. *International Journal of Applied Earth Observation and Geoinformation, 11*, 8-14.

Gamon, J.A., & Surfus, J.S. (1999). Assessing leaf pigment content and activity with a reflectometer. *New Phytologist, 143*, 105-117.

Gamon, J.A., Penuelas, J., & Field, C.B. (1992). A narrow-waveband spectral index that tracks diurnal changes in photosynthetic efficiency. *Remote Sensing of Environment, 41*, 35-44.

Gamon, J.A., Serrano, L., & Surfus, J.S. (1997). The photochemical reflectance index: An optical indicator of photosynthetic radiation use efficiency across species, functional types, and nutrient levels. *Oecologia, 112*, 492-501.

Ganapol, B.D., Johnson, L.F., Hammer, P.D., Hlavka, C.A., & Peterson, D.L. (1998). LEAFMOD: A new within-leaf radiative transfer model. *Remote Sensing of Environment, 63*, 182-193.

Gao, F., Schaaf, C.B., Strahler, A.H., Jin, Y., & Li, X. (2003). Detecting vegetation structure using a kernel-based BRDF model. *Remote Sensing of Environment, 86*, 198-205.

Gao, X., Huete, A.R., Ni, W.G., & Miura, T. (2000). Optical-biophysical relationships of vegetation spectra without background contamination. *Remote Sensing of Environment, 74*, 609-620.

Gastellu-Etchegorry, J.P., & Bruniquel-Pinel, V. (2001). A modeling approach to assess the robustness of spectrometric predictive equations for canopy chemistry. *Remote Sensing of Environment, 76*, 1-15.

Gastellu-Etchegorry, J.P., Gascon, F., & Estève, P. (2003). An interpolation procedure for generalizing a look-up table inversion method. *Remote Sensing of Environment, 87*, 55-71.

Gastellu-Etchegorry, J.P., Guillevic, P., Zagolski, F., Demarez, V., Trichon, V., Deering, D., & Leroy, M. (1999). Modeling BRF and radiation regime of boreal and tropical forests: I. BRF. *Remote Sensing of Environment, 68*, 281-316.

Gemmell, F. (1998). An investigation of terrain effects on the inversion of a forest reflectance model. *Remote Sensing of Environment, 65*, 155-169.

Gemmell, F. (1999). Estimating conifer forest cover with thematic mapper data using reflectance model inversions and two spectral indices in a site with variable background characteristics. *Remote Sensing of Environment, 69*, 105-121.

Gemmell, F., & McDonald, A.J. (2000). View zenith angle effects on the forest information content of three spectral indices. *Remote Sensing of Environment, 72*, 139-158.

Gemmell, F., & Varjo, J. (1999). Utility of reflectance model inversion versus two spectral indices for estimating biophysical characteristics in a boreal forest test site. *Remote Sensing of Environment, 68*, 95-111.

Gemmell, F., Varjo, J., & Strandstrom, M. (2001). Estimating forest cover in a boreal forest test site using thematic mapper data from two dates. *Remote Sensing of Environment, 77*, 197-211.

Gemmell, F., Varjo, J., Strandstrom, M., & Kuusk, A. (2002). Comparison of measured boreal forest characteristics with estimates from TM data and limited ancillary information using reflectance model inversion. *Remote Sensing of Environment, 81*, 365-377.

Gerard, F.F., & North, P.R.J. (1997). Analyzing the effect of structural variability and canopy gaps on forest BRDF using a geometric-optical model. *Remote Sensing of Environment, 62,* 46-62.

Gitelson, A., & Merzlyak, M.N. (1994). Spectral relfectance changes associated with autumn senescence of Aesculus hippocastanum L. and Acer platanoides L. leaves. Spectral features and relation to chlorophyll estimation. *Journal of Plant Physiology, 143*, 286-292.

Gitelson, A.A., Gritz, Y., & Merzlyak, M.N. (2003). Relationships between leaf chlorophyll content and spectral reflectance and algorithms for non-destructive chlorophyll assessment in higher plant leaves. *Journal of Plant Physiology, 160*, 271-282.

Gitelson, A.A., Merzlyak, M.N., & Chivkunova, O.B. (2001). Optical properties and nondestructive estimation of anthocyanin content in plant leaves. *Photochemistry and Photobiology, 74*, 38-45.

Gitelson, A.A., Viña, A., Verma, S.B., Rundquist, D.C., Arkebauer, T.J., Keydan, G., Leavitt, B., Ciganda, V., Burba, G.G., & Suyker, A.E. (2006). Relationship between gross primary production and chlorophyll content in crops: Implications for the synoptic monitoring of vegetation productivity. *Journal of Geophysical Research D: Atmospheres, 111,* D08S11.

Glenn, E.P., Huete, A.R., Nagler, P.L., & Nelson, S.G. (2008). Relationship between remotely-sensed vegetation indices, canopy attributes and plant physiological processes: What vegetation indices can and cannot tell us about the landscape. *Sensors, 8*, 2136-2160.

Gobron, N. (1997). Theoretical limits to the estimation of the leaf area index on the basis of visible and near-infrared remote sensing data. *IEEE Transactions on Geoscience and Remote Sensing, 35*, 1438-1445.

Gobron, N., & Lajas, D. (2002). A new inversion scheme for the RPV model. *Canadian Journal of Remote Sensing, 28*, 156-167.

Gobron, N., Pinty, B., Verstraete, M.M., & Widlowski, J.L. (2000). Advanced vegetation indices optimized for up-coming sensors: design, performance, and applications. *IEEE Transactions on Geoscience and Remote Sensing, 38*, 2489-2505.

Goel, N.S. (1988). Models of vegetation canopy reflectance and their use in estimation of biophysical parameters from reflectance data. *Remote Sensing Reviews, 4*, 1-212.

Goel, N.S., & Thompson, R.L. (2000). A snapshot of canopy reflectance models and a universal nodel for the radiation regime. *Remote Sensing Reviews, 18*, 197-225.

Goetz, S. J., Fiske, G. J., & Bunn, A. G. (2006). Using satellite time-series data sets to analyze fire disturbance and forest recovery across Canada. *Remote Sensing of Environment, 101*, 352-365.

Goetz, S.J. (1997). Multi-sensor analysis of NDVI, surface temperature and biophysical variables at a mixed grassland site. *International Journal of Remote Sensing, 18*, 71-94.

Govaerts, Y.M., & Verstraete, M.M. (1998). Raytran: A Monte Carlo ray-tracing model to compute light scattering in three-dimensional heterogeneous media. *IEEE Transactions on Geoscience and Remote Sensing, 36*, 493-505.

Goward, S.N., & Huemmrich, K.F. (1992). Vegetation canopy PAR absorptance and the normalized difference vegetation index: an assessment using the SAIL model. *Remote Sensing of Environment, 39*, 119-140.

Green, R.O., Eastwood, M.L., Sarture, C.M., Chrien, T.G., Aronsson, M., Chippendale, B.J., Faust, J.A., Pavri, B.E., Chovit, C.J., Solis, M., Olah, M.R., & Williams, O. (1998). Imaging spectroscopy and the Airborne Visible/Infrared Imaging Spectrometer (AVIRIS). *Remote Sensing of Environment, 65*, 227-248.

Guanter, L., Alonso, L., & Moreno, J. (2004). Atmospheric corrections of CHRIS/PROBA data acquired in the SPARC Campaign. In *Proceedings of the 2nd CHRIS/PROBA workshop*, 28-30 April 2004, ESRIN, Frascati, Italy. Compiled by H. Lacaste. ESA SP-578, ESA Publications, ESTEC, Noordwijk, The Netherlands.

Guanter, L., Alonso, L., & Moreno, J. (2005a). A method for the surface reflectance retrieval from PROBA/CHRIS data over land: Application to ESA SPARC campaigns. *IEEE Transactions on Geoscience and Remote Sensing, 43*, 2908-2917.

Guanter, L., Alonso, L., & Moreno, J. (2005b). First results from the PROBA/CHRIS hyperspectral/multiangular satellite system over land and water targets. *IEEE Geoscience and Remote Sensing Letters, 2*, 250-254.

References

Guanter, L., Alonso, L., Gomez-Chova, L., & Moreno, J. (2007). CHRIS/PROBA atmospheric correction module. Algorithm theoretical basis document, ESA ITT SoWENDVI-DTEX-EOPS-SW-06-0008, ESA Publications, ESTEC, Noordwijk, The Netherlands.

Haboudane, D., Miller, J.R., Tremblay, N., Zarco-Tejada, P.J., & Dextraze, L. (2002). Integrated narrow-band vegetation indices for prediction of crop chlorophyll content for application to precision agriculture. *Remote Sensing of Environment, 81*, 416-426.

Haboudane, D., Tremblay, N., Miller, J.R., & Vigneault, P. (2008). Remote estimation of crop chlorophyll content using spectral indices derived from hyperspectral data. *IEEE Transactions on Geoscience and Remote Sensing, 46*, 423-436.

Hapke, B. (1981). Bidirectional reflectance spectroscopy. 1. Theory. *Journal of Geophysical Research, 86*, 3039-3054.

Harris, A.T., Asner, G.P., & Miller, M.E. (2003). Changes in vegetation structure after long-term grazing in Pinyon-Juniper ecosystems: Integrating imaging spectroscopy and field studies. *Ecosystems, 6*, 368-383.

He, Y., Guo, X., & Wilmshurst, J. (2006). Studying mixed grassland ecosystems I: Suitable hyperspectral vegetation indices. *Canadian Journal of Remote Sensing, 32*, 98-107.

Heiskanen, J. (2006). Tree cover and height estimation in the Fennoscandian tundra-taiga transition zone using multiangular MISR data. *Remote Sensing of Environment, 103*, 97-114.

Hilker, T., Coops, N.C., Coggins, S.B., Wulder, M.A., Brownc, M., Black, T.A., Nesic, Z., & Lessard, D. (2009). Detection of foliage conditions and disturbance from multi-angular high spectral resolution remote sensing. *Remote Sensing of Environment, 113*, 421-434.

Homolová, L., Malenovský, Z., Hanuš, J., Tomášková, I., Dvořáková, M., & Pokorný, R. (2007), Comparison of different ground techniques to map leaf area index of Norway spruce forest canopy. In 10th Intl. Symposium on Physical Measurements and Spectral Signatures in Remote Sensing (eds Schaepman, M.E., Liang, S., Groot, N.E. and Kneubühler, M.), Intl. Archives of the Photogrammetry, Remote Sensing and Spatial Information Sciences, Vol. XXXVI, Part 7/C50, pp. 499-504. ISPRS, Davos (CH). ISSN 1682-1777.

Hu, B.X., Inannen, K., & Miller, J.R. (2000). Retrieval of leaf area index and canopy closure from CASI data over the BOREAS flux tower sites. *Remote Sensing of Environment, 74*, 255-274.

Huang, D., Knyazikhin, Y., Wang, W., Deering, D.W., Stenberg, P., Shabanov, N., Tan, B., & Myneni, R.B. (2008). Stochastic transport theory for investigating the three-dimensional canopy structure from space measurements. *Remote Sensing of Environment, 112*, 35-50.

Huemmrich, K.F. (2001). The GeoSail model: a simple addition to the SAIL model to describe discontinuous canopy reflectance. *Remote Sensing of Environment, 75*, 423-431.

Huemmrich, K.F., & Goward, S.N. (1997). Vegetation canopy PAR absorptance and NDVI: An assessment for ten tree species with the SAIL model. *Remote Sensing of Environment, 61*, 254-269

Huete, A., Didan, K., Miura, T., Rodriguez, E.P., Gao, X., & Ferreira, L.G. (2002). Overview of the radiometric and biophysical performance of the MODIS vegetation indices. *Remote Sensing of Environment, 83*, 195-213.

Huete, A.R., Hua, G., Qi, J., Chehbouni, A., & Van Leeuwen, W.J.D. (1992). Normalization of multidirectional red and NIR reflectances with the SAVI. *Remote Sensing of Environment, 41*, 143-154.

Hyvönen, R., Ågren, G.I., Linder, S., Persson, T., Cotrufo, M.F., Ekblad, A., Freeman, M., Grelle, A., Janssens, I.A., Jarvis, P.G., Kellomäki, S., Lindroth, A., Loustau, D., Lundmark, T., Norby, R.J., Oren, R., Pilegaard, K., Ryan, M.G., Sigurdsson, B.D., Strömgren, M., Van Oijen, M., & Wallin, G. (2007). The likely impact of elevated [CO2], nitrogen deposition, increased temperature and management on carbon sequestration in temperate and boreal forest ecosystems: A literature review. *New Phytologist, 173*, 463-480.

Jach, M.E., & Ceulemans, R. (2000). Effects of season, needle age and elevated atmospheric CO2 on photosynthesis in Scots pine (Pinus sylvestris). *Tree Physiology, 20*, 145-157.

Jackson, R.D. Teillet, P.M., Slater, P.N., Fedosejevs, G., Jasinski, M.F., Aase, J.K., & Moran, M.S. (1990). Bidirectional measurements of surface reflectance for view angle corrections of oblique imagery. *Remote Sensing of Environment, 32*, 189-202.

Jacquemoud, S., & Baret, F. (1990). PROSPECT: A model of leaf optical properties spectra. *Remote Sensing of Environment, 34*, 75-91.

Jacquemoud, S., Bacour, C., Poilvé, H., & Frangi, J.P. (2000). Comparison of four radiative transfer models to simulate plant canopies reflectance: Direct and inverse mode. *Remote Sensing of Environment, 74*, 471-481.

Jacquemoud, S., Baret, F., Andrieu, B., Danson, F.M., & Jaggard, K. (1995). Extraction of vegetation biophysical parameters by inversion of the PROSPECT+SAIL models on sugar beet canopy reflectance data. Application to TM and AVIRIS sensors. *Remote Sensing of Environment, 52*, 163-172.

Jacquemoud, S., Verhoef, W., Baret, F., Bacour, C., Zarco-Tejada, P.J., Asner, G.P., François, C., & Ustin, S.L. (2009). PROSPECT + SAIL models: A review of use for vegetation characterization. *Remote Sensing of Environment, 113 (SUPPL. 1)*, S56-S166.

Jia, G.J., Burke, I.C., Goetz, A.F.H., Kaufmann, M.R., & Kindel, B.C. (2006). Assessing spatial patterns of forest fuel using AVIRIS data. *Remote Sensing of Environment, 102*, 318-327

Jin, Y., Gao, F., Schaaf, C.B., Li, X., Strahler, A.H., Bruegge, C.J., & Martonchik, J.V. (2002). Improving MODIS surface BRDF/albedo retrieval with MISR multiangle observations. *IEEE Transactions on Geoscience and Remote Sensing, 40*, 1593-1604.

Kane, V.R., Gillespie, A.R., McGaughey, R., Lutz, J.A., Ceder, K., & Franklin, J.F. (2008). Interpretation and topographic compensation of conifer canopy self-shadowing. *Remote Sensing of Environment, 112*, 3820-3832.

Kaufman, Y.J., & Tanre, D. (1992). Atmospherically resistant vegetation index (ARVI) for EOS-MODIS. *IEEE Transactions on Geoscience and Remote Sensing, 30*, 261-270.

Kayitakire, F., & Defourny, P. (2004). Forest type discrimination using multi-angle hyperspectral data. In, *European Space Agency, (Special Publication) ESA SP* (pp. 72-84).

Keddy, P.A., & Drummond, C.G. (1996). Ecological properties for the evaluation, management, and restoration of temperate deciduous forest ecosystems. *Ecological Applications, 6*, 748-762.

Kimes, D., Gastellu-Etchegorry, J., & Esteve, P. (2002). Recovery of forest canopy characteristics through inversion of a complex 3D model. *Remote Sensing of Environment, 79*, 320-338.

Kimes, D.S. (1983). Dynamics of directional reflectance factor distributions for vegetation canopies. *Applied Optics, 22*, 1364-1372.

Kimes, D.S., Newcomb, W.W., Tucker, C.J., Zonneveld, I.S., Van Wijngaarden, W., De Leeuw, J., & Epema, G.F. (1985). Directional reflectance factor distributions for cover types of Northern Africa. *Remote Sensing of Environment, 18*, 1-19.

Kimes, D.S., Ranson, K.J., Sun, G., & Blair, J.B. (2006). Predicting lidar measured forest vertical structure from multi-angle spectral data. *Remote Sensing of Environment, 100*, 503-511.

Kneubühler, M., Koetz, B., Huber, S., Schaepman, M.E., & Zimmermann, N.E. (2008). Space-based spectrodirectional measurements for the improved estimation of ecosystem variables. *Canadian Journal of Remote Sensing, 34*, 192-205.

Knohl, A., Schulze, E.D., Kolle, O., & Buchmann, N. (2003). Large carbon uptake by an unmanaged 250-year-old deciduous forest in Central Germany. *Agricultural and Forest Meteorology, 118*, 151-167.

Koetz, B., Kneubühler, M., Widlowski, J.L., Morsdorf, F., Schaepman, M., & Itten, K. (2005). Assessment of canopy structure and heterogeneity from multi-angular CHRIS-PROBA data. *The 9th International Symposium on Physical Measurements and Signatures in Remote Sensing (ISPMSRS)*, 17-19 October 2005, Beijing, China, pp. 73-78.

Koetz, B., Sun, G., Morsdorf, F., Ranson, K.J., Kneubühler, M., Itten, K., & Allgöwer, B. (2007). Fusion of imaging spectrometer and LIDAR data over combined radiative transfer models for forest canopy characterization. *Remote Sensing of Environment, 106*, 449-459.

References

Koetz, B., Verrelst, J., Widlowski, J.L., Morsdorf, F., Schaepman, M.E & Kneubühler, M. (2006). Suitability of the parametric model RPV to assess canopy structure and heterogeneity from multi-angular CHRIS-PROBA data. *Proc. 4th CHRIS/PROBA Workshop,* 19-21 September 2006,Frascati Italy.

Kokaly, R.F., Asner, G.P., Ollinger, S.V., Martin, M.E., & Wessman, C.A. (2009). Characterizing canopy biochemistry from imaging spectroscopy and its application to ecosystem studies. *Remote Sensing of Environment, 113 (SUPPL. 1)*, S78-S91.

Kooistra, L., Wamelink, W., Schaepman-Strub, G., Schaepman, M., van Dobben, H., Aduaka, U., & Batelaan, O. (2008). Assessing and predicting biodiversity in a floodplain ecosystem: Assimilation of net primary production derived from imaging spectrometer data into a dynamic vegetation model. *Remote Sensing of Environment, 112*, 2118-2130.

Kötz, B., Schaepman, M., Morsdorf, F., Bowyer, P., Itten, K., & Allgower, B. (2004). Radiative transfer modeling within a heterogeneous canopy for estimation of forest fire fuel properties. *Remote Sensing of Environment, 92*, 332-344.

Kuusk, A., & Nilson, T. (2000). A directional multispectral forest reflectance model. *Remote Sensing of Environment, 72*, 244-252.

Kuusk, A., Nilson, T., Paas, M., Lang, M., & Kuusk, J. (2008). Validation of the forest radiative transfer model FRT. *Remote Sensing of Environment, 112*, 51-58.

Labate, D., Ceccherini, M., Cisbani, A., De Cosmo, V., Galeazzi, C., Giunti, L., Melozzi, M., Pieraccini, S., & Stagi, M. (2009). The PRISMA payload optomechanical design, a high performance instrument for a new hyperspectral mission. *Acta Astronautica, 65*, 1429-1436.

Lacaze, R., & Roujean, J.L. (2001). G-function and HOt SpoT (GHOST) reflectance model - Application to multi-scale airborne POLDER measurements. *Remote Sensing of Environment, 76*, 67-80.

Lang, M., Nilson, T., Kuusk, A., Kiviste, A., & Hordo, M. (2007). The performance of foliage mass and crown radius models in forming the input of a forest reflectance model: A test on forest growth sample plots and Landsat 7 ETM+ images. *Remote Sensing of Environment, 110*, 445-457.

Lavergne, T., Kaminski, T., Pinty, B., Taberner, M., Gobron, N., Verstraete, M.M., Vossbeck, M., Widlowski, J.L., & Giering, R. (2007). Application to MISR land products of an RPV model inversion package using adjoint and Hessian codes. *Remote Sensing of Environment, 107*, 362-375.

Le Maire, G., François, C., & Dufrêne, E. (2004). Towards universal broad leaf chlorophyll indices using PROSPECT simulated database and hyperspectral reflectance measurements. *Remote Sensing of Environment, 89*, 1-28.

Leblanc, S.G., Chen, J.M., & Cihlar, J. (1997). NDVI directionality in boreal forests: A model interpretation of measurements. *Canadian Journal of Remote Sensing, 23*, 369-380.

Leblanc, S.G., Chen, J.M., White, H.P., Latifovic, R., Lacaze, R., & Roujean, J.L. (2005). Canada-wide foliage clumping index mapping from multiangular POLDER measurements. *Canadian Journal of Remote Sensing, 31*, 364-376.

Lenney, M.P., Woodcock, C.E., Collins, J.B., & Hamdi, H. (1996). The status of agricultural lands in Egypt: The use of multitemporal NDVI features derived from landsat TM. *Remote Sensing of Environment, 56*, 8-20.

Lewis, P. (1999). Three-dimensional plant modelling for remote sensing simulation studies using the Botanical Plant Modelling System. *Agronomie, 19*, 185-210.

Lewis, P.E., Disney, M.I., Quaife, T., Nichol, C., & Rebelo, L. (2005). *CTCD CHRIS-Proba activities.* Paper presented at the European Space Agency, (Special Publication) ESA SP, Frascati.

Li, W., Stamnes, K., Chen, B., & Xiong, X. (2001). Snow grain size retrieved from near-infrared radiances at multiple wavelengths. *Geophysical Research Letters, 28*, 1699-1702.

Li, X., & Strahler, A.H. (1992). Geometric-optical bidirectional reflectance modeling of the discrete crown vegetation canopy: Effect of crown shape and mutual shadowing. *IEEE Transactions on Geoscience and Remote Sensing*, 30, 276-292.

Lichtenthaler, H.K. (1987). Chlorophylls and carotenoids: Pigments of photosynthetic biomembranes. *Methods Enzymol., 148*, 350-382.

Lichtenthaler, H.K., Lang, M., Sowinska, M., Heisel, F., & Miehe, J.A. (1996). Detection of vegetation stress via a new high resolution fluorescence imaging system. *Journal of Plant Physiology, 148*, 599-612.

Liesenberg, V., Galvão, L.S., & Ponzoni, F.J. (2007). Variations in reflectance with seasonality and viewing geometry: Implications for classification of Brazilian savanna physiognomies with MISR/Terra data. *Remote Sensing of Environment, 107*, 276-286.

Lillesand, T.M., Kiefer, R.W., & Chipman, J.W. (2004). Remote sensing and image interpretation. Hohn Wiley & Sons

Los, S.O., North, P.R.J., Grey, W.M.F., & Barnsley, M.J. (2005). A method to convert AVHRR Normalized Difference Vegetation Index time series to a standard viewing and illumination geometry. *Remote Sensing of Environment, 99*, 400-411.

Lu, D., & Weng, Q. (2007). A survey of image classification methods and techniques for improving classification performance. *International Journal of Remote Sensing, 28*, 823-870.

Lucht, W., Schaaf, C.B., & Strahler, A.H. (2000). An algorithm for the retrieval of albedo from space using semiempirical BRDF models. *IEEE Transactions on Geoscience and Remote Sensing, 38*, 977-998.

Luyssaert, S., Schulze, E.D., Börner, A., Knohl, A., Hessenmäler, D., Law, B.E., Ciais, P., & Grace, J. (2008). Old-growth forests as global carbon sinks. *Nature, 455*, 213-215.

Maccioni, A., Agati, G., & Mazzinghi, P. (2001). New vegetation indices for remote measurement of chlorophylls based on leaf directional reflectance spectra. *Journal of Photochemistry and Photobiology B: Biology, 61*, 52-61.

Magda, S., Kriegman, D.J., Zickler, T., & Belhumeur, P.N. (2001). Beyond Lambert: Reconstructing surfaces with arbitrary BRDFs. *Proceedings of the IEEE International Conference on Computer Vision*, 2, 391-398.

Majeke, B., Van Aardt, J.A.N., & Cho, M.A. (2008). Imaging spectroscopy of foliar biochemistry in forestry environments. *Southern Forests, 70*, 275-285.

Malenovský, Z., Albrechtova, J., Lhotáková, Z., Zurita-Milla, R., Clevers, J.G.P.W., Schaepman, M.E., & Cudlín, P. (2006). Applicability of the PROSPECT model for Norway spruce needles. *International Journal of Remote Sensing, 27*, 5315-5340

Malenovský, Z., Martin, E., Homolova, L., Gastellu-Etchegorry, J.P., Zurita-Milla, R., Schaepman, M.E., Pokorny, R., Clevers, J.G.P.W., & Cudlin, P. (2008). Influence of woody elements of a Norway spruce canopy on nadir reflectance simulated by the DART model at very high spatial resolution. *Remote Sensing of Environment, 112*, 1-18.

Martínez, P.J., Pèrez, R.M., Plaza, A., Aguilar, P.L., Cantero, M.C., & Plaza, J. (2006). Endmember extraction algorithms from hyperspectral images. *Annals of Geophysics, 49*, 93-101.

Mättus, M., & Rautiainen, M. (2009). Direct retrieval of the shape of leaf spectral albedo from multiangular hyperspectral Earth observation data. *Remote Sensing of Environment, 113*, 1799-1807

McMurtrey Iii, J.E., Chappelle, E.W., Kim, M.S., Meisinger, J.J., & Corp, L.A. (1994). Distinguishing nitrogen fertilization levels in field corn (Zea mays L.) with actively induced fluorescence and passive reflectance measurements. *Remote Sensing of Environment, 47*, 36-44.

Meroni, M., Colombo, R., & Panigada, C. (2004). Inversion of a radiative transfer model with hyperspectral observations for LAI mapping in poplar plantations. *Remote Sensing of Environment, 92*, 195-206.

Middleton, E.M., Sullivan, J.H., Deluca, A.J., Bovard, B.D., Chan, S.S., & Cannon, T.A. (1997). Seasonal variability in foliar characteristics and physiology for boreal forest species at the five Saskatchewan tower sites during the 1994 Boreal Ecosystem-Atmosphere Study. *Journal of Geophysical Research D: Atmospheres, 102*, 28831-28844.

Minnaert, M. (1941). The reciprocity principle in lunar photometry. *Astrophysical Journal, 93*, 403-410

Mishra, V.D., Negi, H.S., Rawat, A.K., Chaturvedi, A., & Singh, R.P. (2009). Retrieval of sub-pixel snow cover information in the Himalayan region using medium and coarse resolution remote sensing data. *International Journal of Remote Sensing, 30*, 4707-4731.

Miura, T., Huete, A., & Yoshioka, H. (2006). An empirical investigation of cross-sensor relationships of NDVI and red/near-infrared reflectance using EO-1 Hyperion data. *Remote Sensing of Environment, 100*, 223-236.

Monteith, J.L. (1972) Solar radiation and productivity in tropical exosystems, *Journal of Applied Ecology, 9*, 747-766.

Moorthy, I., Miller, J.R., & Noland, T.L. (2008). Estimating chlorophyll concentration in conifer needles with hyperspectral data: An assessment at the needle and canopy level. *Remote Sensing of Environment, 112,* 2824-2838.

Morsdorf, F., Meier, E., Kötz, B., Itten, K.I., Dobbertin, M., & Allgöwer, B. (2004). LIDAR-based geometric reconstruction of boreal type forest stands at single tree level for forest and wildland fire management. *Remote Sensing of Environment, 92*, 353-362.

Morsdorf, F., Nichol, C., Malthus, T., & Woodhouse, I.H. (2009). Assessing forest structural and physiological information content of multi-spectral LiDAR waveforms by radiative transfer modelling. *Remote Sensing of Environment, 113*, 2152-2163.

Myneni, R. B., Nemani, R. R., & Running, S. W. (1997). Estimation of global leaf area index and absorbed par using radiative transfer models. *IEEE Transactions on Geoscience and Remote Sensing, 35*, 1380-1393.

Myneni, R.B., Hoffman, S., Knyazikhin, Y., Privette, J.L., Glassy, J., Tian, Y., Wang, Y., Song, X., Zhang, Y., Smith, G.R., Lotsch, A., Friedl, M., Morisette, J.T., Votava, P., Nemani, R.R., & Running, S.W. (2002). Global products of vegetation leaf area and fraction absorbed PAR from year one of MODIS data. *Remote Sensing of Environment, 83*, 214-231.

Myneni, R.B., Maggion, S., Iaquinto, J., Privette, J.L., Gobron, N., Pinty, B., Kimes, D.S., Verstraete, M.M., & Williams, D.L. (1995). Optical remote-sensing of vegetation - modeling, caveats, and algorithms. *Remote Sensing of Environment, 51*, 169-188.

Myneni, R.B., Ross, J., & Asrar, G. (1989). A review of the theory of photon transport in leaf canopies. *Agricultural & Forest Meteorology, 45*, 1-153.

Nichol, C. J., Huemmrich, K. F., Black, T. A., Jarvis, P. G., Walthall, C. L., Grace, J., & Hall, F. G. (2000). Remote sensing of photosynthetic-light-use efficiency of boreal forest. *Agricultural and Forest Meteorology, 101*, 131-142.

Nichol, C.J., Lloyd, J., Shibistova, O., Arneth, A., Röser, C., Knohl, A., Matsubara, S., & Grace, J. (2002). Remote sensing of photosynthetic-light-use efficiency of a Siberian boreal forest. *Tellus, Series B: Chemical and Physical Meteorology, 54*, 677-687.

Nicodemus, F.E., Richmond, J.C., Hsia, J.J., Ginsberg, I.W., & Limperis, T. (1977). Geometrical considerations and nomenclature for reflectance. In: *National Bureau of standards*, *160*. 1-52

Nilson, T., & Peterson, U. (1994). Age dependence of forest reflectance: Analysis of main driving factors. *Remote Sensing of Environment, 48*, 319-331.

Nolin, A.W. (2004). Towards retrieval of forest cover density over snow from the Multi-angle Imaging SpectroRadiometer (MISR). *Hydrological Processes, 18*, 3623-3636.

North, P.R.J. (1996). Three-dimensional forest light interaction model using a Monte Carlo method. *IEEE Transactions on Geoscience and Remote Sensing, 34*, 946-956.

Okin, G.S., Roberts, D.A., Murray, B., & Okin, W.J. (2001). Practical limits on hyperspectral vegetation discrimination in arid and semiarid environments. *Remote Sensing of Environment, 77*, 212-225.

Painter, T.H., & Dozier, J. (2004). The effect of anisotropic reflectance on imaging spectroscopy of snow properties. *Remote Sensing of Environment, 89*, 409-422.

Pearlman, J.S., Barry, P.S., Segal, C.C., Shepanski, J., Beiso, D., & Carman, S.L. (2003). Hyperion, a space-based imaging spectrometer. *IEEE Transactions on Geoscience and Remote Sensing, 41,* 1160-1173.

Peddle, D.R., Johnson, R.L., Cihlar, J., & Latifovic, R. (2004). Large area forest classification and biophysical parameter estimation using the 5-Scale canopy reflectance model in Multiple-Forward-Mode. *Remote Sensing of Environment, 89*, 252-263.

Peltoniemi, J.I., Kaasalainen, S., Naranen, J., Rautiainen, M., Stenberg, P., Smolander, H., Smolander, S., & Voipio, P. (2005). BRDF measurement of understory vegetation in pine forests: dwarf shrubs, lichen, and moss. *Remote Sensing of Environment, 94*, 343-354.

Peñuelas, J., & Inoue, Y. (2000). Reflectance assessment of canopy CO_2 uptake. *International Journal of Remote Sensing, 21*, 3353-3356.

Peñuelas, J., Baret, F., & Filella, I. (1995). Semi-empirical indices to assess carotenoids/chlorophyll a ratio from leaf spectral reflectance. *Photosynthetica, 31*, 221-230.

Pinter Jr, P. J., Zipoli, G., Maracchi, G., & Reginato, R. J. (1987). Influence of topography and sensor view angles on NIR/ red ratio and greenness vegetation indices of wheat. *International Journal of Remote Sensing, 8*, 953-957.

Pinty, B., & Verstraete, M.M. (1992). On the design and validation of surface bidirectional reflectance and albedo models. *Remote Sensing of Environment, 41*, 155-167.

Pinty, B., Gobron, N., Widlowski, J.L., Gerstl, S.A.W., Verstraete, M.M., Antunes, M., Bacour, C., Gascon, F., Gastellu, J.P., Goel, N., Jacquemoud, S., North, P., Qin, W., & Thompson, R. (2001). Radiation transfer model intercomparison (RAMI) exercise. *Journal of Geophysical Research D: Atmospheres, 106*, 11937-11956.

Pinty, B., Gobron, N., Widlowski, J.L., Lavergne, T., & Verstraete, M.M. (2004). Synergy between 1-D and 3-D radiation transfer models to retrieve vegetation canopy properties from remote sensing data. *Journal of Geophysical Research D: Atmospheres, 109*, D21205 1-16.

Pinty, B., Verstraete, M.M., & Dickinson, R.E. (1989). A physical model for predicting bidirectional reflectances over bare soil. *Remote Sensing of Environment, 27*, 273-288.

Pinty, B., Widlowski, J.L., Gobron, N., Verstraete, M.M., & Diner, D.J. (2002). Uniqueness of multiangular measurements - Part I: An indicator of subpixel surface heterogeneity from MISR. *IEEE Transactions on Geoscience and Remote Sensing, 40*, 1560-1573.

Pisek, J., Chen, J.M., Miller, J.R., Freemantle, J.R., Peltoniemi, J.I., & Simic, (2010). A. Mapping forest background reflectance in a boreal region using multiangle compact airborne spectrographic imager data. *IEEE Transactions on Geoscience and Remote Sensing, 48*, 499-510.

Plaza, A., Martínez, P., Pèrez, R., & Plaza, J. (2004). A quantitative and comparative analysis of endmember extraction algorithms from hyperspectral data. *IEEE Transactions on Geoscience and Remote Sensing, 42*, 650-663.

Pocewicz, A., Vierling, L.A., Lentile, L.B., & Smith, R. (2007). View angle effects on relationships between MISR vegetation indices and leaf area index in a recently burned ponderosa pine forest. *Remote Sensing of Environment, 107*, 322-333.

Qi, J., Moran, M.S., Cabot, F., & Dedieu, G. (1995). Normalization of sun/view angle effects using spectral albedo-based vegetation indices. *Remote Sensing of Environment*, 52, 207-217.

Quaife, T., Lewis, P., De Kauwe, M., Williams, M., Law, B.E., Disney, M., & Bowyer, P. (2008). Assimilating canopy reflectance data into an ecosystem model with an Ensemble Kalman Filter. *Remote Sensing of Environment, 112*, 1347-1364.

Radeloff, V.C., Mladenoff, D.J., & Boyce, M.S. (1999). Detecting jack pine budworm defoliation using spectral mixture analysis: Separating effects from determinants. *Remote Sensing of Environment, 69*, 156-169.

Rahman, A.F., Gamon, J.A., Fuentes, D.A., Roberts, D.A., & Prentiss, D. (2001). Modeling spatially distributed ecosystem flux of boreal forest using hyperspectral indices from AVIRIS imagery. *Journal of Geophysical Research D: Atmospheres, 106,* 33579-33591.

Rahman, H., Pinty, B., & Verstraete, M.M. (1993). Coupled surface-atmosphere reflectance (CSAR) model 2. Semiempirical surface model usable with NOAA advanced very high resolution radiometer data. *Journal of Geophysical Research, 98*, 20791-20801.

Rautiainen, M. (2005). Retrieval of leaf area index for a coniferous forest by inverting a forest reflectance model. *Remote Sensing of Environment, 99*, 295-303.

Rautiainen, M., & Stenberg, P. (2005). Application of photon recollision probability in coniferous canopy reflectance simulations. *Remote Sensing of Environment, 96*, 98-107.

Rautiainen, M., Lang, M., Mättus, M., Kuusk, A., Nilson, T., Kuusk, J., & Lükk, T. (2008). Multi-angular reflectance properties of a hemiboreal forest: An analysis using CHRIS PROBA data. *Remote Sensing of Environment, 112*, 2627-2642.

Rautiainen, M., Stenberg, P., Nilson, T., & Kuusk, A. (2004). The effect of crown shape on the reflectance of coniferous stands. *Remote Sensing of Environment, 89*, 41-52.

Rautiainen, M., Suomalainen, J., Mättus, M., Stenberg, P., Voipio, P., Peltoniemi, J., & Manninen, T. (2007). Coupling forest canopy and understory reflectance in the Arctic latitudes of Finland. *Remote Sensing of Environment, 110*, 332-343.

Richter, R. (1998). Correction of satellite imagery over mountainous terrain. *Applied Optics, 37*, 4004-4015.

Richter, R., & Schläpfer, D. (2002). Geo-atmospheric processing of airborne imaging spectrometry data. Part 2: Atmospheric/topographic correction. *International Journal of Remote Sensing, 23*, 2631-2649.

Risch, A.C., Nagel, L.M., Schütz, M., Krüsi, B.O., Kienast, F., & Bugmann, H. (2003). Structure and long-term development of subalpine Pinus montana Miller and Pinus cembra L. forests in the Central European Alps. *Struktur und Langzeitentwicklung von subalpinen Pinus montana Miller und Pinus cembra L. Wäldern in den zentraleuropäischen Alpen, 122*, 219-230.

Roberts, D.A., Smith, M.O., & Adams, J.B. (1993). Green vegetation, nonphotosynthetic vegetation, and soils in AVIRIS data. *Remote Sensing of Environment, 44*, 255-269.

Roberts, D.A., Ustin, S.L., Ogunjemiyo, S., Greenberg, J., Bobrowski, S.Z., Chen, J., & Hinckley, T.M. (2004). Spectral and structural measures of northwest forest vegetation at leaf to landscape scales. *Ecosystems, 7*, 545-562.

Roberts, G. (2001). A review of the application of BRDF models to infer land cover parameters at regional and global scales. *Progress in Physical Geography, 25*, 483-511.

Ross, J. (1981). *The Radiation Regime and Architecture of Plant Stands.*

Roujean, J.-L., Schaaf, C. B. & Lucht, W. (2004). Parametric BRDF models for albedo calculation. In: Schönermark, M. von, Geiger, B., and Röser, H.-P. (Eds.), Reflection Properties of Vegetation and Soil. Wissenschaft & Technik Verlag, Berlin, 352 pp., 105-120.

Sabol Jr, D.E., Gillespie, A.R., Adams, J.B., Smith, M.O., & Tucker, C.J. (2002). Structural stage in Pacific Northwest forests estimated using simple mixing models of multispectral images. *Remote Sensing of Environment, 80*, 1-16.

Salisbury, J.W., D'Aria, D.M., & Wald, A. (1994). Measurements of thermal infrared spectral reflectance of frost, snow, and ice. *Journal of Geophysical Research, 99*, 24,235-24,240.

Sampson, P.H., Zarco-Tejada, P.J., Mohammed, G.H., Miller, J.R., & Noland, T.L. (2003). Hyperspectral remote sensing of forest condition: Estimating chlorophyll content in tolerant hardwoods. *Forest Science, 49*, 381-391.

Sandmeier, S., & Deering, D.W. (1999). Structure analysis and classification of boreal forests using airborne hyperspectral BRDF data from ASAS. *Remote Sensing of Environment, 69*, 281-295.

Santer, R., Ramon, D., Vidot, J., & Dilligeard, E. A surface reflectance model for aerosol remote sensing over land (2007) *International Journal of Remote Sensing, 28,* 737-760.

Saxe, H., Cannell, M.G.R., Johnsen, Ã., Ryan, M.G., & Vourlitis, G. (2001). Tree and forest functioning in response to global warming. *New Phytologist, 149*, 369-400.

Schaaf, C.B., Gao, F., Strahler, A.H., Lucht, W., Li, X., Tsang, T., Strugnell, N.C., Zhang, X., Jin, Y., & Muller, J.-P. (2002). First operational BRDF, albedo nadir reflectance products from MODIS. *Remote Sensing of Environment, 83*, 135-148.

Schaaf., C.B., Li, X., & Strahler, A.H. (1994). Topographic effects on bidirectional and hemispherical reflectances calculated with a geometric-optical canopy model. *IEEE Transactions on Geoscience and Remote Sensing, 32*, 1186-1193.

Schaepman, M.E. (2007) Spectrodirectional remote sensing: from pixels to processes. *International Journal of Applied Earth Observation and Geoinformation*, 9, 204-223.

Schaepman, M.E., Koetz, B., Schaepman-Strub, G., & Itten, K.I. (2005). Spectrodirectional remote sensing for the improved estimation of biophysical and -chemical variables: Two case studies. *International Journal of Applied Earth Observation and Geoinformation, 6*, 271-282.

Schaepman, M.E., Koetz, B., Schaepman-Strub, G., Zimmermann, N.E., & Itten, K.I. (2004). Quantitative retrieval of biogeophysical characteristics using imaging spectroscopy - A mountain forest case study. *Community Ecology, 5*, 93-104.

Schaepman, M.E., Ustin, S.L., Plaza, A., Painter, T., Verrelst, J. & Liang, S. (2009). Earth system science related imaging spectroscopy - An assessment. *Remote Sensing of Environment. 113 (SUPPL. 1)*, S123-S137.

Schaepman, M.E., Ustin, S.L., Plaza, A.J., Painter, T.H., Verrelst, J., & Liang, S. (2009). Earth system science related imaging spectroscopy-An assessment. *Remote Sensing of Environment, 113*, S123-S137.

Schaepman-Strub, G., Schaepman, M.E., Painter, T.H., Dangel, S., & Martonchik, J.V. (2006). Reflectance quantities in optical remote sensing--definitions and case studies. *Remote Sensing of Environment, 103*, 27-42.

Schläpfer, D., Koetz, B., Gruber, S., & Morsdorf, F. (2003). The influence of DEM characteristics on preprocessing of DAIS/ROSIS data in high altitude alpine terrain. In 3rd EARSeL Workshop on Imaging Spectroscopy, Herrsching, Germany, 13-16 May 2003. Edited by M. Habermeyer, A. Müller and S. Holzwarth. European Association of Remote Sensing Laboratories (EARSel) and Deutsches Zentrum für Luft- und Raumfahrt (DLR). pp. 133-139.

Schlerf, M., & Atzberger, C. (2006). Inversion of a forest reflectance model to estimate structural canopy variables from hyperspectral remote sensing data. *Remote Sensing of Environment, 100*, 281-294.

Schlerf, M., Atzberger, C., & Hill, J. (2005). Remote sensing of forest biophysical variables using HyMap imaging spectrometer data. *Remote Sensing of Environment, 95*, 177-194.

Sedano, F., Lavergne, T., Ibañez, L.M., & Gong, P. (2008). A neural network-based scheme coupled with the RPV model inversion package. *Remote Sensing of Environment, 112*, 3271-3283.

Sellers, P.J. (1985). Canopy reflectance, photosynthesis and transpiration. *International Journal of Remote Sensing, 6*, 1335-1372.

Settle, J.J., & Drake, N.A. (1993). Linear mixing and the estimation of ground cover proportions. *International Journal of Remote Sensing, 14*, 1159-1177.

Shabanov, N.V., Wang, Y., Buermann, W., Dong, J., Hoffman, S., Smith, G.R., Tian, Y., Knyazikhin, Y., & Myneni, R.B. (2003). Effect of foliage spatial heterogeneity in the MODIS LAI and FPAR algorithm over broadleaf forests. *Remote Sensing of Environment, 85*, 410-423

Siitonen, J. (2001). Forest management, coarse woody debris and saproxylic organisms: Fennoscandian boreal forests as an example. *Ecological Bulletins, 49*, 11-41.

Simic, A., & Chen, J.M. (2008). Refining a hyperspectral and multiangle measurement concept for vegetation structure assessment. *Canadian Journal of Remote Sensing, 34*, 174-191.

Simic, A., Chen, J.M., Freemantle, J.R., Miller, J.R., & Pisek, J. (2009). Improving clumping and LAI algorithms based on multiangle airborne imagery and ground measurements. *IEEE Transactions on Geoscience and Remote Sensing.* In press.

Sims, D.A., & Gamon, J.A. (2002). Relationships between leaf pigment content and spectral reflectance across a wide range of species, leaf structures and developmental stages. *Remote Sensing of Environment, 81*, 337-354.

Sims, D.A., & Gamon, J.A. (2003). Estimation of vegetation water content and photosynthetic tissue area from spectral reflectance: A comparison of indices based on liquid water and chlorophyll absorption features. *Remote Sensing of Environment, 84*, 526-537.

Smith, R.C., Adams, J., Stephens, D.J., & Hick, P.T. (1995). Forecasting wheat yield in a Mediterranean-type environment from the NOAA satellite. *Australian Journal of Agricultural Research, 46*, 113-125.

Smolander, S., & Stenberg, P. (2003). A method to account for shoot scale clumping in coniferous canopy reflectance models. *Remote Sensing of Environment, 88*, 363-373

Snedecor, G.W., & Cochran, W.G. (1980). *Statistical Methods.* 7th edition, Iowa State University Press, Iowa.

Song, C., & Woodcock, C.E. (2002). The spatial manifestation of forest succession in optical imagery: The potential of multiresolution imagery. *Remote Sensing of Environment, 82*, 271-284

Song, C., Schroeder, T.A., & Cohen, W.B. (2007). Predicting temperate conifer forest successional stage distributions with multitemporal Landsat Thematic Mapper imagery. *Remote Sensing of Environment, 106*, 228-237.

Song, C.H., Woodcock, C.E., & Li, X.W. (2002). The spectral/temporal manifestation of forest succession in optical imagery - The potential of multitemporal imagery. *Remote Sensing of Environment, 82*, 285-302.

Soudani, K., Francois, C., le Maire, G., Le Dantec, V., & Dufréne, E. (2006). Comparative analysis of IKONOS, SPOT, and ETM+ data for leaf area index estimation in temperate coniferous and deciduous forest stands. *Remote Sensing of Environment, 102*, 161-175.

Spanner, M.A., Pierce, L.L., Peterson, D.L., & Running, S.W. (1990). Remote sensing of temperate coniferous forest leaf area index. The influence of canopy closure, understory vegetation and background reflectance. *International Journal of Remote Sensing, 11*, 95-111.

Stenberg, P., Rautiainen, M., Manninen, T., Voipio, P., & Smolander, H. (2004). Reduced simple ratio better than NDVI for estimating LAI in Finnish pine and spruce stands. *Silva Fennica, 38*, 3-14.

Steven, M.D., Malthus, T.J., Baret, F., Xu, H., & Chopping, M.J. (2003). Intercalibration of vegetation indices from different sensor systems. *Remote Sensing of Environment, 88*, 412-422.

Stuffler, T., Förster, K., Hofer, S., Leipold, M., Sang, B., Kaufmann, H., Penné, B., Mueller, A., & Chlebek, C. (2009). Hyperspectral imaging-An advanced instrument concept for the EnMAP mission (Environmental Mapping and Analysis Programme). *Acta Astronautica, 65*, 1107-1112.

Stylinski, C. D., Gamon, J. A., & Oechel, W. C. (2002). Seasonal patterns of reflectance indices, carotenoid pigments and photosynthesis of evergreen chaparral species. *Oecologia, 131*, 366-374.

Su, L., Huang, Y., Chopping, M.J., Rango, A., & Martonchik, J.V. (2009). An empirical study on the utility of BRDF model parameters and topographic parameters for mapping vegetation in a semi-arid region with MISR imagery. *International Journal of Remote Sensing, 30*, 3463-3483.

Suárez, L., Zarco-Tejada, P.J., Sepulcre-Canto, G., Pérez-Priego, O., Miller, J.R., Jiménez-Muñoz, J.C., & Sobrino, J. (2008). Assessing canopy PRI for water stress detection with diurnal airborne imagery. *Remote Sensing of Environment, 112*, 560-575.

Teillet, P.M., Staenz, K., & William, D.J. (1997). Effects of spectral, spatial, and radiometric characteristics on remote sensing vegetation indices of forested regions. *Remote Sensing of Environment 61*, 139-149.

Telesca, L., & Lasaponara, R. (2006). Quantifying intra-annual persistent behaviour in SPOT-VEGETATION NDVI data for Mediterranean ecosystems of southern Italy. *Remote Sensing of Environment, 101*, 95-103.

Toutin, T. (2004). Geometric processing of remote sensing images: Models, algorithms and methods. *International Journal of Remote Sensing, 25*, 1893-1924.

Trishchenko, A.P., Cihlar, J., & Li, Z. (2002). Effects of spectral response function on surface reflectance and NDVI measured with moderate resolution satellite sensors. *Remote Sensing of Environment, 81*, 1-18.

Trotter, G.M., Whitehead, D., & Pinkney, E.J. (2002). The photochemical reflectance index as a measure of photosynthetic light use of efficiency for plants with varying foliar nitrogen contents. *International Journal of Remote Sensing, 23*, 1207-1212.

Tucker, C.J. (1979). Red and photographic infrared linear combinations for monitoring vegetation. *Remote Sensing of Environment, 8*, 127-150.

Ungar, S.G., Pearlman, J.S., Mendenhall, J.A., & Reuter, D. (2003). Overview of the Earth Observing One (EO-1) mission. *IEEE Transactions on Geoscience and Remote Sensing, 41*, 1149-1159.

Ustin, S.L., Gitelson, A.A., Jacquemoud, S., Schaepman, M.E., Asner, G., Gamon, J.A. & Zarco-Tejada, P. (2009). Retrieval of Foliar Information about Plant Pigment Systems from High Resolution Spectroscopy. *Remote Sensing of Environment. 113 (SUPPL. 1)*, S67-S77.

Ustin, S.L., Roberts, D.A., Gamon, J.A., Asner, G.P., & Green, R.O. (2004). Using imaging spectroscopy to study ecosystem processes and properties. *BioScience, 54*, 523-534.

Van Leeuwen, W.J.D., Huete, A.R., & Laing, T.W. (1999). MODIS vegetation index compositing approach: A prototype with AVHRR data. *Remote Sensing of Environment, 69,* 264-280.

Van Leeuwen, W.J.D., Orr, B.J., Marsh, S.E., & Herrmann, S.M. (2006). Multi-sensor NDVI data continuity: Uncertainties and implications for vegetation monitoring applications. *Remote Sensing of Environment, 100*, 67-81.

Verhoef, W. (1984). Light scattering by leaf layers with application to canopy reflectance modeling: The SAIL model. *Remote Sensing of Environment, 16*, 125-141.

Verhoef, W., & Bach, H. (2003). Remote sensing data assimilation using coupled radiative transfer models. *Physics and Chemistry of the Earth, 28*, 3-13.

Verrelst, J., Ac, A, Malenovský, Z., Hanus, J., Marek, M.V., & Schaepman, M.E. (2007). Angular chlorophyll indices estimates derived from ground-based diurnal course data and multiangular CHRIS-PROBA data: Two case studies. In: *Proceedings 5th EARSeL SIG IS workshop,* Brugge, Belgium, 23-25 April 2007.

Verrelst, J., Clevers, J.G.P.W., & Schaepman, M.E. (2010a). Merging minnaert-k parameter with spectral unmixing to map forest heterogeneity with CHRIS-PROBA data. *IEEE Transactions on Geoscience and Remote Sensing.* In review.

Verrelst, J., Koetz, B., Kneubühler, M., & Schaepman, M.E. (2006a). Directional sensitivity analysis of vegetation indices from multi-angular CHRIS/PROBA data. In: *ISPRS 2006: ISPRS mid-term symposium 2006*, Enschede, the Netherlands, 8-11 May 2006.

Verrelst, J., Schaepman, M.E., & Clevers, J.G.P.W. (2008a). A modelling approach for studying forest chlorophyll content in relation to canopy composition. In: *Proceedings of the XXI ISPRS Congress*, Beijing, China, 3-11 July 2008.

Verrelst, J., Schaepman, M.E., & Clevers, J.G.P.W. (2010b). Spectrodirectional Minnaert-k retrieval using CHRIS/PROBA data. *Remote Sensing of Environment,* In review.

Verrelst, J., Schaepman, M.E., & Clevers, J.G.P.W. (2009a). Fusing Minnaert-k parameter with spectral unmixing for forest heterogeneity mapping using CHRIS-PROBA data. In: *first IEEE GRSS WHISPERS*. Grenoble, France, 26-28 August 2009.

Verrelst, J., Schaepman, M.E., Koetz, B., & Clevers, J.G.P.W. (2009b). Spectrodirectional Minnaert-k retrieval using CHRIS-PROBA data. In: *EARSeL Imaging Spectrometry Workshop*. Tel Aviv, Israel, 16-19 March 2009.

Verrelst, J., Schaepman, M.E., Koetz, B., & Kneubühler, M. (2006b). Assessing the angular variability of broandband and narrowband vegetation indices using CHRIS/PROBA data. In: *Proceedings 4th International Workshop on Multiangular Measurements and Models (IWMMM-4)*, Sydney, Australia, 20-24 March 2006.

Verrelst, J., Schaepman, M.E., Koetz, B., & Kneubühler, M. (2008b). Angular sensitivity analysis of vegetation indices derived from CHRIS/PROBA data. *Remote Sensing of Environment, 112*, 2341-2353.

Verrelst, J., Schaepman, M.E., Malenovský, Z., & Clevers, J.G.P.W. (2010c). Effects of woody elements on simulated canopy reflectance: Implications for forest chlorophyll content retrieval. *Remote Sensing of Environment,114*, 647-656

Verstraete, M.M., & Pinty, B. (1996). Designing optimal spectral indexes for remote sensing applications. *IEEE Transactions on Geoscience and Remote Sensing, 34*, 1254-1265.

Verstraete, M.M., Pinty, B., & Dickinson, R.E. (1990). A physical model of the bidirectional reflectance of vegetation canopies: 1. Theory. *Journal of Geophysical Research, 95*, 11755-11765.

Vikhamar, D., & Solberg, R. (2003). Subpixel mapping of snow cover in forests by optical remote sensing. *Remote Sensing of Environment, 84*, 69-82.

Vincent, R.K.J. (1997), *Fundamentals of Geological and Environmental Remote Sensing*. Prentice Hall, Uper Saddle River, New Jersey.

Vuolo, F., Dini, L., & D'Urso, G. (2008). Retrieval of Leaf Area Index from CHRIS/PROBA data: an analysis of the directional and spectral information content. *International Journal of Remote Sensing, 29*, 5063-5072.

Wang, Y., Buermann, W., Stenberg, P., Smolander, H., Hame, T., Tian, Y., Hu, J., Knyazikhin, Y., & Myneni, R.B. (2003). A new parameterization of canopy spectral response to incident solar radiation: case study with hyperspectral data from pine dominant forest. *Remote Sensing of Environment, 85*, 304-315.

Wanner, W., Strahler, A.H., Hu, B., Lewis, P., Muller, J.P., Li, X., Barker Schaaf, C.L., & Barnsley, M.J. (1997). Global retrieval of bidirectional reflectance and albedo over land from EOS MODIS and MISR data: Theory and algorithm. *Journal of Geophysical Research D: Atmospheres, 102*, 17143-17161.

Warren, S.G., Brandt, R.E., & Hinton, P.O. (1998). Effect of surface roughness on bidirectional reflectance of Antarctic snow. *Journal of Geophysical Research E: Planets, 103*, 25789-25807

Wessels, K.J., De Fries, R.S., Dempewolf, J., Anderson, L.O., Hansen, A.J., Powell, S.L., & Moran, E.F. (2004). Mapping regional land cover with MODIS data for biological conservation: Examples from the Greater Yellowstone Ecosystem, USA and Parao State, Brazil. *Remote Sensing of Environment, 92*, 67-83.

White, J.C., Wulder, M.A., Brooks, D., Reich, R., & Wheate, R.D. (2005). Detection of red attack stage mountain pine beetle infestation with high spatial resolution satellite imagery. *Remote Sensing of Environment, 96*, 340-351.

Widlowski, J.L. (2002). Extracting quantitative sub-pixel heterogeneity information form optical remote sensing data. PhD Thesis, University of Fribourg, Switzerland. 173 pp.

Widlowski, J.L., Lavergne, T., Pinty, B., Gobron, N., & Verstraete, M.M. (2008). Towards a high spatial resolution limit for pixel-based interpretations of optical remote sensing data. *Advances in Space Research, 41*, 1724-1732.

Widlowski, J.L., Pinty, B., Gobron, N., Verstraete, M.M., & Davis, A.B. (2001). Characterization of surface heterogeneity detected at the MISR/TERRA subpixel scale. *Geophysical Research Letters, 28*, 4639-4642.

Widlowski, J.L., Pinty, B., Gobron, N., Verstraete, M.M., Diner, D.J., & Davis, A.B. (2004). Canopy structure parameters derived from multi-angular remote sensing data for terrestrial carbon studies. *Climatic Change, 67*, 403-415.

Widlowski, J.L., Pinty, B., Lavergne, T., Verstraete, M.M., & Gobron, N. (2006). Horizontal radiation transport in 3-D forest canopies at multiple spatial resolutions: Simulated impact on canopy absorption. *Remote Sensing of Environment, 103*, 379-397.

Widlowski, J.L., Taberner, M., Pinty, B., Bruniquel-Pinel, V., Disney, M., Fernandes, R., Gastellu-Etchegorry, J.P., Gobron, N., Kuusk, A., Lavergne, T., Leblanc, S., Lewis, P.E., Martin, E., Mõttus, M., North, P.R.J., Qin, W., Robustelli, M., Rochdi, N., Ruiloba, R., Soler, C., Thompson, R.,

Verhoef, W., Verstraete, M.M., & Xie, D. (2007). Third Radiation Transfer Model Intercomparison (RAMI) exercise: Documenting progress in canopy reflectance models. *Journal of Geophysical Research D: Atmospheres, 112,* D09111.

Woldendorp, G., & Keenan, R.J. (2005). Coarse woody debris in Australian forest ecosystems: A review. *Austral Ecology, 30*, 834-843

Xavier, A.C., Theodor Rudorff, B.F., Moreira, M.A., Alvarenga, B.S., De Freitas, J.G., & Salomon, M.V. (2006). Hyperspectral field reflectance measurements to estimate wheat grain yield and plant height. *Scientia Agricola, 63*, 130-138.

Xiao, X., Boles, S., Frolking, S., Li, C., Babu, J.Y., Salas, W., & Moore Iii, B. (2006). Mapping paddy rice agriculture in South and Southeast Asia using multi-temporal MODIS images. *Remote Sensing of Environment, 100*, 95-113.

Xue, L., & Yang, L. (2009). Deriving leaf chlorophyll content of green-leafy vegetables from hyperspectral reflectance. *ISPRS Journal of Photogrammetry and Remote Sensing, 64,* 97-106.

Yu, F., Price, K.P., Ellis, J., & Shi, P. (2003). Response of seasonal vegetation development to climatic variations in eastern central Asia. *Remote Sensing of Environment, 87*, 42-54.

Zarco-Tejada, P.J., Miller, J.R., Harron, J., Hu, B., Noland, T.L., Goel, N., Mohammed, G.H., & Sampson, P. (2004). Needle chlorophyll content estimation through model inversion using hyperspectral data from boreal conifer forest canopies. *Remote Sensing of Environment, 89*, 189-199.

Zarco-Tejada, P.J., Miller, J.R., Mohammed, G.H., & Noland, T.L. (2000). Chlorophyll fluorescence effects on vegetation apparent reflectance: I. Leaf-level measurements and model simulation. *Remote Sensing of Environment, 74*, 582-595.

Zarco-Tejada, P.J., Miller, J.R., Mohammed, G.H., Noland, T.L., & Sampson, P.H. (2002). Vegetation stress detection through chlorophyll a + b estimation and fluorescence effects on hyperspectral imagery. *Journal of Environmental Quality, 31*, 1433-1441.

Zarco-Tejada, P.J., Miller, J.R., Morales, A., Berjón, A., & Agüera, J. (2004). Hyperspectral indices and model simulation for chlorophyll estimation in open-canopy tree crops. *Remote Sensing of Environment, 90*, 463-476.

Zarco-Tejada, P.J., Miller, J.R., Noland, T.L., Mohammed, G.H., & Sampson, P.H. (2001). Scaling-up and model inversion methods with narrowband optical indices for chlorophyll content estimation in closed forest canopies with hyperspectral data. *IEEE Transactions on Geoscience and Remote Sensing, 39*, 1491-1507.

Zarco-Tejada, P.J., Ustin, S.L., & Whiting, M.L. (2005). Temporal and spatial relationships between within-field yield variability in cotton and high-spatial hyperspectral remote sensing imagery. *Agronomy Journal, 97*, 641-653.

Zhang, Q., Xiao, X., Braswell, B., Linder, E., Baret, F., & Moore Iii, B. (2005). Estimating light absorption by chlorophyll, leaf and canopy in a deciduous broadleaf forest using MODIS data and a radiative transfer model. *Remote Sensing of Environment, 99*, 357-371.

Zhang, Q., Xiao, X., Braswell, B., Linder, E., Ollinger, S., Smith, M.L., Jenkins, J.P., Baret, F., Richardson, A.D., Moore Iii, B., & Minocha, R. (2006). Characterization of seasonal variation of forest canopy in a temperate deciduous broadleaf forest, using daily MODIS data. *Remote Sensing of Environment, 105*, 189-203.

Zhang, Y., Chen, J.M., Miller, J.R., & Noland, T.L. (2008). Leaf chlorophyll content retrieval from airborne hyperspectral remote sensing imagery. *Remote Sensing of Environment, 112*, 3234-3247

Zoller, H., (1995). In: *Vegetationskarte des Schweizerischen Nationalparks. Erläuterungen*, National Park Forschung, Zernetz, Switzerland, p. 108.

Zurita-Milla, R., Clevers, J.G.P.W., Schaepman, M.E. & Kneubühler, M. (2007). Effects of MERIS L1b radiometric calibration on regional land cover mapping and land products. *International Journal of Remote Sensing, 28*, 653-673.

Zurita-Milla, R., Clevers, J.G.P.W., & Schaepman, M.E. (2008). Unmixing-based landsat TM and MERIS FR data fusion. *IEEE Geoscience and Remote Sensing Letters, 5*, 453-457

Summary

With the upcoming global warming forests are under threat. To forecast climate change impacts and adaptations, there is need for developing improved forest monitoring services, which are able to record, quantify and map bio-indicators of the forests' health status across the globe. In this context, Earth observation (EO) can provide a substantial amount of up-to-date information about the biochemical and structural conditions of our forests at a local-to-global scale. Among the optical EO instruments in space, one of the most innovative instruments is the experimental Compact High Resolution Imaging Spectrometer (CHRIS) on board the PROBA-1 (Project for On Board Autonomy) satellite. CHRIS is capable of sampling reflected radiation at five viewing angles over the visible and near-infrared (VNIR) region of the solar spectrum with a relatively high spatial resolution (~17 m). The as such acquired spectrodirectional (combined multi-angular and spectroscopy) data may lead to new opportunities for space-based forest monitoring applications, yet the added value of canopy reflectance anisotropy measured over the whole VNIR spectral region is largely unknown. This is why the use of space-borne spectrodirectional data of a forested target has been investigated in this thesis.

An Alpine old-growth forest was chosen as study site because of its large heterogeneity in structure and composition. This heterogeneity in structure can be characterized by variation in canopy cover (CC) and leaf area index (LAI). The heterogeneity in composition can be characterized by variation in non-photosynthetic vegetation (NPV: e.g. dead standing trees and coarse woody debris) and photosynthetic vegetation (PV: e.g. foliage). Such a large heterogeneity exerts influence on reflectance anisotropy in the VNIR and therefore challenges the interpretation of spectrodirectional data. While reflectance anisotropy has traditionally been considered as a source of noise, in turn, when having an improved understanding of its functioning, it may actually become usable for mapping the canopy heterogeneity. The main objective of this thesis is therefore to analyze the link between canopy variables and spectrodirectional data with the purpose of (*i*) evaluating the use of spectrodirectional data, and (*ii*) developing a mapping application that enables to monitor forest heterogeneity at the subpixel scale.

Chapter 1 outlines the radiative transfer processes and models that are of importance for mapping quantitative forest properties, links the models in relation to forest growth development, sketches the potentials of multi-angular imaging spectrometry for forest monitoring, and after that, lists the research objectives of this PhD thesis.

Chapter 2 addresses the phenomena of canopy reflectance anisotropy in the VNIR by means of vegetation indices. For a set of broadband and narrowband vegetation indices the angular reflectance anisotropy of an old-growth forest and an Alpine meadow as measured by CHRIS was statistically evaluated. Not only the conventional broadband greenness indices but also narrowband greenness indices as well as light use efficiency and leaf pigment indices (e.g. Photochemical Reflectance Index: PRI) were subject to canopy anisotropy effects. The

forest produced more pronounced reflectance anisotropy than the meadow due to its heterogeneous canopy structure. A model-based quantification of the underlying forest canopy variables showed that angularity of PRI can be partly explained by the angular-dependent variation in observed PV and NPV proportions.

Chapter 3 builds further on the findings of chapter 2 by assessing the influence of structural and compositional variables on the performance of vegetation indices. Therefore, a sensitivity study was employed in which the detectability of chlorophyll (*Cab*) content at the canopy level was analyzed on the basis of modeled reflectance data. Statistical analysis revealed that most of the chlorophyll indices outperform single wavelengths in assessing *Cab* content, with best results obtained by the Maccioni index ($[R_{780} - R_{710}] / [R_{780} - R_{680}]$). The Maccioni index was highly sensitive to variations in *Cab* content but relatively insensitive to variations in LAI, CC and NPV. The modeling results provided a theoretical framework for evaluating how reliable *Cab* content can be assessed under various canopy conditions. This evaluation was applied for three distinct coniferous forest types (young, early mature and old-growth stands). It is concluded that the presence of woody elements considerably perturb the relationships between a vegetation index and foliar biochemistry.

Having identified some mechanisms that govern reflectance anisotropy in the VNIR, chapter 4 investigated the mappable information content that can be exploited from space-borne measured reflectance anisotropy. More precisely, the anisotropic reflectance of an Alpine old-growth forest was quantified and analyzed across the VNIR using the so-called Minnaert-*k* parameter. This parameter describes the curvature of reflectance anisotropy and is obtained through inversion of the parametric Rahman–Pinty–Verstraete (RPV) model. Results indicated that for a forested ecosystem with a bright underlying snow cover a switch from bell-shaped ($k > 1$) to bowl-shaped ($k < 1$) reflectance anisotropy patterns takes place in the red edge and early NIR part of the spectrum. It was found that CC plays an important role in determining at which wavelength this switch takes place. The strong spectral dependency of reflectance anisotropy dynamics, with in particular the usable information content in the red edge, encourages the use of multi-angular spectrometers for forestry applications.

Chapter 5 implemented the newly acquired knowledge of reflectance anisotropy dynamics into a mapping application. The uniqueness of CHRIS was exploited to the fullest: information on canopy properties was independently derived from both the angular and spectral domains. In the angular domain a map of the Minnaert-*k* parameter was generated while in the spectral domain a CC map was generated. It was evaluated that both maps are complementary in the red edge (722 nm). Both maps provided information on canopy structure but also have there single-source limitations. Merging Minnaert-*k* with CC produced a unique new data layer that provides information on the horizontal and vertical heterogeneity of the forest canopy at the sensor subpixel scale.

Chapter 6 contains the final conclusions and gives recommendations for further research. The overall conclusion is that space-borne spectrodirectional data are able to simultaneously

derive information on forest foliar biochemistry (from the spectral domain) and on forest cover heterogeneity (from the angular domain). This creates new opportunities to monitor heterogeneous ecosystems such as forests, woodlands and shrublands at a local-to-regional scale. The results presented in this thesis should therefore encourage further research in this field as a means to develop future spectrodirectional EO instruments and to apply derived mapping products into forest monitoring schemes across the globe.

Samenvatting

Met de opkomende opwarming van de aarde staan bossen onder druk. Om de gevolgen van klimaatsverandering en de aanpassingen van bosecosystemen te kunnen voorspellen is er behoefte aan de ontwikkeling van verbeterde waarnemingssystemen. Deze waarnemingssystemen dienen in staat te zijn om door middel van bio-indicatoren de gezondheidsstatus van bossen over de hele wereld te kwantificeren, karteren en te monitoren. In deze context is aardobservatie uitermate geschikt om up-to-date informatie over de biochemische en structurele toestand van onze bossen te bezorgen op een schaal die varieert van lokaal to mondiaal niveau. Eén van de meest innovatieve optische instrumenten aanwezig in de ruimte is de experimentele Compact High Resolution Imaging Spectrometer (CHRIS) aan boord van de PROBA-1 (Project for On Board Autonomy) satelliet. CHRIS is in staat om vanuit vijf kijkhoeken gereflecteerde straling te meten over het zichtbare en nabij-infrarood (VNIR) gebied van het elektromagnetisch spectrum bij een relatief hoge ruimtelijke resolutie (~17 m). De zodanig vanuit de ruimte verkregen spectrodirectionele gegevens (multi-kijkhoek en spectroscopie gecombineerd) kan tot nieuwe toepassingen leiden die geschikt zijn voor het monitoren van bossen. Echter, de toegevoegde waarde van reflectie-anisotropie, die gemeten is over het gehele VNIR spectrale gebied, is nog grotendeels onbekend. Dit brengt ons tot de kern van dit proefschrift dat als doelstelling heeft om de mogelijke toepassingen van spectrodirectionele reflectiegegevens van een bebost gebied te onderzoeken.

Een Alpien, oud naaldbos is gekozen als studiegebied vanwege de sterke heterogeniteit in structuur en samenstelling. Deze heterogeniteit in structuur wordt gekenmerkt door variatie in de bedekkingsgraad (CC) en bladoppervlakte-index (LAI). De heterogeniteit in samenstelling wordt gekenmerkt door variatie in niet-fotosynthetische vegetatie (NPV: bijv. dode, staande bomen en houtige elementen) en fotosynthetische vegetatie (PV: bijv. gebladerte). Zo'n grote heterogeniteit heeft zijn weerslag op de reflectie-anisotropie in het VNIR en kan dus de interpretatie van spectrodirectionele gegevens bemoeilijken. Terwijl enerzijds reflectie-anisotropie van oudsher beschouwd wordt als een bron van verstoring, betekent het anderzijds dat een betere kennis van de werking van reflectie-anisotropie deze informatie daadwerkelijk bruikbaar zou kunnen worden voor het karteren van bosheterogeniteit. Het belangrijkste doel van dit proefschrift is dan ook om de relaties tussen bosvariabelen en spectrodirectionele gegevens te analyseren, met het oog op: (*i*) het evalueren van het gebruik van spectrodirectionele gegevens voor bostoepassingen, en (*ii*) het ontwikkelen van een karteringstoepassing die het mogelijk maakt om bosheterogeniteit te kwantificeren op een subpixel schaalniveau. Het proefschrift is opgedeeld in zes hoofdstukken.

Hoofdstuk 1 beschrijft de processen van stralingsoverdracht en de reflectiemodellen die van belang zijn voor het in kaart brengen van kwantitatieve boseigenschappen, en relateert de modellen aan de ontwikkeling van bosgroei. Vervolgens schetst het de mogelijkheden van multi-kijkhoek beeldvormende spectrometers voor het monitoren van bossen en uiteindelijk somt het de onderzoeksdoelstellingen van dit proefschrift op.

Hoofdstuk 2 gaat in op het verschijnsel van reflectie-anisotropie van een Alpien landschap dat door CHRIS vanuit de ruimte onder verschillende kijkhoeken waargenomen is over het VNIR spectrale gebied. Reflectie-anisotropie is gekwantificeerd door middel van vegetatie indices. Voor een reeks van vegetatie indices, gebaseerd op brede en op smalle banden, is de reflectie-anisotropie van zowel een oud naaldbos als een Alpiene weide statistisch geëvalueerd. Niet alleen conventionele indices, maar ook indices gericht op licht-efficiëntie en bladpigmenten (bijvoorbeeld Photochemical Reflectance Index: PRI) tonen anisotropie effecten. De waargenomen reflectie-anisotropie is meer uitgesproken over bossen dan over weiden als gevolg van de grote heterogeniteit in de structuur van de vegetatie. Uit een modelleringsexperiment dat de onderliggende structurele variabelen van de bosbedekking kwantificeert blijkt dat de anisotropie van de gemeten PRI gedeeltelijk verklaard kan worden door de kijkhoek-afhankelijke variatie in waargenomen PV en NPV proporties.

Hoofdstuk 3 gaat dieper in op de bevindingen van hoofdstuk 2. De invloed van structuur- en compositie-variabelen op de prestaties van vegetatie indices is in dit hoofdstuk geanalyseerd. Door middel van gemodelleerde reflectiegegevens is een gevoeligheidsanalyse van de structurele variabelen op de waarneembaarheid van chlorofielgehalte (*Cab*) uitgevoerd op bosniveau. Uit statistische analyse blijkt dat de meeste chlorofiel-indices beter presteren dan een enkele golflengte bij het bepalen van *Cab*-gehalte, met de beste resultaten voor de Maccioni index ($[R_{780} - R_{710}] / [R_{780} - R_{680}]$). De Maccioni index is zeer gevoelig voor schommelingen in *Cab*-gehalte, maar relatief ongevoelig voor variaties in LAI, CC en NPV. Deze modelleringsresultaten vormen een theoretisch kader voor de evaluatie van hoe betrouwbaar het *Cab*-gehalte bepaald kan worden onder verschillende omstandigheden van bosbedekking. Dit is geëvalueerd voor drie verschillende soorten naaldbossen (een jong, een volgroeid en een oud bosbestand). De conclusie luidt dat de aanwezigheid van houtige elementen de relaties tussen een vegetatie index en de blad-biochemie aanzienlijk kan verstoren.

Na een aantal reflectie-anisotropie mechanismen in het VNIR geïdentificeerd te hebben, is in hoofdstuk 4 onderzocht hoe de vanuit de ruimte gemeten reflectie-anisotropie vertaald kan worden in nuttige informatie. Hiervoor is de reflectie-anisotropie van een Alpien oud bos gekwantificeerd en geanalyseerd over het VNIR met behulp van de zogenaamde Minnaert-*k* parameter. Deze parameter beschrijft de kromming van reflectie-anisotropie en wordt verkregen door inversie van het parametrische Rahman-Pinty-Verstraete (RPV) model. Resultaten tonen aan dat voor een bebost ecosysteem met een onderliggend sneeuwtapijt in het 'red edge' en het begin van het NIR deel van het electromagnetisch spectrum een omslag van klokvormige ($k > 1$) tot komvormige ($k < 1$) reflectie-anisotropie patronen plaatsvindt. CC blijkt een belangrijke rol te spelen bij het bepalen van de golflengte waarbij deze omslag plaatsvindt. De sterke spectrale afhankelijkheid van de dynamiek in reflectie-anisotropie, met in het bijzonder de bruikbare informatie-inhoud in de red edge, stimuleert het gebruik van multi-kijkhoek spectrometers voor bostoepassingen.

136

Hoofdstuk 5 heeft als doel de nieuw verworven kennis van reflectie-anisotropie uit te bouwen tot een karteringsapplicatie. Het unieke van CHRIS is maximaal geëxploiteerd: informatie over bosbedekkingseigenschappen is onafhankelijk van elkaar bepaald uit zowel het kijkhoek- als het spectrale domein. In het kijkhoek-domein is een kaart van de Minnaert-k parameter gegenereerd, terwijl in het spectrale domein een CC-kaart is gegenereerd. Elke kaart verstrekt informatie over bosstructuur maar elke heeft zijn specifieke beperkingen. Anderzijds zijn beide kaarten complementair bevonden in de red edge (722 nm). Door het samenvoegen van Minnaert-k met CC is een unieke nieuwe datalaag gecreëerd die informatie over de horizontale en verticale heterogeniteit van het bos bezorgt op het subpixel-schaalniveau van de sensor.

Hoofdstuk 6 bevat de uiteindelijke conclusies en geeft aanbevelingen voor verder onderzoek. De eindconclusie is dat de vanuit de ruimte waargenomen spectrodirectionele gegevens in staat zijn om gelijktijdig informatie te genereren over de biochemie van het gebladerte (vanuit het spectrale domein), als ook over de structurele heterogeniteit van het bos (vanuit het kijkhoek-domein). Deze kennis creëert nieuwe mogelijkheden om heterogene ecosystemen te monitoren, zoals bossen en struiken op een schaal die varieert van lokaal tot regionaal niveau. De in dit proefschrift gepresenteerde resultaten stimuleren verder onderzoek op het gebied van aardobservatie, met in het bijzonder de ontwikkeling van toekomstige spectrodirectionele instrumenten en de toepassing van karteringsproducten die in staat zijn om bossen over de hele wereld te monitoren.

Acknowledgements

Being a regular PhD student at Wageningen University requires writing four papers in four years time. These four papers have then to be complied with an introduction and a synthesis, and that is basically it. It essentially requires writing one paper per year. It is as simple as that. At least in theory. In practice, however, it was not always that simple. I had to cope with small delays, motivation dips, poor results and rigorous reviewers. Each year again there were moments of stress and uncertainties, and I am fully aware that finishing the PhD would not have been possible without the help of many precious people. It is a pleasure that I have now the opportunity to thank all of them.

I express my deepest gratitude to my promoter, Prof. Michael Schaepman. You were like a father figure to me and kept an eye on that I stayed on track, step-by-step, paper-by-paper, year-by-year. You provided me sufficient freedom, patient supervision, important advice, many helpful suggestions and occasional mental support in times of need. I always appreciated that when we 'went for a coffee' our conversations were each time in a positive tone and balanced between work and private life.

When I started with the PhD – and basically for the whole first year – I was a novice in the field of remote sensing. Regarding this first year I am especially grateful to Ben Koetz, who eventually became a remote co-promoter. You immediately showed confidence in me, introduced me in radiative transfer modeling, was patient with all my hastily written emails and helped a great deal in shaping the first paper.

There were many inspiring people around me at the Centre for Geo-Information (CGI), which in my second year inspired me to speed up the work by automating the modeling work. I am especially indebted to Raul Zurita and Allard de Wit who encouraged me to move away from software packages towards scripting own codes. Raul and Allard introduced me in programming languages, which quickly resulted in the maximal use of all available computers around for running hundred thousands of simulations.

When maturing a bit in the field during my third year I had the luck that former PhD student Zbyněk Malenovský returned to the CGI for a post-doc. You helped me enormously forward, not only thanks to your broad and detailed knowledge, but mostly thanks to your persistence and critical attitude. You forced me to double-check simulations, even to start over from scratch, to question over findings and above all not to lose touch with the complexity of true nature. Although at the very moment I did not always like your comments, at the end I benefited from your inspiring enthusiasm and scientific sincerity.

I am extremely grateful to my daily supervisor, Jan Clevers. Your patience, responsibility, carefulness and guidance gave me great assistance to finish my thesis in my last year. Your

138

commitment, constructive comments and careful corrections were very helpful to me. You read my numerous drafts, and – despite all efforts – continued to find typos. You taught me how to write a scientific paper that is to the point and in good English. Thanks.

For these four years I mainly worked at CGI, and I have done so with great pleasure. The energetic and dynamic working environment at CGI is the product of the interactions of many people and all of the following colleagues have contributed in motivating me to write this thesis. To start with my roommates: Gerd Weitkamp and Valerie Laurent. For keeping the office lively, for the chitchats and for the good times.

Many thanks go to all the staff members of the CGI. Special thanks go to: Harm Bartholomeus, who made me enthusiastic about remote sensing and for the IT support. Sytze de Bruin, for helping with statistical problems, and Lammert Kooistra, for the many RS-related discussions. Other precious people that were for many reasons important for me: Ignas Heitkönig, Gabriela Schaepman, Arnold Bregt, Karle Sykora, Gertjan Geerling.

It was a pleasure to accomplish this thesis in the inspiring ambiance of the fellow PhD students at CGI. These people were always in for a coffee and chitchat, and occasionally even for jumping into the 'wild' nightlife of Wageningen: Watze, Lucas, Lucía, Lucie, Titia, Rogier, Jacob, Yuan, Sander, Pepijn, Maaike, El-Sayed, Roberto, Silvia, Daniel & Daniela.

Within the PhD I received the freedom to visit a few laboratories abroad. I am grateful to Prof. Klaus Itten and later Michael Schaepman that I was always welcome at Remote Sensing Laboraties (RSL), University of Zurich, Switzerland. At RSL I learned new preprocessing techniques and RS software packages. I especially want to thank Mathias Kneubühler who was always there for me. I also enjoyed the inspiring environment of the PhD crew: Juerg, Joerg, Yves, Felix, Alexander, Daniel, Andreas, Francesco, Edoardo, Petra & Alemu.

I will never forget the trip to sunny Valencia with a mobil home, packed with 5 people and furniture for a whole family. I am very grateful to Prof. Jose Moreno who was so kind to offer me a working place in his group at the Lab for Earth Observation (LEO). I enjoyed the pleasant company of Jordi Garcia Llongo, Gloria Fernandez and especially Luis Guanter, for helping me with atmospherically correcting CHRIS images, and Luis Alonso, for the many fruitful discussions and introducing us into the Valencian life.

I want to thank my MSc students: Valerie, Jan-Martijn and Erika, for working on CHRIS-related topics.

I am very grateful to Joy Burrough for proof reading some of the articles. At the very end of the writing process you taught me to write proper English (which I continue to do wrong). I

also want to express special gratitude to the anonymous reviewers. Their numerous critical comments definitely contributed to improving the thesis.

I want to thank all my friends, former housemates and family that supported me in these past years, but above all my parents and relatives, Kris Aerden & Koen Buys and Koen Verrelst, thank you for your unconditional patience and support. Also thanks to Armand van Damme and da bro and sis: Janus and Even & Bjorn.

I owe my loving thanks to Agata Jakubowska and her beloved kids Misia and Franek. Agata was everything to me throughout this PhD period and beyond. Your heartfelt love, intellect, sweetness and realism have supported me in countless ways during the entire thesis process. Without you I would never have started a PhD, and even if so, I would never have been able to finish. You showed me that a PhD is just a job with many pleasant moments. You were always there for me and during the years living in separation you were my biggest motivation to finish on time. I therefore dedicate this thesis to you.

Color plates

Figure 1.1: Stand age study site compared for year of publication per radiative transfer model used. The open symbols represent biophysical retrievals (e.g. fraction cover, LAI), while the closed symbols represent biochemical retrievals (e.g. chlorophyll). Symbols are plotted on the averaged age. The grey lines represent the full range of stand age of the used study site. (Referenced legend *a*: Bruniquel-Pinel & Gastellu-Etchegorry, 1998; *b*: Gemmell, 1998; *c*: Gemmell and Varjo, 1999; *d*: Gastellu-Etchegorry et al., 1999; *e*: Gemmell, 1999; *f*: Brown et al., 2000; *g:*Demarez & Gastellu-Etchegorry, 2000; *h*: Kuusk & Nilson, 2000; *i*: Hu et al., 2000; *j*: Gao et al., 2000; *k*: Huemmrich, 2001; *l*: Gastellu-Etchegorry & Bruniquel-Pinel, 2001 *m*: Lacaze & Roujean, 2001; *n*: Gemmell et al., 2001*; o*: Kimes et al., 2002; *p*: Gemmell et al., 2002; *q*: Song et al., 2002; *r*: Wang et al., 2003; *s*: Shabanov et al., 2003; *t*: Gastellu-Etchegorry et al., 2003; *u*: Rautiainen et al., 2004; *v*: Zarco-Tejeda et al., 2004; *w*: Peddle et al., 2004; *x*: Fernandes et al., 2004; *y*: Meroni et al., 2004; *z*, *aa*: Kötz et al., 2004; *ab*, *ac*: Fang et al., 2003; *ad*: Zhang et al., 2005; *ae*: Rautiainen & Stenberg, 2005; *af*: Rautiainen, 2005; *ag*: Disney et al., 2006; *ah*: Schlerf & Atzberger, 2006; *ai:* Eriksson et al., 2006; *aj*: Soudani et al., 2006; *ak*, *al*: Cheng et al., 2006; *am*: Zhang et al., 2006; *an* Song et al., 2007; *ao*: Koetz et al., 2007; *ap*: Colombo et al., 2008; *aq*: Lang et al., 2007; *ar*: Malenovský et al., 2008; *as*, *at*: Kuusk et al., 2008; *au*: Huang et al., 2008; *av*: Suarez et al., 2008; *aw*: Verrelst et al., 2008b; *ax*: Quaife et al., 2008; *ay*: Moorthy et al., 2008).

Figure 3.4: $\Delta y / \Delta x$ of the Maccioni index for three templates (a: CC − LAI; b: LAI − NPV; c: CC − NPV, with fixed variables according to Swiss National Park: LAI: 2.5; CC: 60%; NPV: 30%, respectively). Error bars per structural variable span the range of values specific for each site The three study sites used: d: ●) young Norway spruce stand, e: **x**) old-growth pine forest and, f: *****) early mature beetle-infected lodgepole pine.
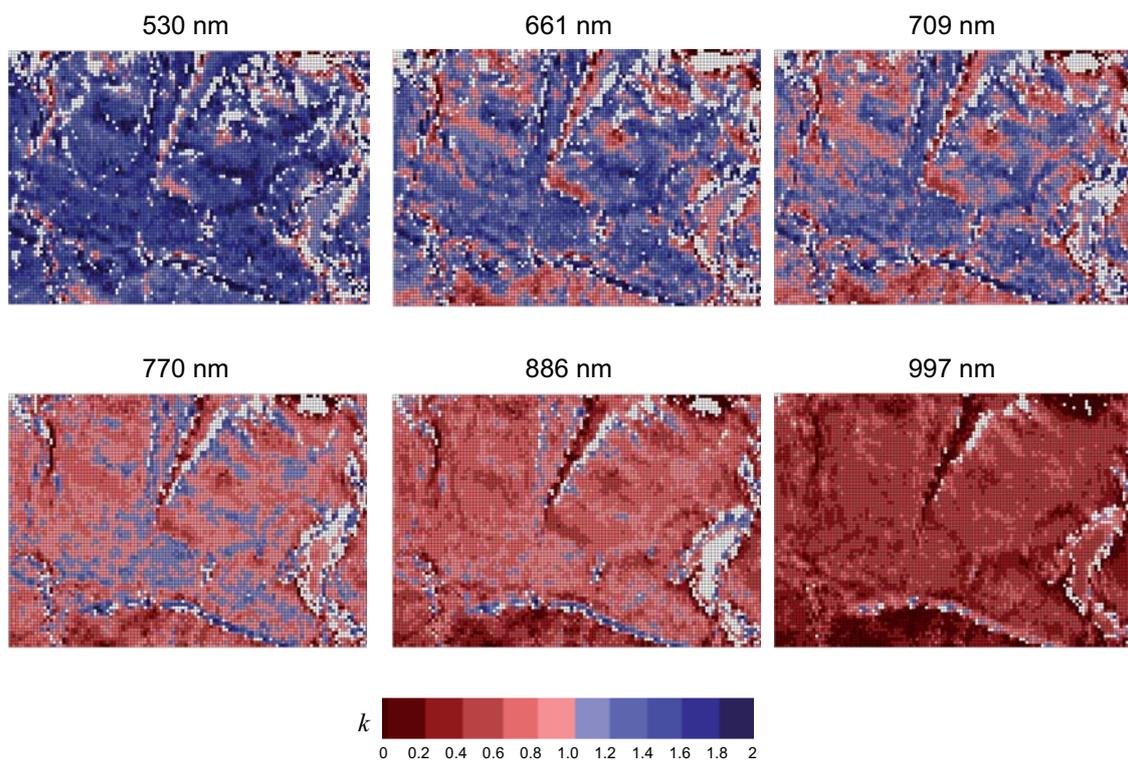
Figure 4.4: Minnaert-k maps for various CHRIS wavelengths. The white pixels are those in which the reflectance anisotropy of the CHRIS-HDRF data and the RPV-reconstructed HDRF data was significantly different.
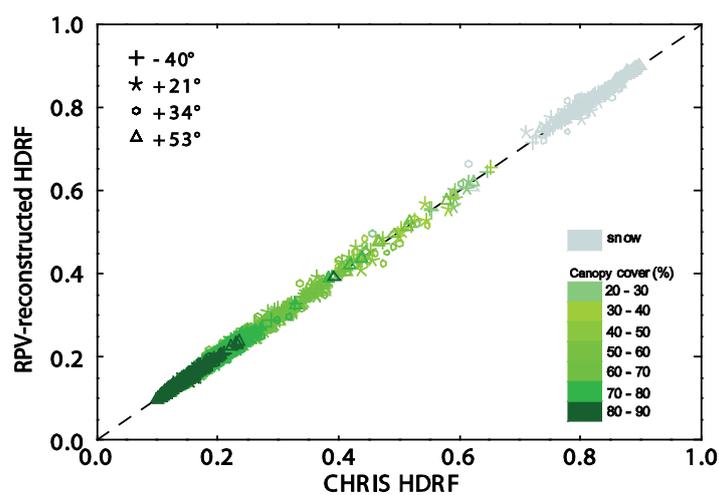
Figure 4.6: Comparison of CHRIS–HDRF and RPV-reconstructed HDRF at 631 nm for various canopy cover classes.
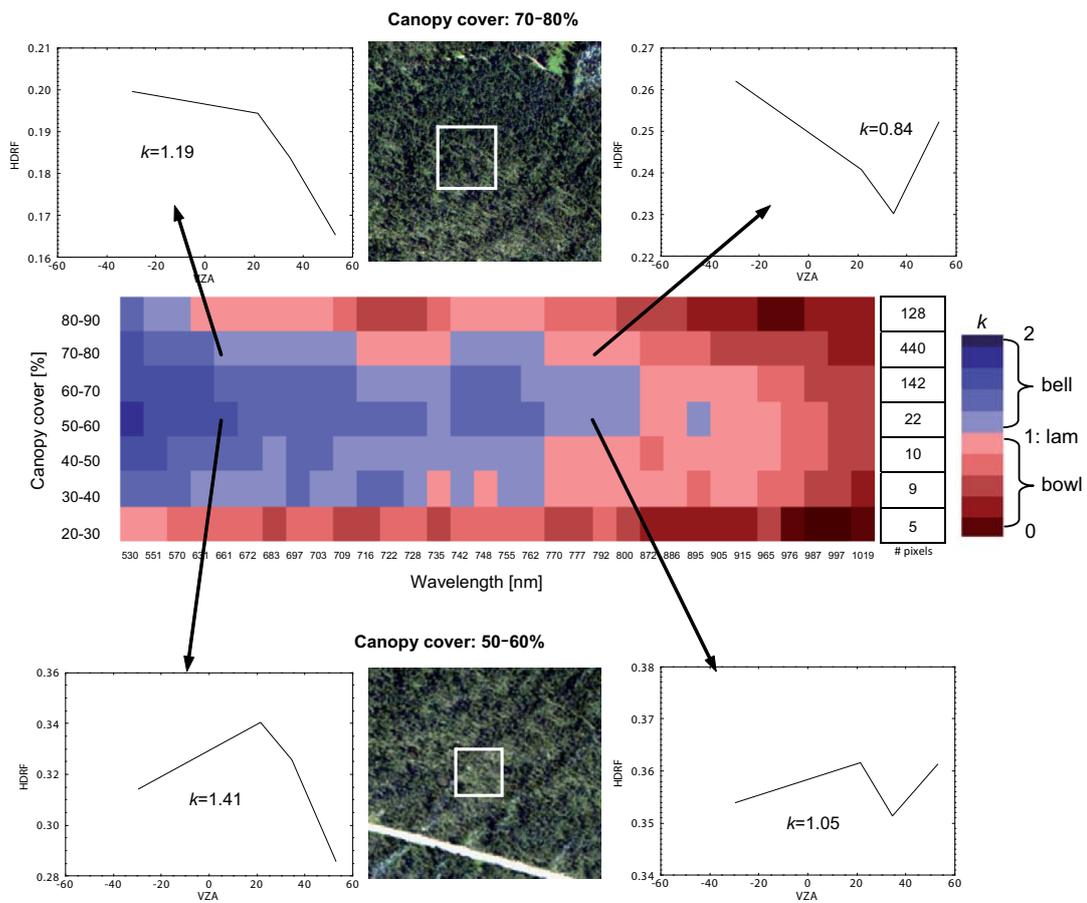
Figure 4.7: Averaged Minnaert-k values as a function of canopy cover and wavelength. The number of pixels per canopy cover class is given and some examples of the original angular signatures are shown. The RGB snapshots for a given canopy cover (white square) are derived from an HRSC (High Resolution Stereo Camera) acquisition in summer 2003. (lam= Lambertian)
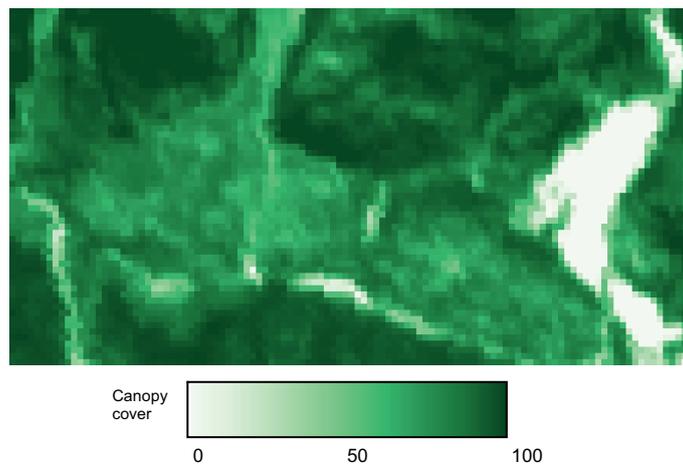
Figure 5.2: Map of canopy cover based on constrained LSU of the nadir CHRIS image of March 17, 2007.
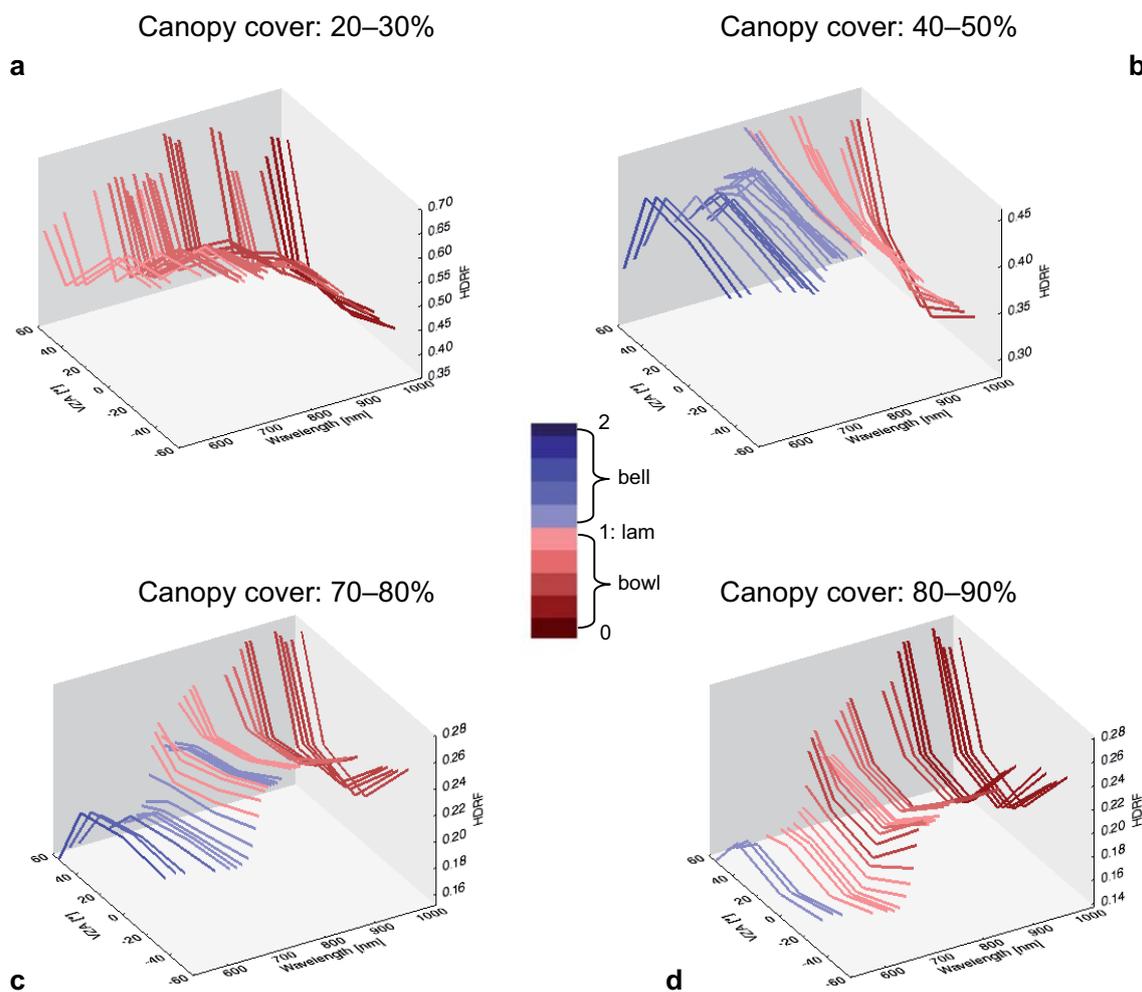
Figure 4.8: Averaged angular HDRF signatures for 4 canopy cover classes (a: 20−30%; b: 40−50%; c: 70−80%; d: 80−90%) with a color depending on the Minnaert-*k* value. Negative View Zenith Angles (VZA) represent the backscattering directions, positive VZAs represent forward scattering directions (lam= Lambertian).
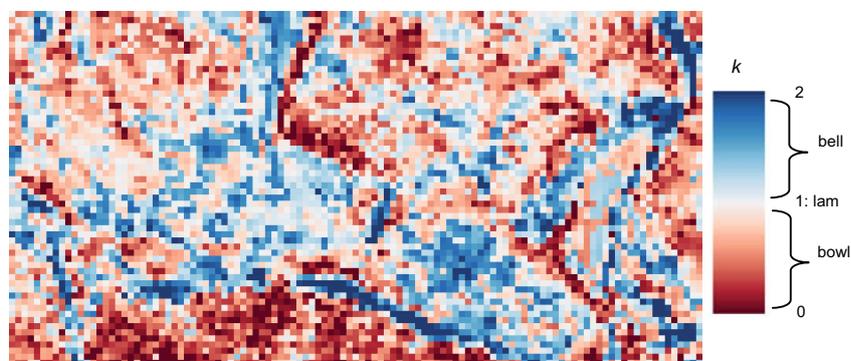
Figure 5.6: Minnaert-*k* parameter obtained by RPV model inversion at 722 nm (lam= Lambertian).
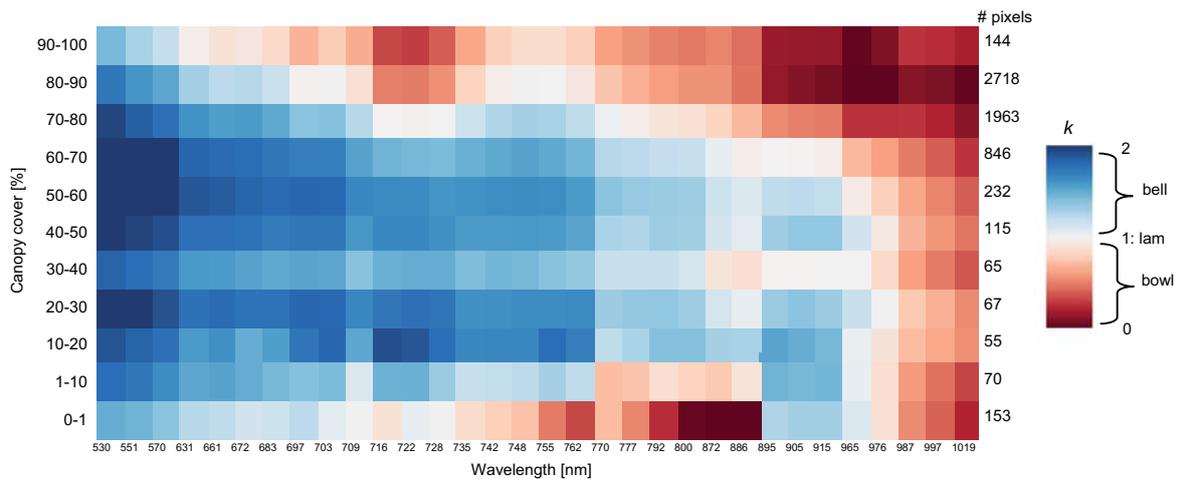
Figure 5.4: Averaged Minnaert-k values as a function of canopy cover and wavelength. The numbers on the right represent the number of pixels for each class (lam= Lambertian).
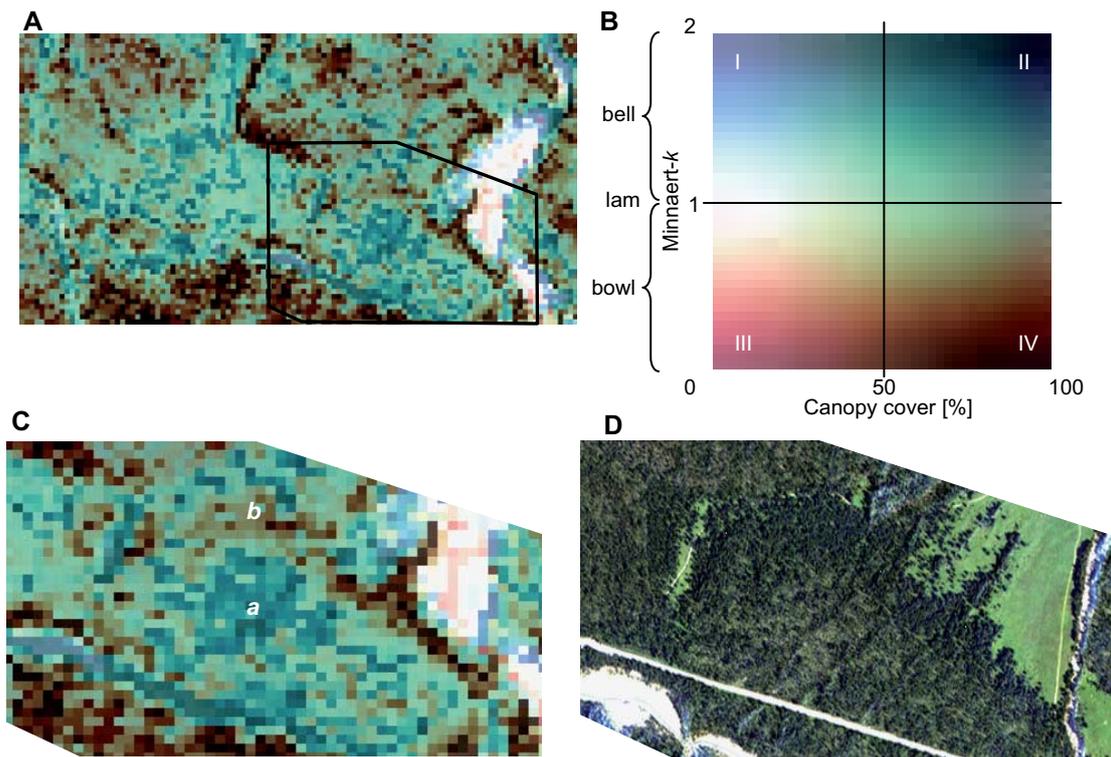
Figure 5.8: A) The RGB result of merging the Minnaert-*k* map with the canopy cover map. B) 2D color chart based on the color bar of the canopy cover map (*x*-axis) and the color bar of the Minnaert-*k* map (*y*-axis) (lam=Lambertian). C) Zoom-in of the merged map as presented in panel A. D) The reference image as derived from a high resolution stereo camera (HRSC) acquisition in summer 2003 (true color).

Glossary

Acronym	Meaning
1D	One-dimensional
2D	Two-dimensional
3D	Three-dimensional
AirMISR	Air Multiangle Imaging SpectroRadiometer
ALI	Advanced Land Imager
ANOVA	ANalysis Of VAriance
AOD	Aerosol Optical Depth
ARI	Anthocyanin Reflectance Index
ARVI	Atmospherically Resistant Vegetation Index
ASD	Analytical Spectral Devices
ATCOR-3	Atmospheric/Topographic CORrection for spaceborne imagery, v.3
BEAM	Basic ERS & Envisat (A)ATSR and Meris Toolbox
BHR	bihemispherical reflectance
BRDF	Bidirectional Reflectance Distribution Function
BRF	Bidirectional Reflectance Factor
Cab	Chlorophyll a+b concentration
CC	Crown Cover
CHRIS	Compact High Resolution Imaging Spectrometer
COP15	15th United Nations Climate Change Conference
CWD	Coarse Woody Debris
DART	Discrete Anisotropic Radiative Transfer (model)
DBH	Diameter at Breast Height
DDV	Dark Dense Vegetation
DEM	Digital Elevation Model
DHR	Directional-Hemispherical Reflectance
drat	aDvanced Radiometric Ray Tracer (model)
DTM	Digital Terrain Model
EnMAP	hyperspectral sensor for Environmental Mapping and Analysis Program
ENVI	Environment for Visualizing Images
EO	Earth Observation
EO-1	Earth Observer-1
EOS	Earth Observing System (http://eospso.gsfc.nasa.gov/)
ESA	European Space Agency
FLIGHT	Forest LIGHT interaction model
FLIM	Forest Light Interaction Model
FOV	Field OF View
FRT	Forest Radiative Transfer (model)
FWHM	Full Width at Half Maximum

Acronym	Meaning
FZA	Fly-by Zenith Angle
GEMI	Global Environmental Monitoring Index
GeoSAIL	Geometrical Scattering by Arbitrarily Inclined Leaves (model)
GEOSS	Global Earth Observation System of Systems (http://www.earthobservations.org/)
GHOST	G-function and Hot SpoT (model)
GMES	Global Monitoring for Environment and Security (http://www.gmes.info/)
gNDVI	green Normalized Difference Vegetation Index
GOFC	Global Observations of Forest Cover (http://www.fao.org/gtos/gofc-gold/)
GORT	Geometric-Optical Radiative Transfer (model)
HDRF	Hemispherical-Directional Reflectance Factor
HRSC	High Resolution Stereo Camera
IDL	Interactive Data Language
LAI	Leaf Area Index
LIBERTY	Leaf Incorporating Biochemistry Exhibiting Reflectance and Transmittance Yields (model)
LiDAR	Light Detection and Ranging
LSU	Linear Spectral Unmixing
LUE	Light Use Efficiency
MC	Monte Carlo
MCRM	Markov Chain Canopy Reflectance Model
MERIS	Medium Resolution Imaging Spectrometer
MISR	Multiangle Imaging SpectroRadiometer
$mNDVI_{705}$	modified Normalized Difference Vegetation Index $_{705}$ (narrowband index)
MODIS	MOderate Resolution Imaging Spectrometer
MODTRAN-4	MODerate resolution atmospheric TRANsmission, v.4
$mSRI_{705}$	modified Simple Ratio Index $_{705}$ (narrowband index)
NASA	National Aeronautics and Space Administration
NDVI	Normalized Difference Vegetation Index
$NDVI_{705}$	Normalized Difference Vegetation Index $_{705}$ (narrowband index)
NIR	Near Infra-Red (part of the electromagnetic spectrum)
NPP	Net Primary Productivity
NPV	Non-Photosynthetic Vegetation
OSAVI	Optimized Soil-Adjusted Vegetation Index
PDF	Probability Density Function
PRI	Photochemical Reflectance Index
PRISMA	PRecursore IperSpettrale della Missione Applicativa

Acronym	Meaning
PROBA-1	PROject for On Board Autonomy-1 (space platform)
PROFLIGHT	PROSPECT & FLIGHT (model coupling)
PROSPECT	leaf optical PROperties SPECTral model
PV	Photosynthetic Vegetation
RGB	Red Green Blue (color composition)
RGRI	Red Green Ratio Index
RM	Repeated Measurements
RMSE	Root Mean Square Error
RPV	Rahman-Pinty-Verstraete (model)
RT	Radiative Transfer
SAIL	Scattering by Arbitrarily Inclined Leaves (model)
SAIL2	Scattering by Arbitrarily Inclined Leaves (coupled model with the PROSPECT model)
SAILH	Scattering by Arbitrarily Inclined Leaves, with implemented Hot spot (model)
SAVI	Soil Adjusted Vegetation Index
SD	Standard Deviation
SEM	Standard Error of Mean
SIPI	Structure Insensitive Pigment Index
SLF	Swiss Federal Institute for Snow and Avalanche Research
SNP	Swiss National Park
SPREAD	fire SPREAD and mitigation (campaign)
SRI	Simple Ratio Index
SWIR	Short Wavelength Infra-Red
TCARI	Transformed Chlorophyll Absorption in Reflectance Index
TOA	Top Of Atmosphere
TOC	Top Of Canopy
VALERI	Validation of LAnd European Remote sensing Instruments
VI	Vegetation Index
VIS	VISible (part of the electromagnetic spectrum)
VNIR	Visible and Near Infra-Red (part of the electromagnetic spectrum)
VZA	View Zenith Angle
WFC	World Forestry Congress (http://www.fao.org/forestry/wfc/en/)

Short biography

Jochem Verrelst was born in Mortsel, located South of Antwerpen, Belgium on December 30, 1978, and lived his childhood in the region of South Antwerpen until he was 18. After finishing secondary school (Pius X-institute, Antwerpen) in 1997, he spent one year living with a Bolivian family in Oruro, a mining city in the Andes. Having seen a bit of the world, he wanted to become a development worker, with special interest in sustainable development in the tropics. In 1998 he went to Wageningen University, Netherlands to study Tropical Land Use.

As a student Jochem's academic interests developed towards environmental sciences and specifically towards tropical ecology. After the *propedeuse* (initial academic year at Dutch Universities) he chose to follow the tropical nature conservation program. In 2001 he went together with R.Verweij for 8 months to Bénoué National Park, Cameroon, for his first MSc thesis, entitled *"The creations of lawns: Oases in a West African savannah. Grazing facilitation by the common hippo and the Buffon's kob in Bénoué N.P., Cameroon"*. This research was conducted in cooperation with the *Institute of Environmental Science, Leiden* (CML) and the *Centre d'Etude de l'Environment et du Développement au Cameroun (*CEDC). The thesis was awarded with the *C.T. de Wit scriptie prijs* (best thesis award) at Wageningen University. Due to this research, academic interests shifted more towards the spatial compound of land dynamics and he started following courses offered by the Masters Geo-Information Science. Within this Masters, in 2004 he defended a second thesis about mapping floodplain vegetation *"Adopting plant community data for floodplain vegetation mapping using an image fusion of CASI and LiDAR data"*. As an internship, in 2004 he went to Chiapas, Southern Mexico to explore and map patches of fern vegetation in the Monte Azules tropical rain forest, functioning as an indicator of abandoned Mayan agricultural lands. This project was conducted in cooperation with the *Centro de Investigaciones en Ecosistemas* (CIEco) of the *Unversidad Nacional Autónoma de México* (UNAM). In March 2005 he graduated both in Tropical Land Use (Ir. Degree, equivalent to MSc) and Geo-Information Science (MSc).

After graduation, Jochem started working as a research assistant at the Centre for Geo-Information, Wageningen University, to map the 2004 Indonesian tsunami aftermath for the region of Banda Aceh. In September 2005 he started working as a PhD candidate at the same departments on mapping forest properties and four years and four months later he handed in the final draft of this thesis. During his PhD Jochem undertook various lab visits at Remote Sensing Laboratories (RSL), University of Zurich (Switzerland) and at the Lab for Earth Observation (LEO), Universty of Valencia (Spain).

Jochem professional interests are related to remote sensing science with links to vegetation, such as canopy radiative transfer modeling, plant phytosociology and physiology. Furthermore, he has always kept an interest in topics related to dynamics of tropical land cover and land use.

List of publications

Peer reviewed journals:

Leyequien, E., **Verrelst, J.**, Slot, M., Schaepman-Strub, G., Heitkönig, I.M.A., & Skidmore, A. (2007). Capturing the fugitive: Applying remote sensing to terrestrial animal distribution and diversity. *International Journal of Applied Earth Observation and Geoinformation, 9*, 1-20.

Romijn, E., **Verrelst, J**., & Kooistra, L. (2010). Mapping vegetation sructure in a river floodplain using multi-angular CHRIS/PROBA data. In preparation.

Schaepman, M.E., Ustin, S.L., Plaza, A.J., Painter, T.H., **Verrelst, J.**, & Liang, S. (2009). Earth system science related imaging spectroscopy-An assessment. *Remote Sensing of Environment, 113*, S123-S137.

Verrelst, J., Clevers, J.G.P.W., & Schaepman, M.E. (2010). Merging minnaert-k parameter with spectral unmixing to map forest heterogeneity with CHRIS/PROBA data. *IEEE Transactions on Geoscience and Remote Sensing.* In review.

Verrelst, J., Geerling, G.W., Sykora, K.V., & Clevers, J.G.P.W. (2009). Mapping of aggregated floodplain plant communities using image fusion of CASI and LiDAR data. *International Journal of Applied Earth Observation and Geoinformation, 11*, 83-94.

Verrelst, J., Schaepman, M.E., Koetz, B., & Kneubühler, M. (2008). Angular sensitivity analysis of vegetation indices derived from CHRIS/PROBA data. *Remote Sensing of Environment, 112*, 2341-2353.

Verrelst, J., Schaepman, M.E., & Clevers, J.G.P.W. (2010). Spectrodirectional Minnaert-k retrieval using CHRIS/PROBA data. *Remote Sensing of Environment,* In review.

Verrelst, J., Schaepman, M.E., Malenovský, Z., & Clevers, J.G.P.W. (2010). Effects of woody elements on simulated canopy reflectance: Implications for forest chlorophyll content retrieval. *Remote Sensing of Environment, 114*, 647-656.

Verweij, R.J.T., **Verrelst, J.**, Loth, P.E., Heitkönig, I.M.A., & Brunsting, A.M.H. (2006). Grazing lawns contribute to the subsistence of mesoherbivores on dystrophic savannas. *Oikos, 114*, 108-116.

Book chapter:

Verrelst, J.; Geerling, G.W.; Sykora, K.V.; Clevers, J.G.P.W. (2008). Mapping floodplain plant communities: clustering and ordination techniques adopted in remote sensing. In: Changing Rivers: Analysing fluvial landscape dynamics using remote sensing, PhD thesis G.W. Geerling. Centre for sustainable management of resources. Radboud University of Nijmegen, The Netherlands. ISBN: 978-90-810586-3-6.

Other scientific publications:

Koetz, B., Widlowski, J.-L., Morsdorf, F., **Verrelst, J.**, & Schaepman, M.E. (2007). Suitability of the parametric model RPV to assess canopy structure and heterogeneity from multi-angular CHRIS-PROBA data. In: *Proceedings 4th CHRIS PROBA workshop*, Frascati, Italy, 19-21 September, 2006.

Romijn, E., **Verrelst, J.**, & Kooistra, L. (2009). Mapping vegetation structure in river floodplain ecosystems using multi-angular CHRIS-PROBA data (abstract). In: *3rd EARSeL SIG Woskhop of Remote Sensing of Land Use & Land Cover*, Bonn, Germany, 25-27 November 2009.

Verrelst, J., Ac, A, Malenovský, Z., Hanus, J., Marek, M.V., & Schaepman, M.E. (2007). Angular chlorophyll indices estimates derived from ground-based diurnal course data and multiangular CHRIS-PROBA data: Two case studies. In: *Proceedings 5th EARSeL SIG IS workshop,* Brugge, Belgium, 23-25 April 2007.

Verrelst, J., Clevers, J.G.P.W., & Schaepman, M.E (2009). Combining Minnaert-*k* parameter with spectral unmixing for forest heterogeneity mapping using CHRIS-PROBA data (abstract). In: *3rd EARSeL SIG Woskhop of Remote Sensing of Land Use & Land Cover*, Bonn, Germany, 25-27 November 2009.

Verrelst, J., Clevers, J.G.P.W., & Schaepman, M.E (2009). Using the Minnaert-*k* parameter derived from CHRIS-PROBA data for mapping forest heterogeneity (abstract). In: *Hyperspectral workshop 2010*, Frascati, Italy, 17-19 March 2010.

Verrelst, J., Koetz, B., Kneubühler, M., & Schaepman, M.E. (2006). Directional sensitivity analysis of vegetation indices from multi-angular CHRIS/PROBA data. In: *ISPRS 2006: ISPRS mid-term symposium 2006*, Enschede, the Netherlands, 8-11 May 2006.

Verrelst, J., Schaepman, M.E. (2007). Damage assessment of a coastal plain based on satellite imagery. In: Your environment is our concern : a catalogue of worldwide environmental research by Alterra and the Environmental Sciences Department of Wageningen University. - Wageningen : Environmental Sciences Group, - p. 78 - 81.

Verrelst, J., Schaepman, M.E., & Clevers, J.G.P.W. (2008). A modelling approach for studying forest chlorophyll content in relation to canopy composition. In: *Proceedings of the XXI ISPRS Congress*, Beijing, China, 3-11 July 2008.

Verrelst, J., Schaepman, M.E., & Clevers, J.G.P.W. (2009). Fusing Minnaert-k parameter with spectral unmixing for forest heterogeneity mapping using CHRIS-PROBA data. In: *first IEEE GRSS WHISPERS*. Grenoble, France, 26-28 August 2009.

Verrelst, J., Schaepman, M.E., Koetz, B., & Clevers, J.G.P.W. (2009). Spectrodirectional Minnaert-k retrieval using CHRIS-PROBA data. In: *EARSeL Imaging Spectrometry Workshop*. Tel Aviv, Israel, 16-19 March 2009.

Verrelst, J., Schaepman, M.E., Koetz, B., & Kneubühler, M. (2006). Assessing the angular variability of broandband and narrowband vegetation indices using CHRIS/PROBA data. In: *Proceedings 4th International Workshop on Multiangular Measurements and Models (IWMMM-4)*, Sydney, Australia, 20-24 March 2006.

Verrelst, J., Zurita Milla, R., Koetz, B., Clevers, J.G.P.W., & Schaepman, M.E. (2007). Angular unmixing of photosynthetic and non-photosynethetic vegetation within a coniferous forest using CHRIS-PROBA. In: *Proceedings of the 10th ISPMSRS congress*, Davos, Switzerland, 12-14 March 2007.

PE&RC PhD Education Certificate

With the educational activities listed below the PhD candidate has complied with the educational requirements set by the C.T. de Wit Graduate School for Production Ecology and Resource Conservation (PE&RC) which comprises of a minimum total of 32 ECTS (= 22 weeks of activities)

Review of Literature (5.6 ECTS)
- Review on structural and biochemical canopy properties mapping of forests
  Review on remote sensing and terrestrial fauna (2005-2009)

Laboratory Training and Working Visits (4.3 ECTS)
- Laboratory visits for geometric and atmospheric correction of satellite images; Remote Sensing Laboratories (RSL), University of Zürich , Switzerland (2006, 2007, 2009)
- Visiting scientists; Department of physic University of Valencia, Spain (2007)

Post-Graduate Courses (14 ECTS)
- Application development for remote sensing; IDL (Interactive Data Language); CREASO (2006)
- The art of modelling; PE&RC-SENSE (2006)
- First Hyper-I-et summer schools; Caceres, Spain (2007)
- Second Hyper-I-et summer schools; PE&RC (2008)
- Advanced IDL programming; Fanning Consulting (2008)
- ESA Summer school "Land"; ESA, Prague, Czech Republic (2009)

Deficiency, Refresh, Brush-up Courses (2.8 ECTS)
- Advanced statistics PE&RC (2006)

Competence Strengthening / Skills Courses (1.4 ECTS)
- Techniques for writing and presenting a scientific paper; Wageningen Graduate Schools (2006)

Discussion Groups / Local Seminars and Other Scientific Meetings (9.8 ECTS)
- Spatial Method discussion group; PE&RC (2005-2008)
- Remote sensing thematic group; CGI-WUR (2005-2009)

PE&RC Annual Meetings, Seminars and the PE&RC Weekend (0.9 ECTS)
- PE&RC Day "The scientific agenda. Who pulls the strings?"(2006)
- PE&RC Day "Scaling from molecules to ecosystems" (2008)
- PE&RC Day "Intelligent Nature: On the Origin of Communication" (2009)

International Symposia, Workshops and Conferences (7.7 ECTS)
- 4th International Workshop on Multiangular Measurements and Models; Sydney, Australia (2006)
- ISPRS Commission VII mid-term symposium; Enschede, Netherlands (2006)
- ISPRS Working Group VII/I; Davos, Switzerland (2007)
- ISPRS Conference; Beijing, China (2008)
- EARSel Imaging Spectrocopy workshop; Tel Aviv, Israel (2009)
- IEEE WHISPERS hyperspectral workshop; Grenoble, France (2009)

Courses in Which the PhD Candidate Has Worked as a Teacher (1/2 day)
- Remote Sensing; GRS-WUR (2006-2009)

Supervision of MSc Students (3 students, 20 days)
- Remote Sensing